NAVAL POSTGRADUATE SCHOOL

MONTEREY, CALIFORNIA

THESIS

INVESTIGATION ON NOVEL METHODS TO INCREASE SPECIFIC THRUST IN PULSE DETONATION ENGINES VIA IMPLODING DETONATIONS

by

Ivan Chin Kian Ho

December 2009

Thesis Advisor:	Jose O. Sinibaldi
Co-Advisor:	Christopher M .Brophy

Approved for public release; distribution is unlimited

REPORT DOCUMENTATION PAGE			Form Approved OMB No. 0704-0188
Public reporting burden for this collection of information is estimated to average 1 hour per response, including the time for reviewing instruction, searching existing data sources, gathering and maintaining the data needed, and completing and reviewing the collection of information. Send comments regarding this burden estimate or any other aspect of this collection of information, including suggestions for reducing this burden, to Washington headquarters Services, Directorate for Information Operations and Reports, 1215 Jefferson Davis Highway, Suite 1204, Arlington, VA 22202-4302, and to the Office of Management and Budget, Paperwork Reduction Project (0704-0188) Washington DC 20503.			
1. AGENCY USE ONLY ***(Leave blank)***	**2. REPORT DATE** December 2009	**3. REPORT TYPE AND DATES COVERED** Master's Thesis	
4. TITLE AND SUBTITLE Investigation on Novel Methods to Increase Specific Thrust in Pulse Detonation Engines via Imploding Detonations		**5. FUNDING NUMBERS**	
6. AUTHOR(S) Ivan Chin Kian Ho			
7. PERFORMING ORGANIZATION NAME(S) AND ADDRESS(ES) Naval Postgraduate School Monterey, CA 93943-5000		**8. PERFORMING ORGANIZATION REPORT NUMBER**	
9. SPONSORING /MONITORING AGENCY NAME(S) AND ADDRESS(ES) N/A		**10. SPONSORING/MONITORING AGENCY REPORT NUMBER**	
11. SUPPLEMENTARY NOTES The views expressed in this thesis are those of the author and do not reflect the official policy or position of the Department of Defense or the U.S. Government.			
12a. DISTRIBUTION / AVAILABILITY STATEMENT Approved for public release; distribution is unlimited		**12b. DISTRIBUTION CODE**	

13. ABSTRACT (maximum 200 words)

Pulse Detonation Engines (PDE) are seen to be the next generation propulsion systems due to enhanced thermodynamic efficiencies based on the Humphrey cycle. One of the limitations in fielding practical designs has been attributed to tube diameters not exceeding 5 inches as the shock wave takes a long run distance for transition to detonation, thus, potentially affecting specific thrust. Novel methods via imploding detonations were investigated to remove such limitations. During the study, a practical computational cell size was first determined, so as to capture the required physics for transient detonation wave propagation using a Hydrogen-Air test case. Through a grid sensitivity analysis, one-quarter of the induction length was found sufficient to capture the experimentally observed initial wave transients. Test case models utilizing axi-symmetric head-on implosions were studied in order to understand how the implosion process reinforces a detonation wave as it expands. This in effect creates localized overdriven regions, which maintains the transition process to full detonation. A parametric study was also performed to determine the extent of diameter increase and it was found that the detonations could be supported with no change in run distance even when the tube diameter exceeds 5 inches.

14. SUBJECT TERMS Pulse Detonation Engines, Shock Wave, Detonation Implosions, Induction Length, Detonation Cell Width, Deflagration-to-Detonation Transition, Specific Thrust			**15. NUMBER OF PAGES** 113
			16. PRICE CODE
17. SECURITY CLASSIFICATION OF REPORT Unclassified	**18. SECURITY CLASSIFICATION OF THIS PAGE** Unclassified	**19. SECURITY CLASSIFICATION OF ABSTRACT** Unclassified	**20. LIMITATION OF ABSTRACT** UU

NSN 7540-01-280-5500 Standard Form 298 (Rev. 2-89)
Prescribed by ANSI Std. 239-18

THIS PAGE INTENTIONALLY LEFT BLANK

Approved for public release; distribution is unlimited

INVESTIGATION ON NOVEL METHODS TO INCREASE SPECIFIC THRUST IN PULSE DETONATION ENGINES VIA IMPLODING DETONATIONS

Ivan Chin Kian Ho
Engineer, Defence Science & Technology Agency (Singapore)
B.S., National University of Singapore, 2001

Submitted in partial fulfillment of the
requirements for the degree of

MASTER OF SCIENCE IN MECHANICAL ENGINEERING
and
MASTER OF SCIENCE IN APPLIED PHYSICS

from the

NAVAL POSTGRADUATE SCHOOL
December 2009

Author: Ivan Chin Kian Ho

Approved by: Jose O. Sinibaldi
Thesis Advisor

Christopher M. Brophy
Co-Advisor

Knox T. Millsaps
Chairman, Department of Mechanical and Astronautical Engineering

Andres Larraza
Chairman, Department of Physics

THIS PAGE INTENTIONALLY LEFT BLANK

ABSTRACT

Pulse Detonation Engines (PDE) are seen to be the next generation propulsion systems due to enhanced thermodynamic efficiencies based on the Humphrey cycle. One of the limitations in fielding practical designs has been attributed to tube diameters not exceeding 5 inches as the shock wave takes a long run distance for transition to detonation, thus potentially affecting specific thrust. Novel methods via imploding detonations were investigated to remove such limitations. During the study, a practical computational cell size was first determined so as to capture the required physics for transient detonation wave propagation using a Hydrogen-Air test case. Through a grid sensitivity analysis, one-quarter of the induction length was found sufficient to capture the experimentally observed initial wave transients. Test case models utilizing axi-symmetric head-on implosions were studied in order to understand how the implosion process reinforces a detonation wave as it expands. This in effect creates localized overdriven regions, which maintains the transition process to full detonation. A parametric study was also performed to determine the extent of diameter increase and it was found that the detonations could be supported with no change in run distance even when the tube diameter exceeds 5 inches.

THIS PAGE INTENTIONALLY LEFT BLANK

TABLE OF CONTENTS

I. INTRODUCTION....1
A. MOTIVATION....1
B. BACKGROUND....1
C. OBJECTIVES....3

II. THEORY....5
A. PULSE DETONATION ENGINES....5
B. DETONATION THEORY....6
C. DEFLAGRATION-TO-DETONATION TRANSITION....11
D. DETONATION WAVE STRUCTURE....13
E. DETONATION CELL WIDTH....14
F. REDUCED CHEMICAL KINETIC REACTION MODELS....16
G. EQUIVALENCE RATIO OF FUEL-OXIDIZER MIXTURE....16
H. COMPUTATIONAL NUMERICAL SCHEMES....17

III. SIMULATION SETUP (GRID SENSITIVITY)....19
A. WAVE IMPLOSION....19
B. HIGH FIDELITY SIMULATIONS (GRID SENSITIVITY ANALYSIS)....20
C. DETONATION CELL WIDTH OF H_2-AIR FOR DIFFERENT EQUIVALENCE RATIOS....22
D. PDE CONFIGURATION....23
E. SIMULATION PARAMETERS....24

IV. DISCUSSION OF RESULTS AND ANALYSIS....27
A. INITIAL COMPARISON OF DIFFERENT GRID SIZES....27
1. Computation of Detonation Velocity....28
2. Results from Initial Comparison....29
B. FURTHER GRID SENSITIVITY ANALYSIS....32
C. IMPLOSION ANALYSIS....39
1. Implosion Along the Mid-axis Inlet....40
2. Implosion Analysis Along Symmetry Axis....50
D. PARAMETRIC STUDY....58
1. Parametric Analysis Along Mid-inlet Axis....59
2. Parametric Analysis Along Symmetry Axis....66

V. WAY FORWARD AND RECOMMENDATIONS....77

VI. CONCLUSION....79

APPENDIX A: NASA CHEMICAL EQUILIBRIUM ANALYSIS OUTPUT....81

APPENDIX B: CONVERGENCE PLOTS FOR RESIDUAL ERRORS....85
A. GLOBAL RESIDUAL ERROR PLOT FOR MESH SIZE OF 0.25 MM....85
B. INNER RESIDUAL ERROR PLOT FOR MESH SIZE OF 0.25 MM....85

C. GLOBAL RESIDUAL ERROR PLOT FOR MESH SIZE OF 0.50 MM 86
D. INNER RESIDUAL ERROR PLOT FOR MESH SIZE OF 0.50 MM 86
E. GLOBAL RESIDUAL ERROR PLOT FOR MESH SIZE OF 1.00 MM 87
F. INNER RESIDUAL ERROR PLOT FOR MESH SIZE OF 1.00 MM 87
G. GLOBAL RESIDUAL ERROR PLOT FOR MESH SIZE OF 0.0625 MM 88
H. INNER RESIDUAL ERROR PLOT FOR MESH SIZE OF 0.0625 MM 88
I. GLOBAL RESIDUAL ERROR PLOT FOR MESH SIZE OF 0.05 MM 89
J. INNER RESIDUAL ERROR PLOT FOR MESH SIZE OF 0.05 MM 89
K. GLOBAL RESIDUAL ERROR PLOT FOR IMPLOSION (76.2 MM) .. 90
L. INNER RESIDUAL ERROR PLOT FOR IMPLOSION (76.2 MM)..... 90
M. GLOBAL RESIDUAL ERROR PLOT FOR IMPLOSION (114.30 MM)..... 91
N. INNER RESIDUAL ERROR PLOT FOR IMPLOSION (114.30 MM)... 91
O. GLOBAL RESIDUAL ERROR PLOT FOR IMPLOSION (133.35 MM)..... 92
P. INNER RESIDUAL ERROR PLOT FOR IMPLOSION (133.35 MM)... 92
LIST OF REFERENCES 93
INITIAL DISTRIBUTION LIST 95

LIST OF FIGURES

Figure 1. Pressure-volume plot based on Humphrey cycle [From 2] 2
Figure 2. PDE cycle – fill phase 5
Figure 3. PDE cycle – fire phase 6
Figure 4. PDE cycle – purge phase 6
Figure 5. One-dimensional combustion wave model [From 3] 7
Figure 6. Hugoniot curve for fuel-air mixtures [From 3] 10
Figure 7. Transition process to superdetonation [From 3] 12
Figure 8. Thermodynamic properties of the ZND model [From 3] 14
Figure 9 Soot foil imprint produced by JP10-Air detonation wave [From 4] 15
Figure 10. Detonation front structure with triple point [From 4] 15
Figure 11. Computational molecule based on implicit scheme 18
Figure 12. Collapsible toroidal wave implosion [From 1] 19
Figure 13. Comparison of detonation velocities for Jet A/Air mixture [From 9] 21
Figure 14. Comparison of C-J temperatures for Jet A/Air mixtures [From 9] 21
Figure 15. Graph of detonation cell width vs equivalence ratio for H_2-Air mixture [From 14] 22
Figure 16. 2-dimensional axisymmetric cylinder model 23
Figure 17. 2-D axisymmetric model (Unstructured mesh size) 24
Figure 18. Modified implosion PDE configuration 24
Figure 19. Pressure contour for H_2-Air mixture at 3 microsecond time step 28
Figure 20. Pressure contour for H_2-Air mixture at 4 microsecond time step 28
Figure 21. Schematic of the 5-point stencil method 29
Figure 22. Plot of wave velocity/CJ velocity against run distance for different mesh sizes 30
Figure 23. Plot of wave velocity/CJ velocity against run distance for different implicit time schemes 31
Figure 24. Plot of wave velocity/CJ velocity against run distance for different mesh sizes for Courant number of 1 32
Figure 25. H_2 – Air pressure contour plot at 65 mm 34
Figure 26. H_2 – Air pressure history plot at 65 mm 34
Figure 27. H_2 – Air temperature contour plot at 65 mm 35
Figure 28. H_2 – Air temperature history plot at 65 mm 35
Figure 29. H_2 – Air pressure contour plot at 122 mm 36
Figure 30. H_2–Air pressure history plot at 122 mm 37
Figure 31. H_2 – Air temperature contour plot at 122 mm 37
Figure 32. H_2 – Air temperature history plot at 122 mm 38
Figure 33. Close-up view of detonation wave structure 38
Figure 34. Evaluation of C-J wave speed for implosion study 40
Figure 35. Plot of wave velocity/CJ velocity against tube radius along mid-axis of inlet 41
Figure 36. Pressure contour for imploding geometry at run distance of 10 mm along inlet axis 42

Figure 37. Temperature contour for imploding geometry at run distance of 10 mm along inlet axis 42
Figure 38. Pressure contour for imploding geometry at run distance of 20 mm along inlet axis 44
Figure 39. Temperature contour for imploding geometry at run distance of 20 mm along inlet axis 44
Figure 40. Close-up view of temperature contour 45
Figure 41. Pressure history of imploding wave at run distance of 20 mm along inlet axis 46
Figure 42. Temperature history of imploding wave at run distance of 20 mm along inlet axis 46
Figure 43. Pressure contour for imploding geometry at run distance of 38 mm along inlet axis 47
Figure 44. Pressure history of imploding wave at run distance of 38 mm along inlet axis 48
Figure 45. Temperature contour for imploding geometry at run distance of 38 mm along inlet axis 49
Figure 46. Temperature history for imploding geometry at run distance of 38 mm along inlet axis 49
Figure 47. Plot of wave velocity/CJ velocity against run distance along symmetry axis 50
Figure 48. Pressure contour for imploding geometry at run distance of 23 mm along symmetry axis 51
Figure 49. Temperature contour for imploding geometry at run distance of 23 mm along symmetry axis 52
Figure 50. Pressure history of imploding wave at run distance of 23 mm along symmetry axis 52
Figure 51. Temperature history of imploding wave at run distance of 23 mm along symmetry axis 53
Figure 52. Pressure contour for imploding geometry at run distance of 50 mm along symmetry axis 54
Figure 53. Temperature contour for imploding geometry at run distance of 50 mm along symmetry axis 54
Figure 54. Pressure history of imploding wave at run distance of 50 mm along symmetry axis 55
Figure 55. Temperature history of imploding wave at run distance of 50 mm along symmetry axis 55
Figure 56. Pressure contour for imploding geometry at run distance of 98 mm along symmetry axis 56
Figure 57. Temperature contour for imploding geometry at run distance of 98 mm along symmetry axis 57
Figure 58. Pressure history of imploding wave at run distance of 98 mm along symmetry axis 57
Figure 59. Temperature history of imploding wave at run distance of 98 mm along symmetry axis 58

Figure 60. Plot of wave velocity/CJ Velocity against tube radius along inlet axis for different imploding shock tube diameters....59
Figure 61. Pressure contour for imploding geometry at run distance of 28.75 mm for tube diameter of 114.30 mm along inlet axis....60
Figure 62. Temperature contour for imploding geometry at run distance of 28.75 mm for tube diameter of 114.30 mm along inlet axis....61
Figure 63. Pressure contour for imploding geometry at run distance of 33.34 mm for tube diameter of 133.35 mm along inlet axis....61
Figure 64. Temperature contour for imploding geometry at run distance of 33.34 mm for tube diameter of 133.35 mm along inlet axis....62
Figure 65. Pressure contour for imploding geometry at run distance of 52 mm for tube diameter of 114.30 mm along inlet axis....64
Figure 66. Temperature contour for imploding geometry at run distance of 52 mm for tube diameter of 114.30 mm along inlet axis....64
Figure 67. Pressure contour for imploding geometry at run distance of 62 mm for tube diameter of 133.35 mm along inlet axis....65
Figure 68. Temperature contour for imploding geometry at run distance of 62 mm for tube diameter of 133.35 mm along inlet axis....65
Figure 69. Plot of wave velocity/CJ Velocity against run distance along symmetry axis for different imploding shock tube diameters....66
Figure 70. Pressure history of imploding wave at run distance of 60 mm along symmetry axis (diameter 114.3 mm)....67
Figure 71. Temperature history of imploding wave at run distance of 60 mm along symmetry axis (diameter 114.3 mm)....68
Figure 72. Pressure contour for imploding geometry at run distance of 60 mm for tube diameter of 114.3 mm along symmetry axis....68
Figure 73. Pressure history of imploding wave at run distance of 91 mm along symmetry axis (diameter 114.3 mm)....69
Figure 74. Temperature history of imploding wave at run distance of 91 mm along symmetry axis (diameter 114.3 mm)....70
Figure 75. Pressure contour for imploding geometry at run distance of 91 mm for tube diameter of 114.3 mm along symmetry axis....70
Figure 76. Pressure history of imploding wave at run distance of 30 mm along symmetry axis (diameter 133.35 mm)....71
Figure 77. Temperature history of imploding wave at run distance of 30 mm along symmetry axis (diameter 133.35 mm)....72
Figure 78. Pressure contour for imploding geometry at run distance of 30 mm for tube diameter of 133.35 mm along symmetry axis....72
Figure 79. Pressure contour for imploding geometry at run distance of 88 mm for tube diameter of 133.35 mm along symmetry axis....73
Figure 80. Pressure history of imploding wave at run distance of 88 mm along symmetry axis (diameter 133.35 mm)....74
Figure 81. Temperature history of imploding wave at run distance of 88 mm along symmetry axis (diameter 133.35 mm)....74

THIS PAGE IS INTENTIONALLY LEFT BLANK

LIST OF TABLES

Table 1. Physical validity of states on the Hugoniot curve.....10
Table 2. Reduced chemical kinetic mechanism for H_2-Air mixture.....20
Table 3. Simulation setup on CFD++ platform 25
Table 4. C-J parameters for stoichometric H_2-Air mixtures.....27
Table 5. Single-step reaction for stoichometric H_2-Air mixtures 27
Table 6. Set of evaluation parameters for different mesh sizes 31

THIS PAGE INTENTIONALLY LEFT BLANK

ACKNOWLEDGMENTS

First and foremost, I would like to thank Drs. Jose O. Sinibaldi and Christopher M. Brophy for their mentorship during the course of this research and throughout my graduate studies.

Also, special thanks to Office of Naval Research (ONR) and especially to Dr. Gabriel Roy for sponsoring this project. Also, special note of appreciation to Mr. Sukumar Chakvarathy and the people from Metacomp for providing support and technical advice on CFD++ that is the simulation platform used for the course of this research.

Last, but not least, I would like to thank Dr. Jeff Haferman and Mr. Eric Adint for their technical support for the parallel supercomputer cluster codenamed King Lear and Hamming/Skunkworks on which CFD++ is operated from.

THIS PAGE INTENTIONALLY LEFT BLANK

I. INTRODUCTION

A. MOTIVATION

Pulse Detonation Engines (PDEs) have tremendous potential to replace current state-of-the art propulsion systems, which can operate up to supersonic cruise speeds for missiles, fighter jets, unmanned aerial vehicles, etc. Much of this potential stems from the fact that PDEs operates on the detonation mode of combustion, which has a higher thermodynamic efficiency than current propulsion systems based upon constant pressure. However, no practical design has been fielded to date and one key limitation is due to the fact that detonation can only be supported in main detonation chambers of up to five inches in diameter without requiring unreasonably long tube lengths. This impairs the specific thrust substantially as multiple tubes are required to generate thrust required by a typical cruise missile. As a result, thrust density decreases and potential cross flow mixing problems from the efflux of five separate tubes reduce the efficiency even further. To increase the diameter of the main tube and yet maintain the tube length, simulation studies involving novel means using shock-focusing techniques via toroidal wave implosion first investigated by Jackson et al. [1] is conducted. This reinforces the wave propagation process and effectively shortens the deflagration-to-detonation run distance such that a detonation wave can be supported for larger diameter tubes.

B. BACKGROUND

Pulse Detonation Engines (PDEs) operates on the detonation mode of combustion, which can be best approximated by the Humphrey (Constant-Volume) cycle in contrast to the Brayton (Constant-Pressure) cycle for gas turbine engines, as illustrated in Figure 1. The amount of work done (Pressure-Volume) by the Humphrey cycle as heat energy is introduced under constant volume conditions from 2 to 3 is much greater as compared to the Brayton cycle under constant pressure conditions, resulting in higher thermodynamic efficiencies.

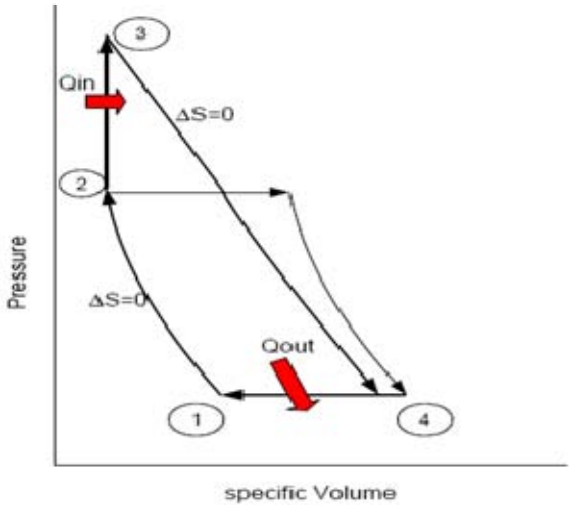

Figure 1. Pressure-volume plot based on Humphrey cycle [From 2]

In order to create detonation shock waves that can propagate at supersonic speeds, a finite run length distance is required for such transitions from deflagration-to-detonation known as a DDT process for a typical confined tube configuration. As tube diameters become larger, a longer DDT run distance is required in order to support the transition to a fully developed detonation wave. This limitation results in multiple tube configurations for a practical cruise missile design.

A novel method is being proposed using shock focusing techniques via toroidal wave implosion such that the shock wave propagation in the main shock tube is reinforced and consequently, the resulting pressures generated are much higher than the Chapman-Jouguet (C-J) conditions defined for a fully-developed steady state wave. The extreme high pressure environment favors much higher reaction rates for the fuel-oxidizer reactant mixtures and this will allow for a near direct generation of a detonation (without the need for DDT) as the fuel-air mixtures react violently in order to support the shock front.

In order to explore such implosion concepts accurately, it is imperative to capture the full physics and chemical kinetics behind such complex and highly transient fluid flows governing the shock wave behavior followed by chemical reactions based on a reduced set of chemical reaction mechanisms. Simulations of such complex flow field

behavior are only achievable via a practical computational cell mesh topology that is sufficiently small enough on the order of the induction length to describe the reaction zone behind the propagating shock front. Validation of such simulation studies based on well known reduced kinetic models for Hydrogen-Air mixtures can be conducted via comparison with experimental data available in the literature.

The required computational cell size for such high fidelity simulations can then be further extended to generic hydrocarbon fuel-air mixtures such as acetylene-air, ethylene-air, propane-air and even JP10-air mixtures based on the required length of the induction zone supporting the shock front. Utilizing the practical computational cell size, further analysis for a simulation case model based on an axi-symmetric head-on toroidal implosion can be conducted and analyzed for similar configuration types.

Parametric studies are then performed to investigate the extent of the increase in tube diameters for a fixed practical propulsion tube length based on the test case model.

C. OBJECTIVES

The research objective is to enhance current PDE applications by carrying out simulation studies to investigate the extent of possible combustor diameter increase using shock focusing techniques via toroidal implosions with modified PDE tube configurations without introducing the need for longer tube lengths.

Simulation studies were conducted on the CFD++ computational platform and carried out via the following order:

i) Determination of a practical computational cell size for high fidelity capturing of detonation wave propagation in a simple PDE tube configuration based on well known Hydrogen-Air reduced reaction models

ii) Simulation and analysis of head-on axi-symmetric toroidal implosions for Hydrogen-Air mixture based on the required computational cell size

iii) Performance of parametric studies used to evaluate the extent of the diameter increase for a fixed practical tube length using toroidal implosion based on an enhanced PDE design configuration

II. THEORY

A. PULSE DETONATION ENGINES

Pulse Detonation Engines are essentially intermittent propulsion systems where thrust is provided by repetitive triggering of detonation waves propagating at supersonic speeds in a long tube enclosed at the head end. The process takes place under nearly constant volume conditions and its operating cycle can be effectively described by three distinct phases. The first phase consists of introducing a reactive component such as hydrogen fuel and an oxidizing component such as air into the main combustion chamber. Initiation of the fuel-air mixture near the enclosed portion of the chamber occurs in the second phase via an energy sparking source. A high pressure detonation wave as a result of the initiation ensues in the third phase. The remaining fuel-air mixture in the tube is compressed in a thin reaction zone by the traversing detonation wave and reacts violently under extreme high pressure conditions to feed the leading edge of the shock front followed by an expansion zone of detonation products. The last phase consists of effectively purging the gaseous products out of the main chamber and the entire cycle repeats. Thrust is produced as the gaseous products exit out of the main propulsion tube. Figures 2 to 4 describes each phase of a PDE cycle.

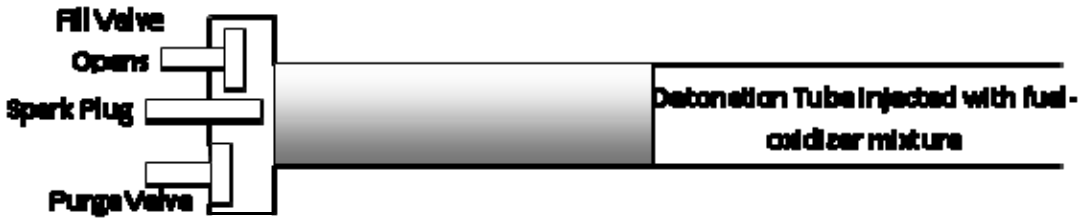

Figure 2. PDE cycle – fill phase

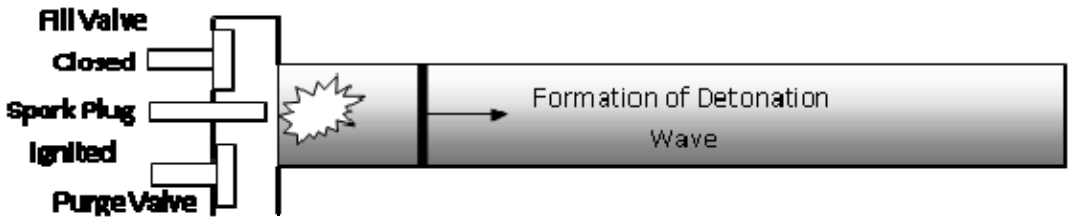

Figure 3. PDE cycle – fire phase

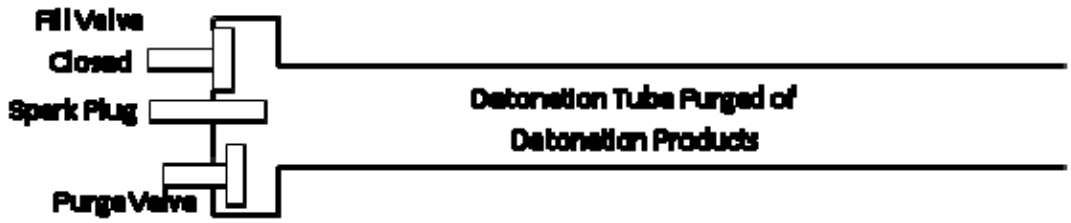

Figure 4. PDE cycle – purge phase

B. DETONATION THEORY

Detonation or deflagration by itself is an exothermic reaction caused by transition of unstable reactive molecular reactions to a stable state. The amount of energy required to trigger such reactions is known as the Activation Energy. When such energy levels are reached, the original reactant molecules come apart and re-arrange themselves back into a more stable state producing shock waves as a result of a sudden sharp increase in thermodynamic properties due to the exothermic reaction.

Combustion of fuel-air mixtures produces either a deflagration or detonation wave. Properties such as pressure (P), temperature (T) and density (ρ) of the reactant and products across the combustion wave front change discontinuously. Figure 5 illustrates the change across such properties for a constant area duct where the flame front is envisioned as stationary.

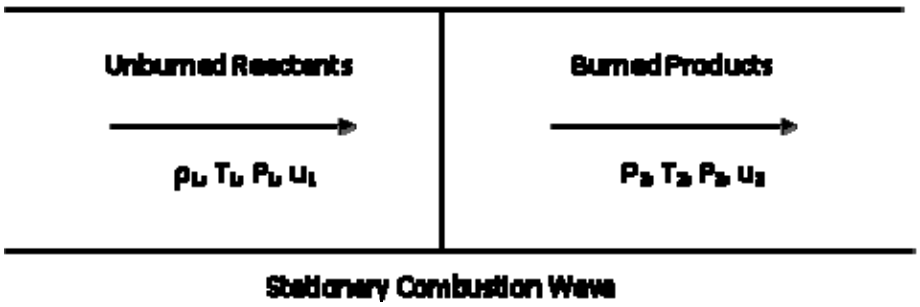

Figure 5. One-dimensional combustion wave model [From 3]

In order to relate properties across a one-dimensional combustion wave front, the corresponding mass conservation, momentum conservation, energy conservation and equation of state must be invoked. For the state equation, the ideal gas law serves as a good approximation to model the properties of the gases during combustion. These relations assume that the combustion wave is steady state and the process across the wave front is adiabatic and remain in chemical and thermodynamic equilibrium [3].

Mass Conservation:

$$\rho_1 u_1 = \rho_2 u_2 \tag{1}$$

Momentum Conservation:

$$P_1 + \rho_1 u_1^2 = P_2 + \rho_2 u_2^2 \tag{2}$$

Energy Conservation:

$$C_p T_1 + \frac{u_1^2}{2} + q = C_p T_2 + \frac{u_2^2}{2} \tag{3}$$

Equation of State (Ideal Gas Law):

$$P = \rho RT \tag{4}$$

Specific heat relation:

$$C_p = \frac{\gamma}{\gamma - 1} R \tag{5}$$

where:

R = Gas Constant

q = Specific heat energy added to the system via the combustion process

C_p = Specific heat at constant pressure

γ = Ratio of specific heats

In order to gain further insight into all possible states that the burned gas products can exist, a Hugoniot relation must be determined. A Hugoniot curve is basically a plot of pressure (P_2) versus specific volume ($\frac{1}{\rho_2}$) corresponding to the burned gas products for a fixed heat release mass, q and the relation can be derived by combining equations (2), (3) and (4) to obtain the given Hugoniot relation.

Hugoniot Relation:

$$\frac{\gamma}{\gamma-1}\left(\frac{P_2}{\rho_2}-\frac{P_1}{\rho_1}\right)-\frac{1}{2}\left(P_2-P_1\right)\left(\frac{1}{\rho_1}+\frac{1}{\rho_2}\right)=q \tag{6}$$

The slope of the Hugoniot relation indicates the velocity of the detonation wave. The Rayleigh Line relation is obtained by combining equations (1) and (2).

Rayleigh Line Relation:

$$\rho_1^2 u_1^2 = \frac{P_2 - P_1}{\frac{1}{\rho_1}-\frac{1}{\rho_2}} \tag{7}$$

The Hugoniot curve is illustrated in Figure 6. From the curve, the origin A represents the pressure (P_1) and specific volume ($\frac{1}{\rho_1}$) of the unburned reactants. The two tangent points intersecting origin A are defined as upper and lower Chapman-Jouget (C-J) points. From the Hugoniot curve, the C-J points can be obtained via the slope of the Hugoniot curve as follows:

C-J relation:

$$\frac{dP_2}{d\left(1/\rho_2\right)} = \frac{\left(P_2 - P_1\right)}{\left(\frac{1}{\rho_2} - \frac{1}{\rho_1}\right)} \tag{8}$$

The C-J relation can also be obtained via differentiation of equation (6) with respect to $d\left(1/\rho_2\right)$.

$$\frac{dP_2}{d\left(1/\rho_2\right)} = \frac{\left(P_2 - P_1\right) - \left(\frac{2\gamma}{\gamma - 1}\right)P_2}{\left(\frac{2\gamma}{\gamma - 1}\right)\frac{1}{\rho_2} - \left(\frac{1}{\rho_2} - \frac{1}{\rho_1}\right)} \tag{9}$$

The speed of sound, c_2 for the burned products is given by the following relation:

$$c_2 = \sqrt{\gamma R T_2} \tag{10}$$

Equating (8) and (9) along with the Rayleigh-Line relation in (7) gives the following:

$$u_2^2 = \frac{\gamma P_2}{\rho_2} = c_2^2 \tag{11}$$

This implies that the particle velocity of the gases leaving the detonation wave are traveling at sonic velocity. In a shock-frame of reference, this means that the product gases leaving the detonation wave are leaving at the sonic velocity of the products. Therefore equilibrating the amount of energy that reaches the shock front from the chemical reactions and thus allowing a sustained steady-state detonation wave to propagate at what is known as the Chapman-Jouguet velocity. Should this not be the case, detonation would undergo an unsteady process that will most likely asymptote to the C-J condition.

Five distinct regions can be infered from the Hugioniot curve, however, not all regions are physically valid. Table 1 describes the validity of the states in these regions.

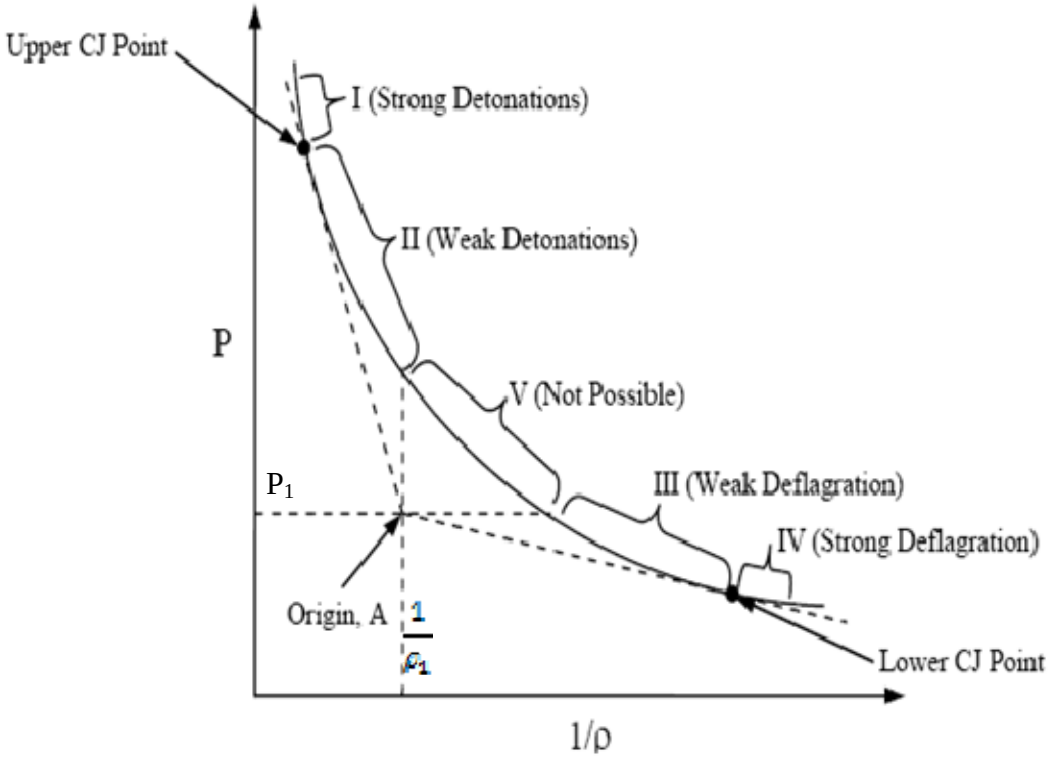

Figure 6. Hugoniot curve for fuel-air mixtures [From 3]

Table 1. Physical validity of states on the Hugoniot curve

Region	Remarks
I	Region I is defined as transient states where the combustion waves propagate as strong overdriven detonations above the upper C-J point. Under such conditions, the lead shock front travels at a much faster rate than the product gases resulting in a larger induction zone. The induction zone will eventually increase to such an extent such that any heat release generated by the combustion of the fuel-oxidizer reactants will not affect the lead shock front, thus slowing it down. As such, strong detonation waves will always decay back to the upper C-J point.
II	Region II is defined as transient states where the combustion waves propagate

Region	Remarks
	as weak detonations below the upper C-J point. Under such conditions, the velocity of the gas products travels at a faster rate than the lead shock front and as such the spatial extent of the induction zone decreases. The same heat release energy generated from the combustion reaction starts to have an increasing effect on the lead shock front due to the decreasing induction zone length and the additional heat release supplied starts to accelerate the lead shock front away from the reaction zone back towards the upper C-J point.
III	Region III represents states where the combustion waves propagate as weak deflagrations. They exist as expansion or rarefaction waves where the density of the burned products is lower than that corresponding to the reactants. They are observed experimentally during the initial deflagration-to-detonation process at ignition and the gas velocity relative to the wave front is accelerated from lower to higher sub-sonic speeds.
IV	Region IV represents states where the combustion waves propagate as strong deflagration waves. These are physically impossible states where the gas velocity relative to the wave front must be accelerated from sub-sonic to super-sonic speeds, which are forbidden for a wave structure propagating in a constant area duct.
V	The solution states for region V is mathematically impossible. The solution to the Rayleigh-Line equation (7) results in an imaginary number for $u_{1.}$

From the analysis given in Table 1, the physically validity of regions 1 and 3 are most likely observed during a detonation process and this has been confirmed in shock tube experiments as well [3].

C. DEFLAGRATION-TO-DETONATION TRANSITION

A detonation wave requires a finite run distance for the shock wave to transit from a deflagration to a detonation wave known as DDT. During initiation of a fuel-oxidizer

mixture in a PDE tube, a deflagration leading shock wave ensues and propagates at a wave speed characteristic of the reactant temperature conditions followed by a series of compression waves produced by the combustion process. The compression waves further heats up the region behind the leading shock wave creating localized high temperature regions and consequently increase the velocity of the compression waves. The compression waves eventually catch up with the leading wave front coalescing into a detonation wave [3]. The tube confinement as well as the turbulence generated by the motion of the product gases from the detonation shock front leads to the onset of "an explosion in an explosion," which produces an overdriven forward shock wave into the unburned reactants known as superdetonation and an opposite shock wave moving into the gas products known as retonation with transverse oscillating shocks in between. This finally leads to a self-sustained steady state detonation wave propagating at C-J velocity. Figure 7 illustrates this phenomenon.

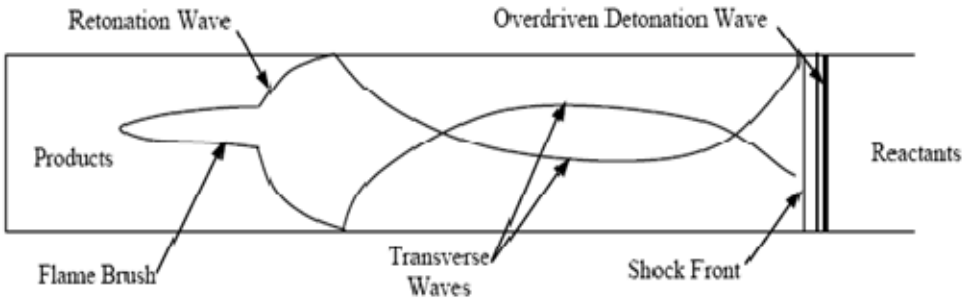

Figure 7. Transition process to superdetonation [From 3]

The DDT run distance is impractically long for current applications and therefore obstacles such as swept rams or spirals are used in PDE configurations to shorten the DDT length via turbulent flow regimes to promote higher chemical reaction kinetics. However, generation of high pressure losses as a consequence of such obstacles degrades the propulsive efficiency tremendously.

D. DETONATION WAVE STRUCTURE

Sustainment of the detonation wave can be described simply by the one-dimensional model developed independently by Zeldovich, von Neumann and Döring [3]. This is known as the ZND model illustrated in Figure 8. The model consists of a shock wave moving at detonation velocity followed by a rarefaction region. The shock wave region is extremely thin in the order of a few mean free paths thick of molecules; therefore limited reactions occur in this region. Across the shock region, there is a sharp almost discontinuous increase of pressure, temperature and density. The rarefaction region is comparatively much thicker usually on the order of 1 cm and consists of an induction and reaction zone. The thermodynamic properties in the induction zone immediately behind the shock front remain almost constant. Reaction rates as a function of temperature begin to increase slowly. Once the induction period is completed, temperatures start to climb sharply with extremely high heat release energies caused by the violent reactions of the fuel-oxidizer mixture defined by the reaction zone, which sustains the propagation of the shock wave. The gasdynamic properties reach their equilibrium states at the end of the reaction zone. Therefore, the induction period or induction zone is extremely important in order to capture the correct thermodynamic properties of temperature, pressure and density for an accurate simulation of a detonation wave.

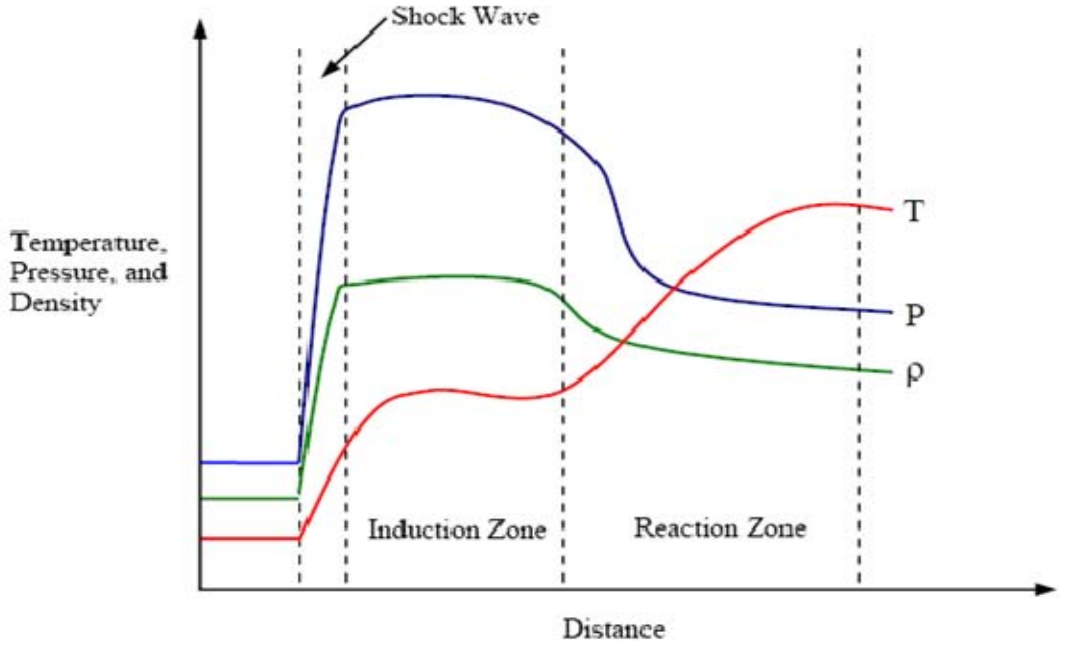

Figure 8. Thermodynamic properties of the ZND model [From 3]

E. DETONATION CELL WIDTH

Detonation cell widths are multi-dimensional detonation wave effects experimentally measured by soot foil imprint techniques where a detonation wave created by a typical fuel-air mixture leaves a fish scale pattern signature on soot coated aluminum sheet lined on the inner surface of a shock tube. Figure 9 illustrates a typical soot foil imprint produced by a detonating shock wave from JP10-Air mixture where JP10 is a liquid hydrocarbon fuel ($C_{10}H_{16}$). The non-planar detonation shock front induced by the energy release arising from the combustion of the fuel-oxidizer mixture is a resultant of the Mach stem, incident shock and reflected shock, which is a necessary condition for a self-sustained detonation front. The interaction of the three waves produces a shear discontinuity known as the triple point. Figure 10 illustrates such a detonation front structure. As a result, the waves propagate down the tube leaving the characteristic fish scale pattern signature. The transverse distance between each fish scale is known as the cell width, which is regarded as a fundamental parameter to characterize the detonability of a gaseous fuel-air mixture. A more reactive fuel such as hydrogen as compared to a

typical hydrocarbon fuel such as ethylene (C_2H_4) will correspondingly have a smaller detonation cell width. Similarly, reaction of hydrogen in the presence of a less reactive oxidizer such as air with respect to pure oxygen will have larger cell widths.

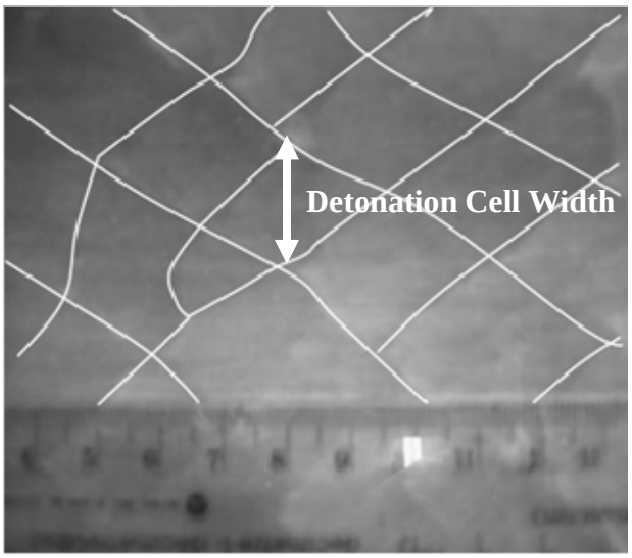

Figure 9 Soot foil imprint produced by JP10-Air detonation wave [From 4]

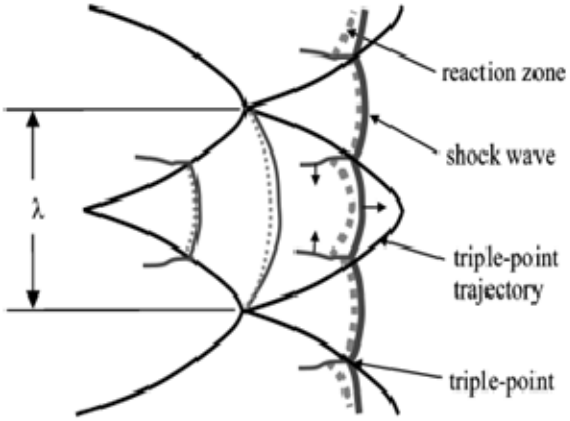

Figure 10. Detonation front structure with triple point [From 4]

F. REDUCED CHEMICAL KINETIC REACTION MODELS

Chemical kinetics governs the rate at which the species concentration of a fuel-oxidizer mixture is transformed into its product species and vice versa depending on pressure and temperature reaction conditions as well as complexity of the involved species. The dependence of the reaction rate constant, k as a function of temperature, T can be inferred from the Arrhenius Equation [3].

Arrhenius Equation:

$$k = AT^{n} \exp\left(-\frac{E_a}{RT}\right) \tag{12}$$

The pre-exponential parameter A describes the frequency of collisions for the species that result in a reaction as well as the preferred orientation of the molecular species that favor a reaction. The exponent n expresses the temperature dependence of the pre-exponential parameter. Activation energy, E_a defines the minimum amount of energy required for a reaction to occur and R is the universal gas constant.

While it is desired to include a detailed chemical reaction model governing a reactive fuel-oxidizer mixture, which can involve up to hundreds of reactions and species under all operating conditions, it is computationally demanding especially for complex flows involving cellular detonation wave structures even for super-computers of today. To ensure that computational times required for CFD simulations to be tractable under reasonable time frames, it is imperative to reduce detailed chemical mechanisms into simpler models where only certain chemical reactions are significant for example during a detonation process and yet able to capture the physics of the shock wave propagation with correct heat release rates in the reaction zone. This can be done via approximation of individual reactions to be in equilibrium or some of the species concentration can be assumed to be in quasi-steady state [5].

G. EQUIVALENCE RATIO OF FUEL-OXIDIZER MIXTURE

Typically, combustion of fuel-oxidizer mixtures is specified in terms of the equivalence ratio, ϕ. The equivalence ratio is independent of the mass, m or the number

of moles, n that is used to characterize the proportion of the fuel to oxidizer mixture. It is defined as the ratio of the fuel-oxidizer ratio to the stoichiometric fuel-oxidizer ratio and can be mathematically represented as follows:

$$\phi = \frac{m_{fuel} / m_{oxidizer}}{\left(m_{fuel} / m_{oxidizer}\right)_{stoichiometric}} = \frac{n_{fuel} / n_{oxidizer}}{\left(n_{fuel} / n_{oxidizer}\right)_{stoichiometric}} \tag{13}$$

The composition and thermodynamic properties of fuel-oxidizer mixtures during combustion/detonation are dependent on the equivalence ratio and consequently the detonation cell width if the wave propagates at supersonic speeds. A ratio greater than 1 would imply excess fuel or fuel rich mixtures than would be required for a stoichiometric reaction and conversely a ratio less than 1 would imply excess oxidizer or fuel lean mixtures.

H. COMPUTATIONAL NUMERICAL SCHEMES

In computational fluid dynamics, there are primarily two main schemes, explicit and implicit schemes implemented in order to discretize the resulting differential equations and resolve the required flow field. Explicit or forward differencing schemes suffer from conditional stability issues where a solution may blow up if the specified time step is too large and/or the computational cell size is too small. Implicit schemes are inherently stable as the forward solution is coupled together with the previous solution and hence will not generate an output that will increase to infinitely large values. Schemes of such types will be employed as the main scheme in study for simulation of detonation waves in PDE configurations. Figure 11 show a computational molecule based on an implicit scheme where p defines the spatial grid points in space and q defines the temporal grid points on an x-t diagram.

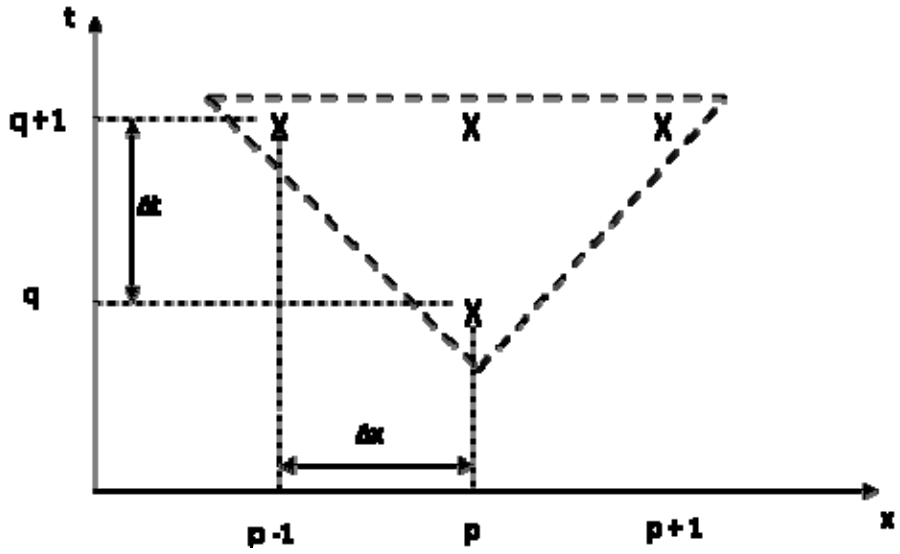

Figure 11. Computational molecule based on implicit scheme

For a mathematical representation of an implicit scheme, consider a simple one-dimensional scalar equation:

$$\frac{\partial u}{\partial x} + a\frac{\partial u}{\partial t} = 0 \tag{14}$$

Discretization of the above equation based on an implicit scheme results in the following:

$$u_p^{q+1} - u_p^q + \frac{a\Delta t}{\Delta x}\left(u_{p+1}^{q+1} - u_{p-1}^{q+1}\right) = 0 \tag{15}$$

$\frac{a\Delta t}{\Delta x}$ is also known as the Courant-Fredrichs-Lewy or CFL number. Numerical solution of the resulting flow field can be specified either in terms of a fixed time step or the CFL number where the time step is computed based on the computational mesh size. For a sufficiently small fixed time step, specification of the CFL number will result in faster numerical computations [6].

III. SIMULATION SETUP (GRID SENSITIVITY)

A. WAVE IMPLOSION

Wave implosion is a technique that focuses a shock front to generate a region of high pressure and temperature gases due to adiabatic compression of gas products as it flows into a region of decreasing area [1]. As a result, extremely high energy density localized regions are formed due to interacting compression waves and this raises the pressure of a typical fuel-oxidizer mixture above the C-J pressure, resulting in an overdriven detonation wave. Figure 12 illustrates an example of a collapsing toroidal wave front implosion. This concept is being explored to increase specific thrust of PDEs by harnessing the extremely high pressures as a result of the overdriven imploding shock front to increase the maximum diameter for a DDT process assuming a reasonable run distance required for transition to detonation. A commercial Computational Fluid Dynamics (CFD) platform used to perform simulation studies on the implosion concepts for PDEs is CFD++ from Metacomp Technologies. It is widely used by commercial companies such as General Electric and Air Force Research Laboratories (AFRL) as a computational tool for development on proof of concept PDEs and also supported by Office of Naval Research (ONR).

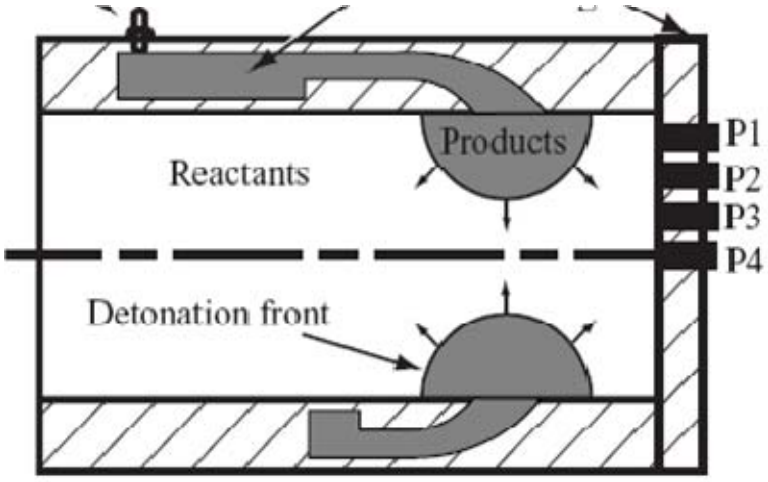

Figure 12. Collapsible toroidal wave implosion [From 1]

B. HIGH FIDELITY SIMULATIONS (GRID SENSITIVITY ANALYSIS)

In order to explore implosion concepts, high fidelity computational fluid dynamic (CFD) models based on reduced chemical kinetic mechanisms are pertinent for accurate and robust simulation to describe and analyze the physics of detonation wave propagation in pulse detonation engines. High fidelity models are sensitive to the induction length for a specific fuel-oxidizer mixture such that the transient flow kinetics and shock physics can be accurately captured as shown by the ZND model in the previous section.

Using a test case model for Hydrogen-Air (H_2-Air) mixtures, a grid sensitivity analysis was performed on a typical PDE tube configuration using a kinetic reaction model based on a reduced set of 18 reactions and 9 species [7] and [8] highlighted in Table 2.

Table 2. Reduced chemical kinetic mechanism for H_2-Air mixture

Number	Reaction	A[a]	n[a]	E_a[a]
1	$H_2 + O_2 \leftrightarrow 2OH$	0.17e11	0	0.2015e9
2	$O_2 + H \leftrightarrow 2OH$	0.142e12	0	0.6866e8
3	$H_2 + OH \leftrightarrow H_2O + H$	0.316e5	1.8	0.12686e8
4	$H_2 + O \leftrightarrow OH + H$	0.207e12	0	0.57568e8
5	$2OH \leftrightarrow H_2O + O$	0.55e11	0	0.29307e8
6	$OH + H + M \leftrightarrow H_2O + M$	0.2211e17	-2	0
7	$H + H + M \leftrightarrow H_2$	0.653e12	-1	0
8	$O_2 + H + M \leftrightarrow HO_2 + M$	0.32e13	-1	0
9	$OH + HO_2 \leftrightarrow O_2 + H_2O$	0.5e11	0	0.4186e7
10	$H + HO_2 \leftrightarrow H_2 + O_2$	0.253e11	0	0.29307e7
11	$H + HO_2 \leftrightarrow 2OH$	0.199e12	0	0.7536e7
12	$O + HO_2 \leftrightarrow O_2 + OH$	0.5e11	0	0.4186e7
13	$2HO_2 \leftrightarrow O_2 + H_2O_2$	0.199e10	0	0
14	$H_2 + HO_2 \leftrightarrow H + H_2O_2$	0.301e9	0	0.7829e8
15	$OH + H_2O_2 \leftrightarrow H + H_2O_2$	0.102e11	0	0.7954e7
16	$H + H_2O_2 \leftrightarrow H_2O + OH$	0.5e12	0	0.4186e8
17	$O + H_2O_2 \leftrightarrow OH + HO_2$	0.199e11	0	0.247e8
18	$H_2O_2 + M \leftrightarrow 2OH + M$	0.121e15	0	0.19049e9

[a] $k = AT^n e^{-E_a/RT}$ in units of kmol,m^3, s, K and J/kmol

Nitrogen and carbon chemistry reactions were excluded in the reaction model so as to optimize the required computational effort. Only slight differences in CJ detonation wave speeds and temperatures for typical hydrocarbon fuel-air mixtures on the order of 6% to 9% respectively [9] were observed as compared to the full kinetic model comprising the full nitrogen and carbon chemistry for Jet A/Air mixture, as shown in Figures 13 and 14, which was deemed as acceptable.

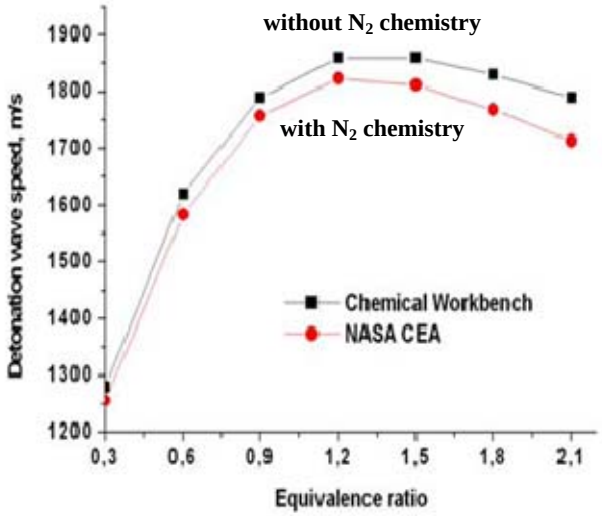

Figure 13. Comparison of detonation velocities for Jet A/Air mixture [From 9]

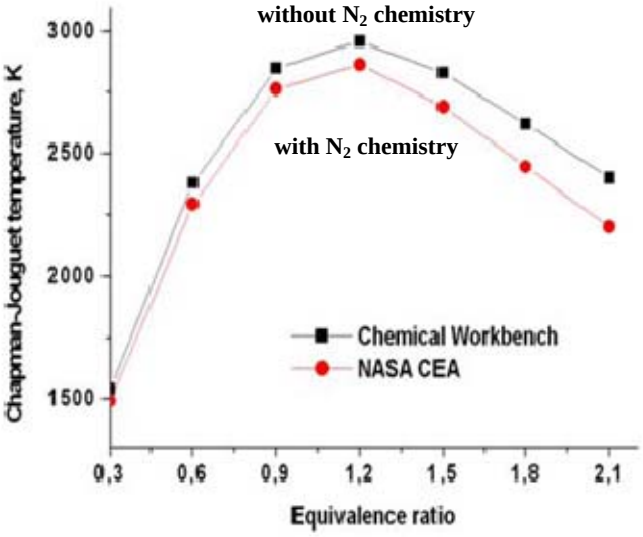

Figure 14. Comparison of C-J temperatures for Jet A/Air mixtures [From 9]

C. DETONATION CELL WIDTH OF H_2-AIR FOR DIFFERENT EQUIVALENCE RATIOS

Determination of the computational mesh size for the model was focused mainly on stoichiometric H_2-Air mixtures. This is because it is well defined in literature that experimental results at which detonation cell width occurs at a minimum corresponds to ϕ = 1 as indicated in Figure 15 referenced from [10], [11], [12] and [13] for a H_2-Air mixture. The induction length is in turn proportional to the detonation cell width and the relation is typically a linear one with a proportionality constant for different fuel-oxidizer mixtures. Therefore, this would present the baseline mesh size required for accurate simulation of detonation shock physics.

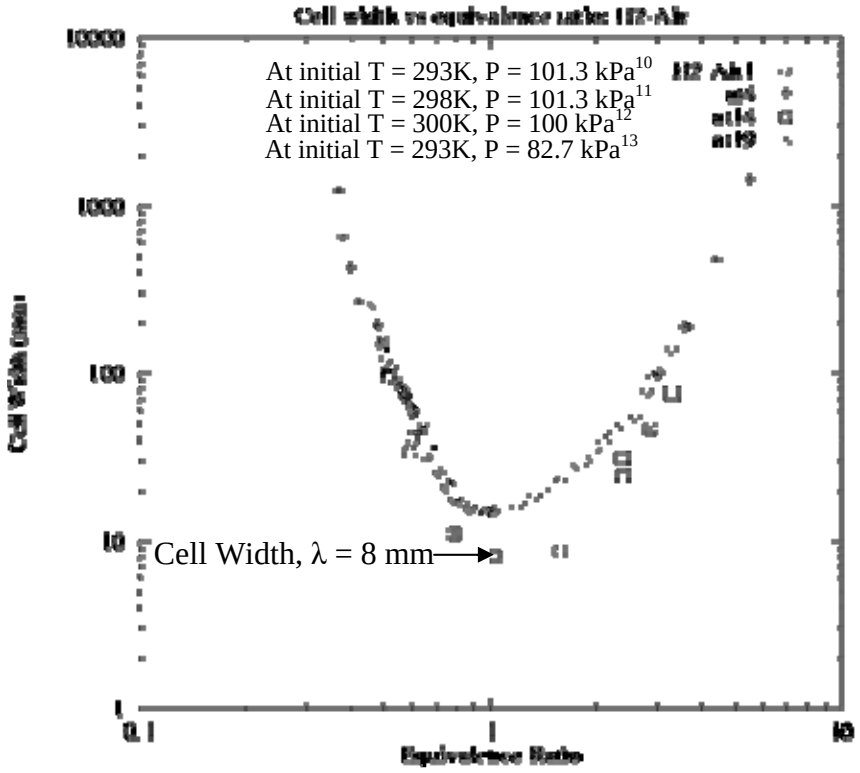

Figure 15. Graph of detonation cell width vs equivalence ratio for H_2-Air mixture [From 14]

D. PDE CONFIGURATION

For the grid sensitivity analysis, a 2-D axisymmetric cylinder model was generated on the Solid Works platform with the dimensions outlined in Figure 16. A detonation wave consisting of the detonation products was assumed to be initiated at CJ Pressure and CJ Temperature conditions characteristic of the fuel-oxidizer mixture as part of the initial conditions. Mass fraction of the detonation products are obtained from NASA Chemical Equilibrium Analysis (CEA) [15] and included in Appendix A. The reactant initial conditions were assumed to be at 1 atmosphere and 298 K, which would mimic experimental conditions for further validation.

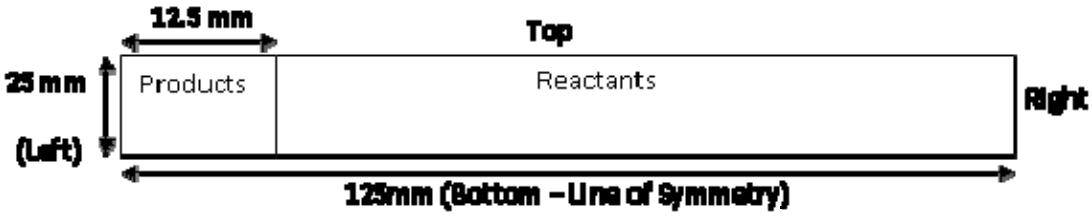

Figure 16. 2-dimensional axisymmetric cylinder model

The model was gridded on the Multipurpose Intelligent Meshing Environment (MIME) platform for an unstructured mesh (triangles) topology, which was optimized as a pre-processor for CFD++. It would have been ideal to resolve the flow field in terms of a structured mesh topology (quadrilaterals) so as to minimize the computational workload; however MIME did not have the capability to generate structured grids. An illustration of the cylinder model for unstructured mesh topology can be found in Figure 17.

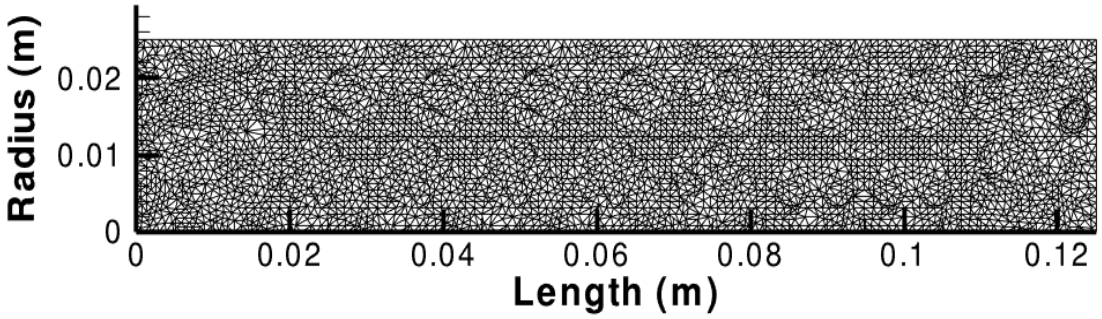

Figure 17. 2-D axisymmetric model (Unstructured mesh size)

For the implosion study, a modified PDE configuration was conceived based on a 2-D cylinder model as depicted in Figure 18 with an axi-symmetric axis. This model utilizes the concept of implosion with an assumption of a starting detonation wave propagating at the inlet. The lead shock front of the detonation wave should be sustained by the implosion concept and will not decay to a rarefaction wave as it expands into the tube space. Further parametric studies are then conducted by increasing the radius of the model until the detonation wave fails, thereby compromising the DDT length that is required for such geometric configurations.

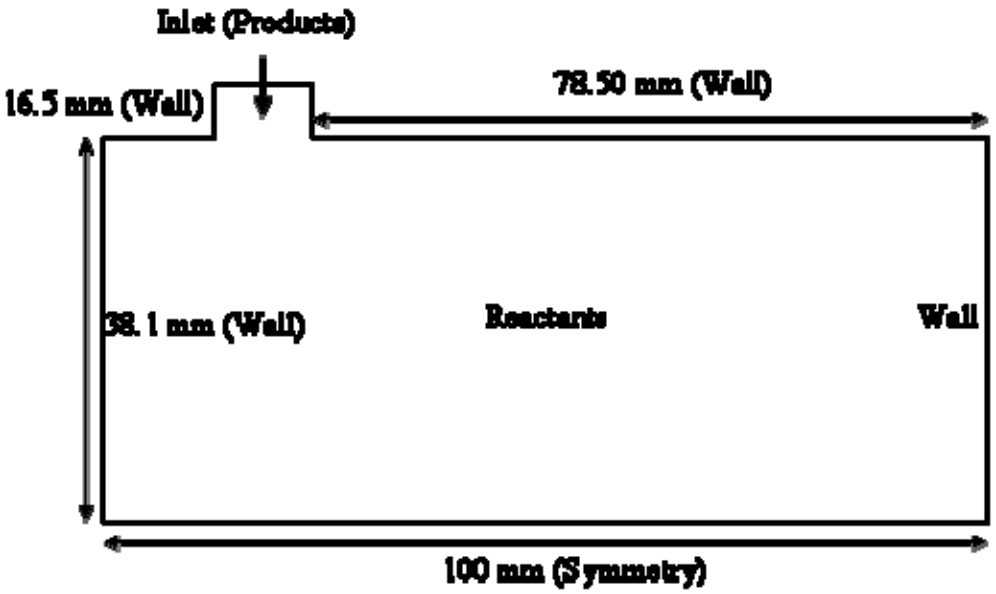

Figure 18. Modified implosion PDE configuration

E. SIMULATION PARAMETERS

The simulation parameters used to perform the grid sensitivity analysis is summarized in Table 3. The unsteady compressible Euler equation (no viscosity terms) was chosen as the main equation set governing the numerical computations. The parameter of interest was to evaluate the thermodynamic parameters and wave speed along the symmetry axis so as to capture the detonation wave physics rather than near the

walls (where viscous effects become significant). A Total Variation Diminishing (TVD) limiter scheme based on the minmod function was used in order to prevent spurious oscillation of the resolved flow field in the vicinity of strong gradients, which represent shocks. Near flow field regions where shocks are encountered, they switch the spatial discretization scheme to a first order accurate method while second-order accurate numerical schemes are computed for the rest of the flow field.

Table 3. Simulation setup on CFD++ platform

Equation Set Type	
i)	Unsteady Compressible Euler
ii)	Equation of State: Ideal Gas
Riemann Solver	
i)	Minimum Dissipation: LHS & RHS
ii)	Activate Pressure Switch: Supersonic
iii)	Activate Pressure Gradient Normal
Boundary Conditions (See Figure 17)	
i)	Top: Multi-species inviscid surface tangency (Wall)
ii)	Left: Multi-species inviscid surface tangency (Wall)
iii)	Right: Multi-species inviscid surface tangency (Wall)
iv)	Bottom: X-axis symmetry
Boundary Conditions (See Figure 18)	
i)	Inlet: Specified by inlet stagnation temperature, pressure and detonation products
ii)	Wall: Multi-species inviscid surface tangency
iii)	Symmetry: X-axis symmetry
Time Integration	
i)	Implicit
Spatial Discretization	
i)	2^{nd} Order Accuracy in Space
ii)	Dimension of polynomial: 2-D axisymmetric
iii)	Axis stability enhancement: Yes
iv)	Types of Total Variation Diminishing (TVD) Limiter: Minmod

THIS PAGE INTENTIONALLY LEFT BLANK

IV. DISCUSSION OF RESULTS AND ANALYSIS

A. INITIAL COMPARISON OF DIFFERENT GRID SIZES

A grid size from 0.25 mm to 1.0 mm was first considered in the grid sensitivity analysis so as to determine a computational mesh size that is sufficiently small enough to capture the physics of the detonation wave. The ZND induction length for detonation of stoichometric H_2-Air mixtures (0.23 mm) was used as a baseline comparison [16].

As outlined previously in the PDE configuration description, a detonation wave was assumed to propagate at the start with conditions pertaining to C-J pressure and temperature obtained from NASA CEA code. This is outlined in Table 4. (Note that the initial reactants were assumed to be at Pressure = 1 atm and Temperature = 298K). This would mimic experimental conditions for purpose of validation. The single step reaction equation is indicated in Table 5.

Table 4. C-J parameters for stoichometric H_2-Air mixtures

ϕ	V_{CJ} (m/s)	T_{CJ} (K)	P_{CJ} (MPa)
1.0	1964.8	2942	1.58

Table 5. Single-step reaction for stoichometric H_2-Air mixtures

ϕ	Reaction
1.0	$H_2 + ½(O_2 + 3.76N_2) \rightarrow H_2O + 3.76/2N_2$

An implicit scheme with a fixed time step of 1 nanosecond was first used during the initial comparison process. In order to validate the accuracy of the simulation run for each computational mesh size, the computed detonation velocity between each time step along the symmetry axis was computed using a first order finite difference method and compared against the C-J velocity. The C-J velocity is the velocity at which a steady state detonation wave propagates, which has been verified in shock tube experiments, as noted by Fickett and Davis [17].

1. Computation of Detonation Velocity

Detonation velocity was determined by noting the location of the shock front in the form of a pressure discontinuity along the symmetry axis of the cylinder configuration between each subsequent time step as illustrated in Figures 19 and 20.

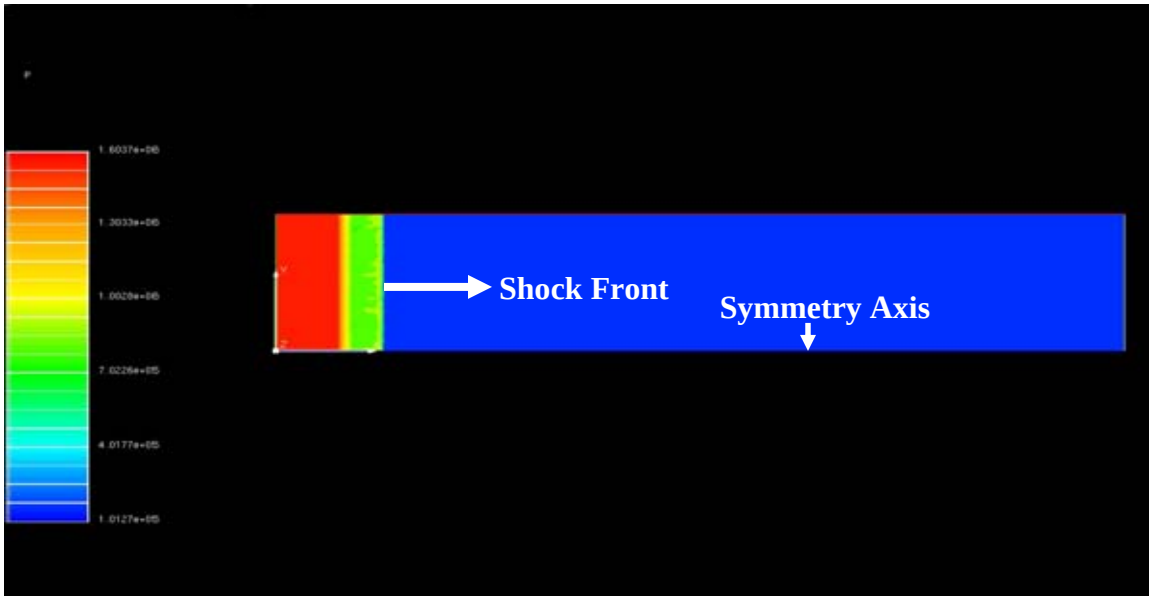

Figure 19. Pressure contour for H_2-Air mixture at 3 microsecond time step

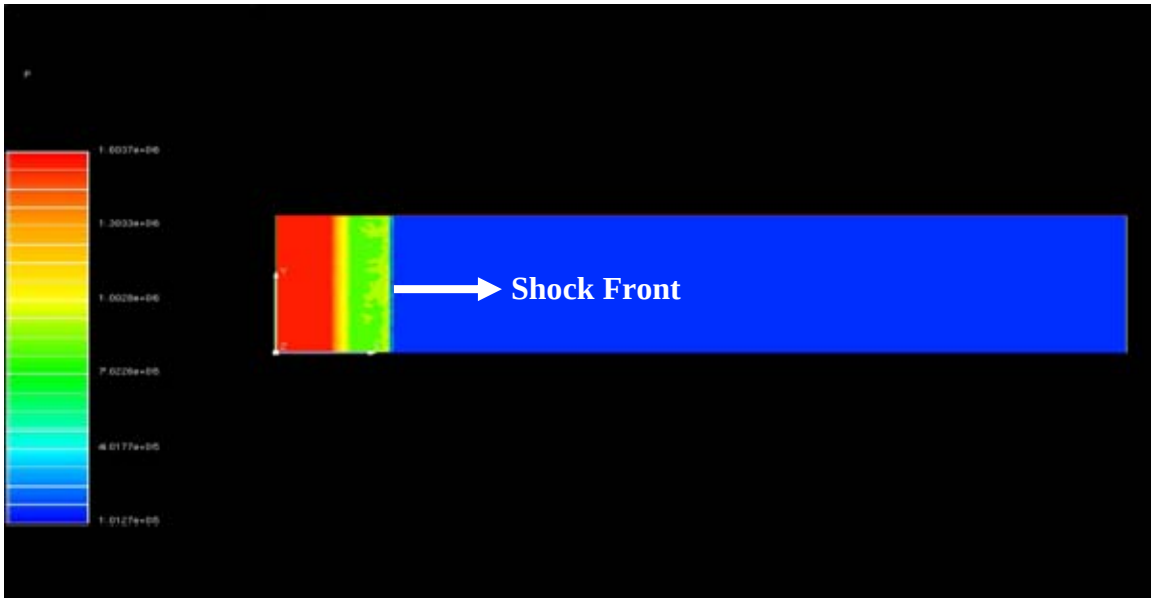

Figure 20. Pressure contour for H_2-Air mixture at 4 microsecond time step

To obtain the wave speed, a five-point stencil first order finite difference method [18] as shown in Figure 21 is performed in one-dimension where x represents the spatial discretized location of the shock front and t represents the fixed time step pertaining to the shock front location.

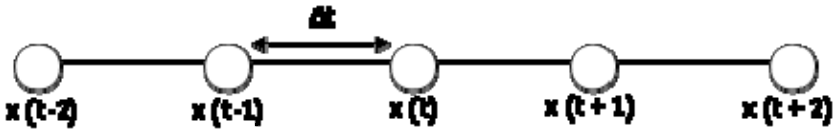

Figure 21. Schematic of the 5-point stencil method

The detonation wave speed, V_{DET} is then obtained via:

$$V_{DET} = \frac{-x(t+2)+8x(t+1)-8x(t-1)+x(t-2)}{12\Delta t} \tag{16}$$

2. Results from Initial Comparison

Results of the normalized detonation velocity with C-J velocity based on cell mesh sizes of 0.25 mm (~ One ZND length), 0.5 mm (~ Two ZND lengths) and 1.0 mm (~ Four ZND lengths) for stoichiometric H_2-Air mixtures against run distance along the symmetry axis of the PDE cylinder is plotted in Figure 22. Convergence plots for each of the simulation runs pertaining to each individual mesh size are included in Appendix B to verify that the resolved flow field solutions are bounded.

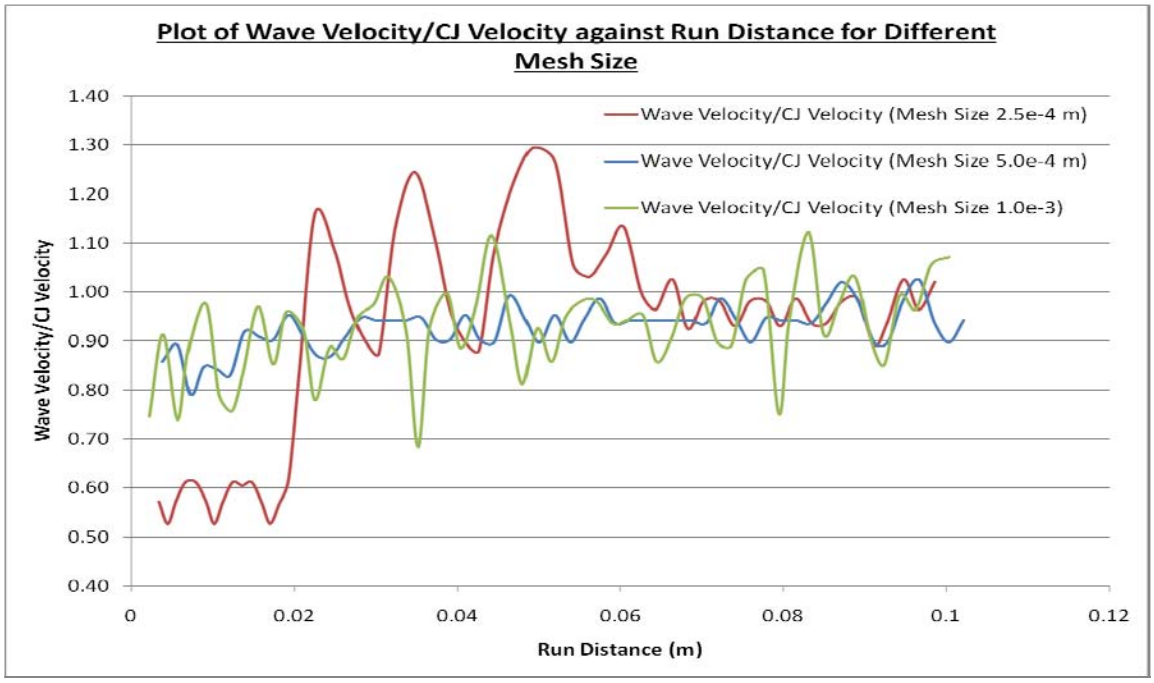

Figure 22. Plot of wave velocity/CJ velocity against run distance for different mesh sizes

All 3 cell sizes indicate good agreement with the predicted C-J velocity towards the end of the PDE cylinder. The detonation waves decay towards the steady state C-J velocity at the end where the order of accuracy from the mean C-J velocity ranged from 3% to 5%. Table 6 gives a statistical summary of the detonation wave velocities in terms of the standard deviation and the average normalized detonation wave speeds. This clearly implies that for simulation of a fully developed detonation wave propagating at C-J velocity, the cell sizes are clearly sufficient. However, the specified initial conditions were not enough to induce the 'wave' transient two-dimensional effects constituting the longitudinal and transverse wave interactions that have been observed in PDE detonation soot foil imprint experiments. Hence, further grid sensitivity studies were performed with the initial detonation wave propagating at temperature and pressure conditions specified by Zaev et al [8].

Table 6. Set of evaluation parameters for different mesh sizes

Mesh Size (mm)	Average Detonation Wave Velocity (m/s)	Standard Deviation of Detonation Wave Velocity (m/s)	Average Detonation Wave Velocity / CJ Velocity
0.25 (1 ZND Length)	1892.58	70.88	0.96
0.50 (2 ZND Lengths)	1864.54	77.87	0.95
1.00 (4 ZND Lengths)	1898.81	175.55	0.97

Also, the computational effort required to complete a simulation run for 0.25 mm took 8 days based on an implicit scheme with a fixed time step. To reduce and optimize the computational time, an implicit scheme with CFL number equal to one was adopted. In order to validate the implicit scheme based on CFL number, the same test case model using a mesh size of 0.25 mm was simulated using these two employed schemes and shown in Figure 23. The results indicate good agreement with each other with the numerical accuracy not compromised by adopting a different scheme.

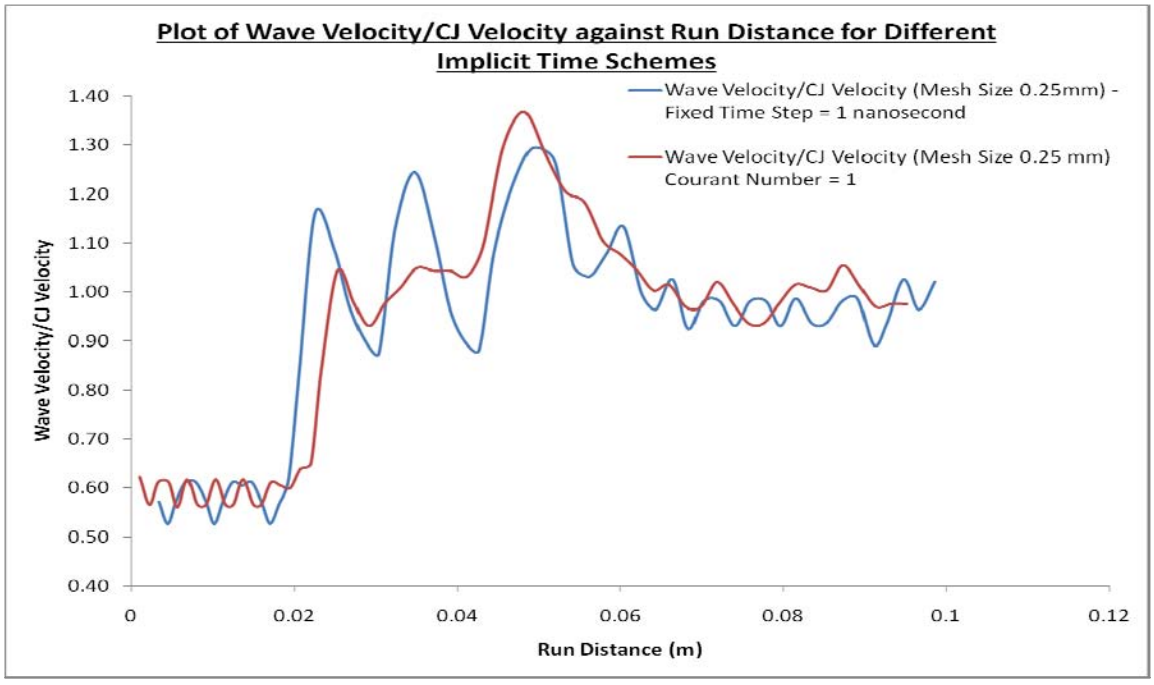

Figure 23. Plot of wave velocity/CJ velocity against run distance for different implicit time schemes

B. FURTHER GRID SENSITIVITY ANALYSIS

Further analysis was performed on cell sizes ranging from 0.25 mm (~ One ZND length), 0.0625 mm (~ One-quarter ZND length) and 0.05 mm (~ One-fifth ZND length). A plot of the normalized wave speeds along the symmetry axis with the C-J velocity as a function of the run distance of the cylinder is shown in Figure 24. Initial conditions for a starting detonation wave are specified at a pressure of 3.95 MPa and a temperature of 2942 K.

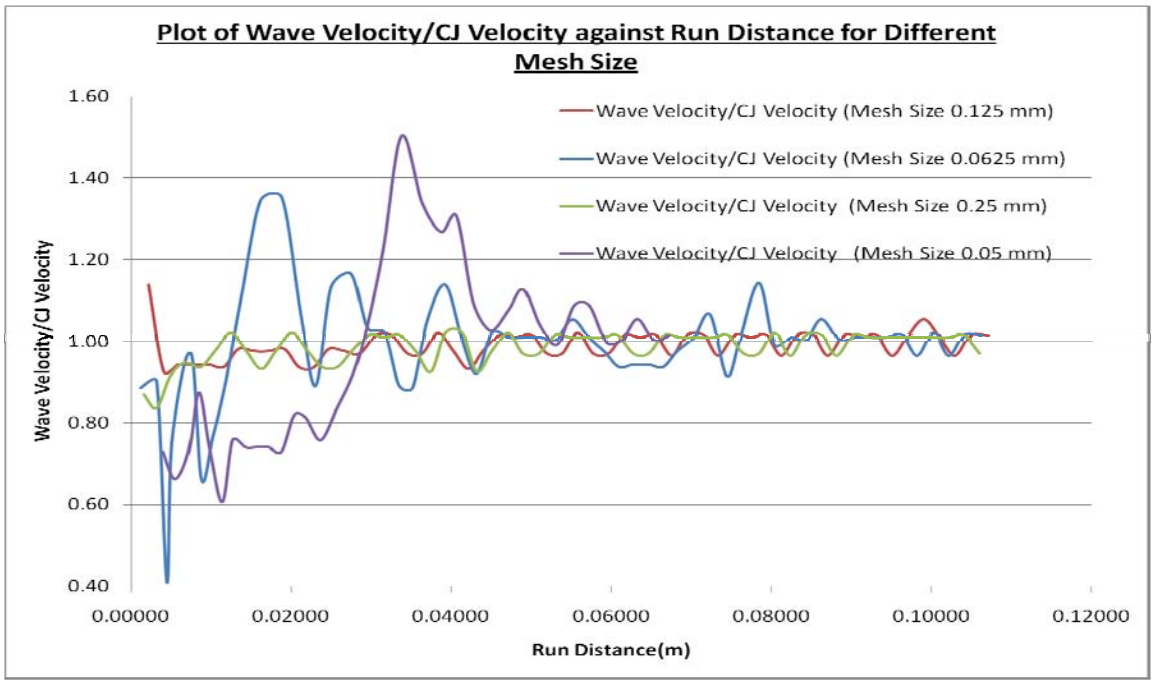

Figure 24. Plot of wave velocity/CJ velocity against run distance for different mesh sizes for Courant number of 1

At a computational mesh size of 0.0625 mm, initial wave transients could be observed for an under-driven wave propagating at a sub-CJ speed and increase after a small run distance to an over-driven detonation wave before decaying and oscillating about the steady state C-J velocity. This clearly shows the transition to detonation or the DDT process. Decreasing the cell size from 0.0625 mm to 0.05 mm shows no change in the initial transients as well as the decay behavior to the steady state C-J velocity, which

allows us to determine that 0.0625 mm would be a practical cell size to capture the detonation physics, as well as apply to other fuel-oxidizer mixtures.

Further insight could also be gained by first analyzing the pressure and temperature contours as well as the histories for the given mesh size of 0.0625 mm at the mid-point of the cylinder configuration as indicated in Figures 25, 26, 27 and 28 respectively.

Behind the shock front, the detonation wave structure comprising of transverse wave interactions along with the longitudinal propagating wave front are observed, which are clearly multi-dimensional effects for both pressure and temperature contours. The thin shock front layer is propagating at a pressure state of 2.4 MPa that is higher than the C-J pressure of 1.58 MPa. Just behind the shock front, the detonation wave structure approximately 45 mm long comprising of the triple points are close coupled, which is fueling the detonation wave process followed by an expansion zone. Similarly, the H_2-Air mixture reacts at an almost constant C-J temperature condition of 3000 K throughout the detonation wave structure zone.

From the pressure history data, the pressure state for lead shock front relaxes to 1.0 MPa before increasing back up to 2.0 MPa. The initial decrease is due to the interaction of the transverse wave propagating from the side walls and the symmetry axis of the cylinder. However, when the triple points intersect, the waves reinforce each other and the superposition process increases the localized pressure points. This promotes conditions that sustain the propagation of the detonation wave.

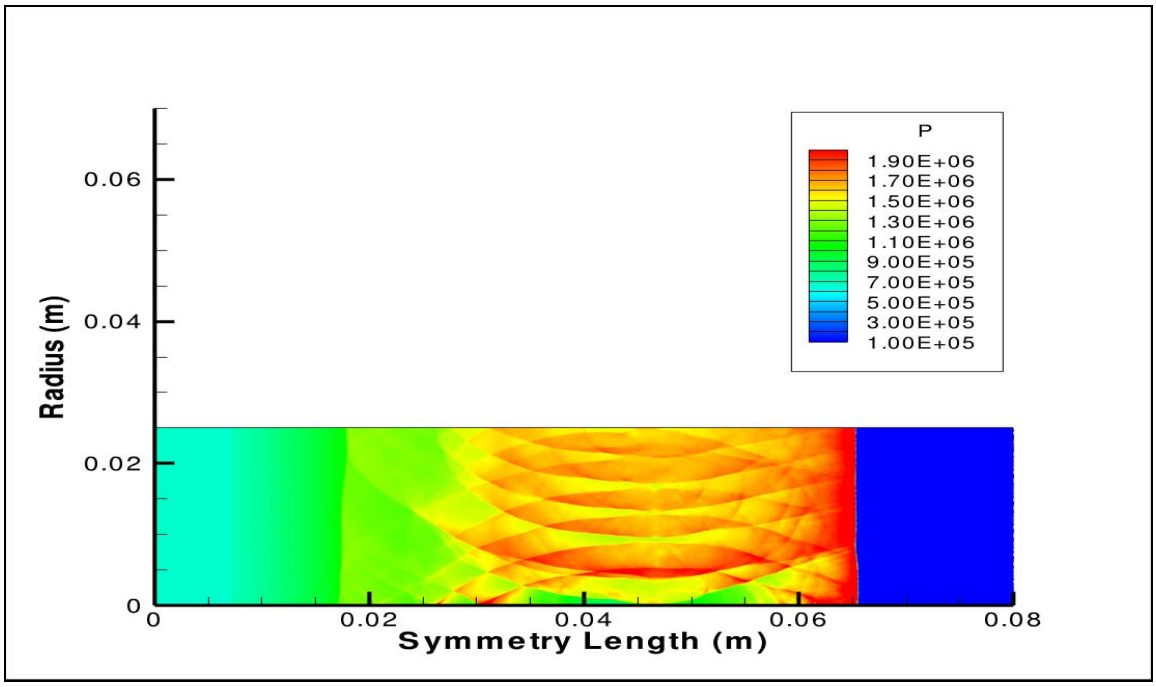

Figure 25. H_2 – Air pressure contour plot at 65 mm

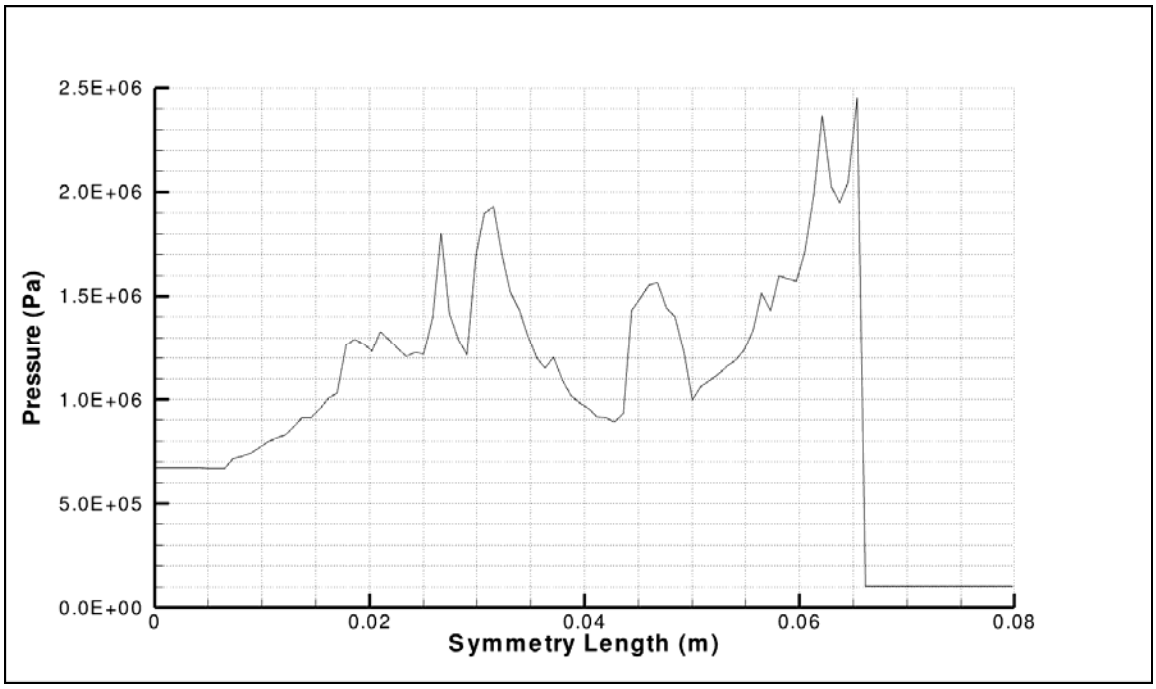

Figure 26. H_2 – Air pressure history plot at 65 mm

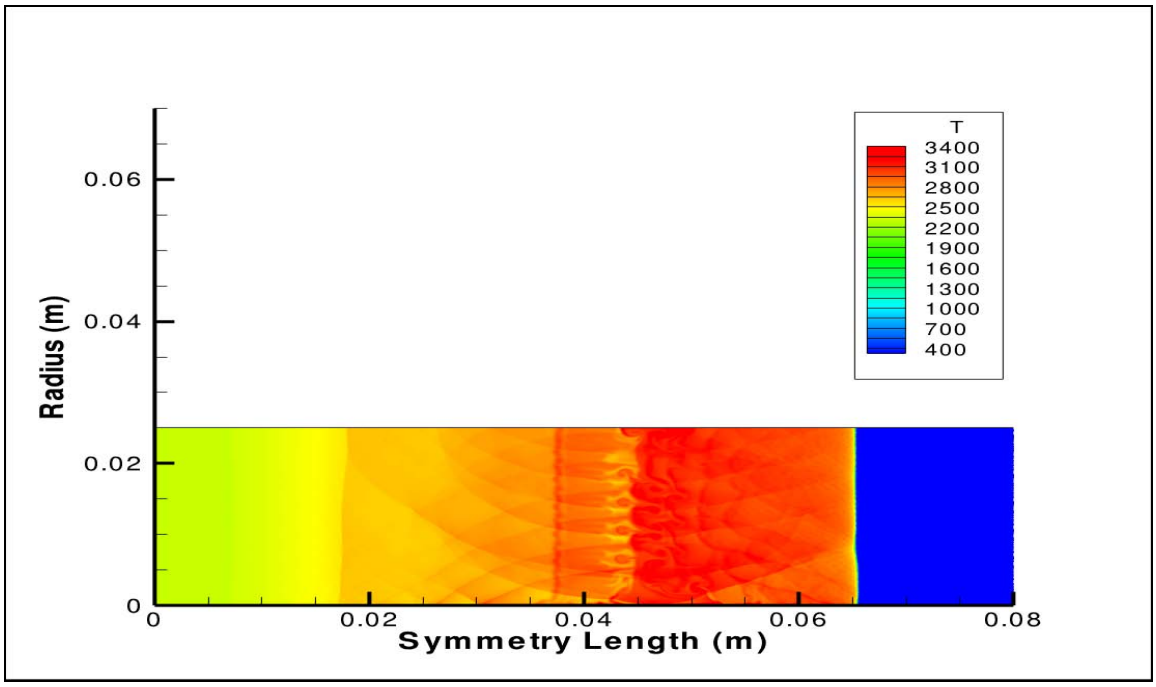

Figure 27. H_2 – Air temperature contour plot at 65 mm

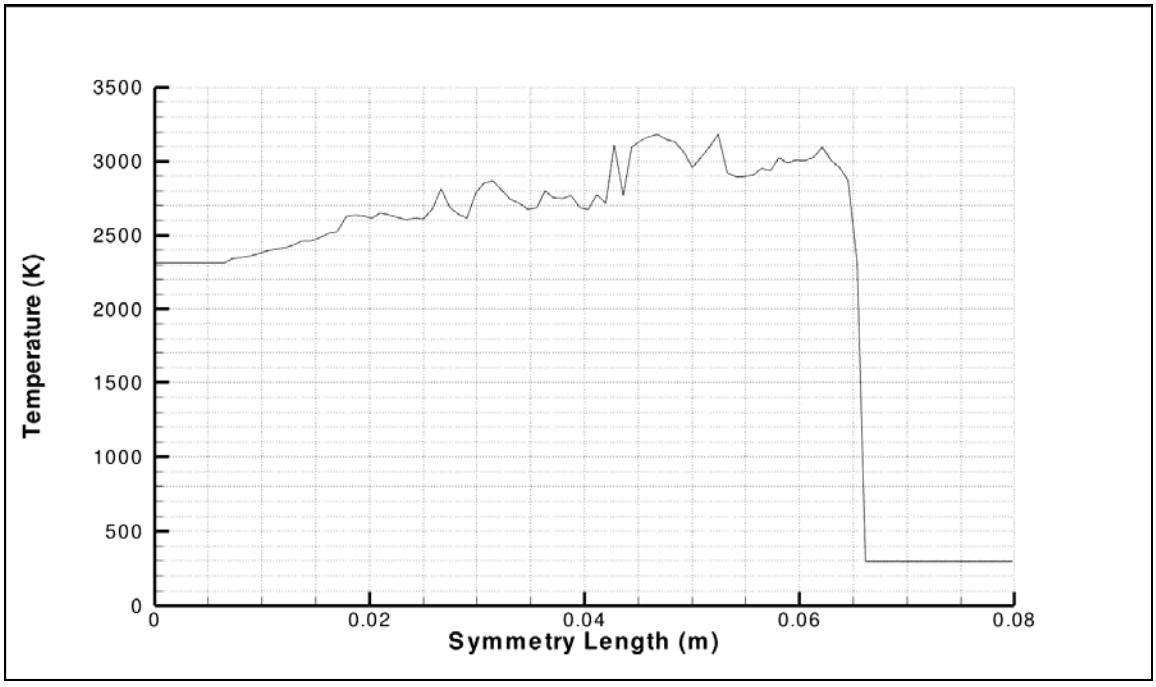

Figure 28. H_2 – Air temperature history plot at 65 mm

The detonation wave is sustained throughout by analyzing the contour and histories pertaining to conditions of pressure and temperature at the cylinder end. This is illustrated in Figures 29, 30, 31 and 32. The same detonation wave structure closely coupled to the shock front is observed with no change in the reaction zone length with a larger expansion zone. The lead shock front is propagating at a slightly lower pressure state of 2.3 MPa. As before, the pressure decreases before increasing back up to 2.4 MPa due to the interaction of the wave transients. The reaction zone conditions are approximately constant at 3000 K.

One interesting feature to take note is when the detonation wave structure is closely analyzed, as shown in Figure 33, the detonation cell width, which characterizes the triple point intersection of the mach stem, incident shock and reflected shock is approximately 8 mm, which was taken to be the largest cell size since the detonation cell width is irregular in nature. This coincides with experimental observations as predicted in Figure 15.

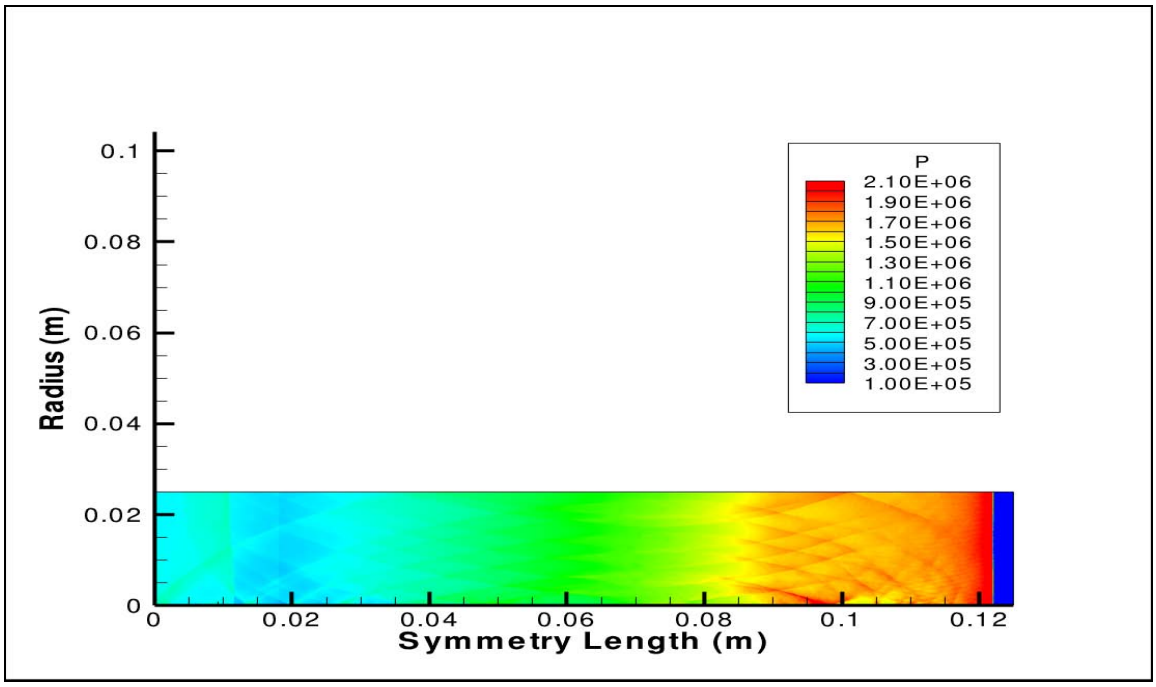

Figure 29. H_2 – Air pressure contour plot at 122 mm

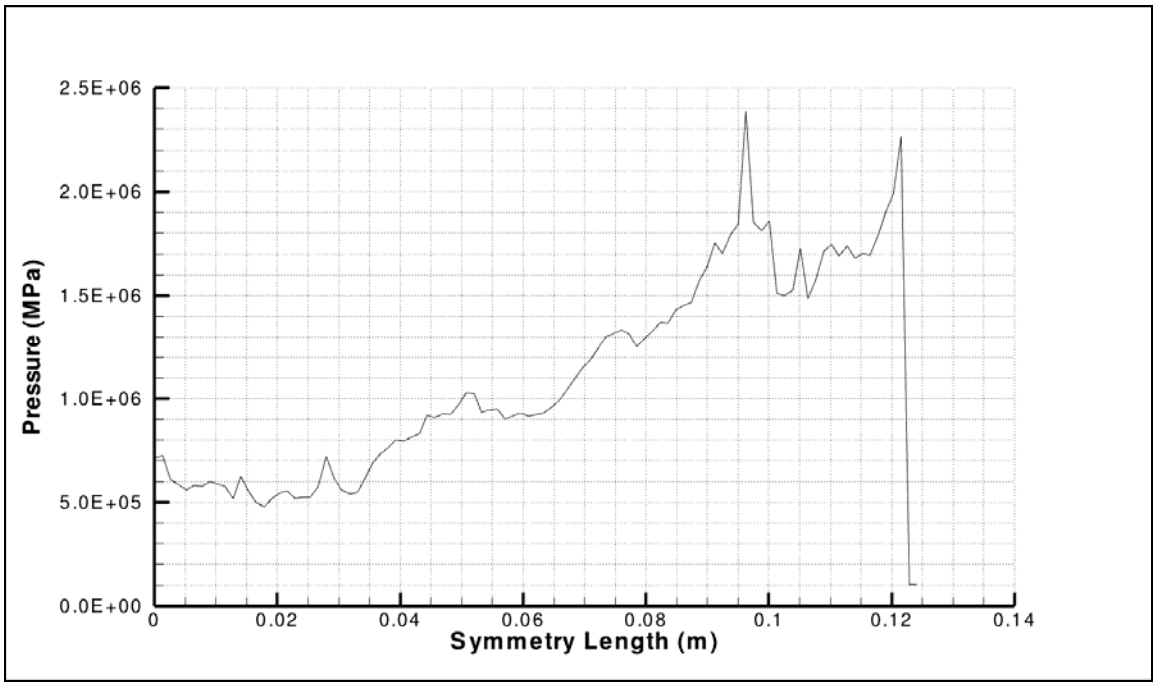

Figure 30. H_2–Air pressure history plot at 122 mm

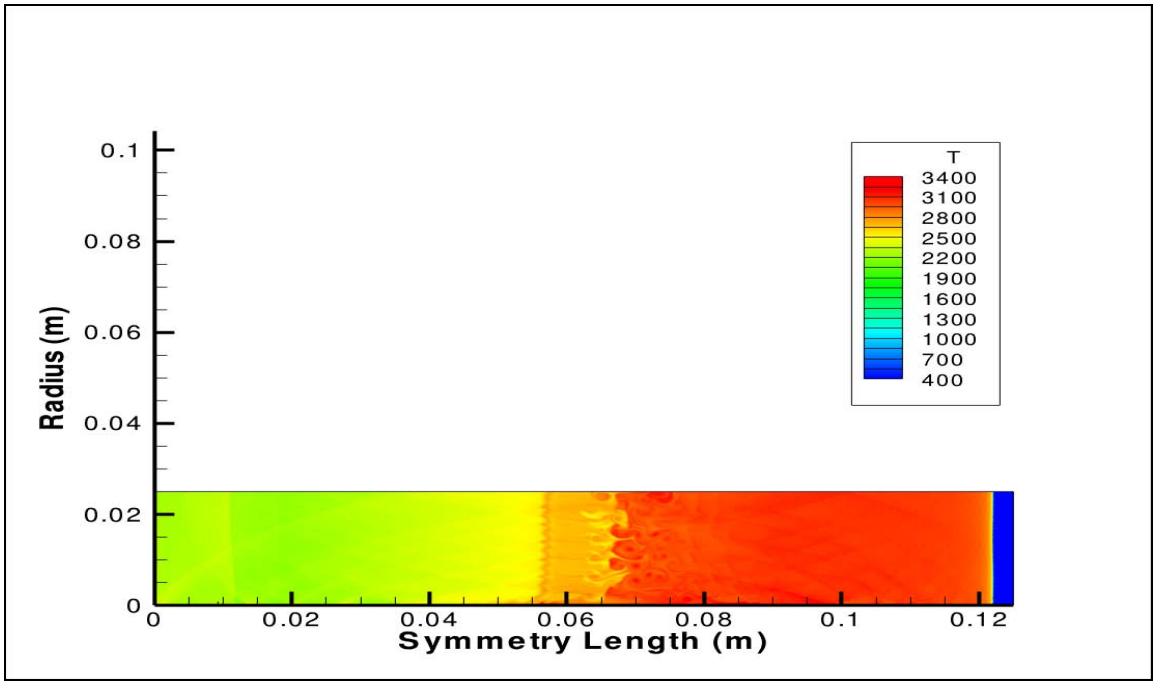

Figure 31. H_2 – Air temperature contour plot at 122 mm

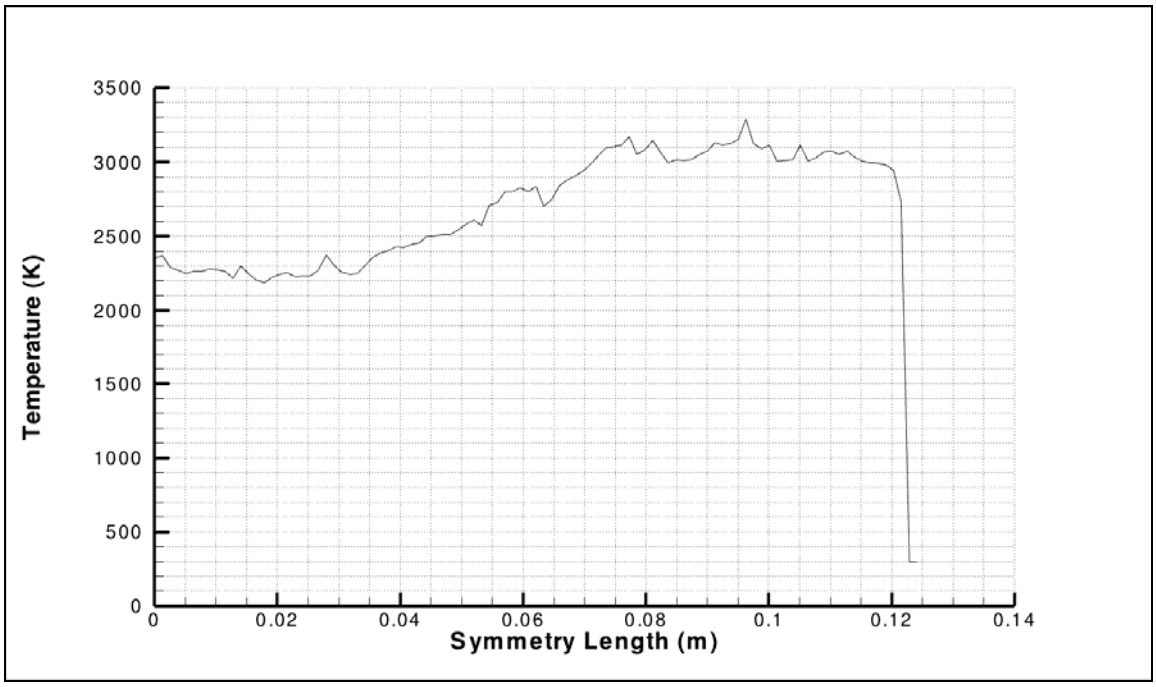

Figure 32. H_2 – Air temperature history plot at 122 mm

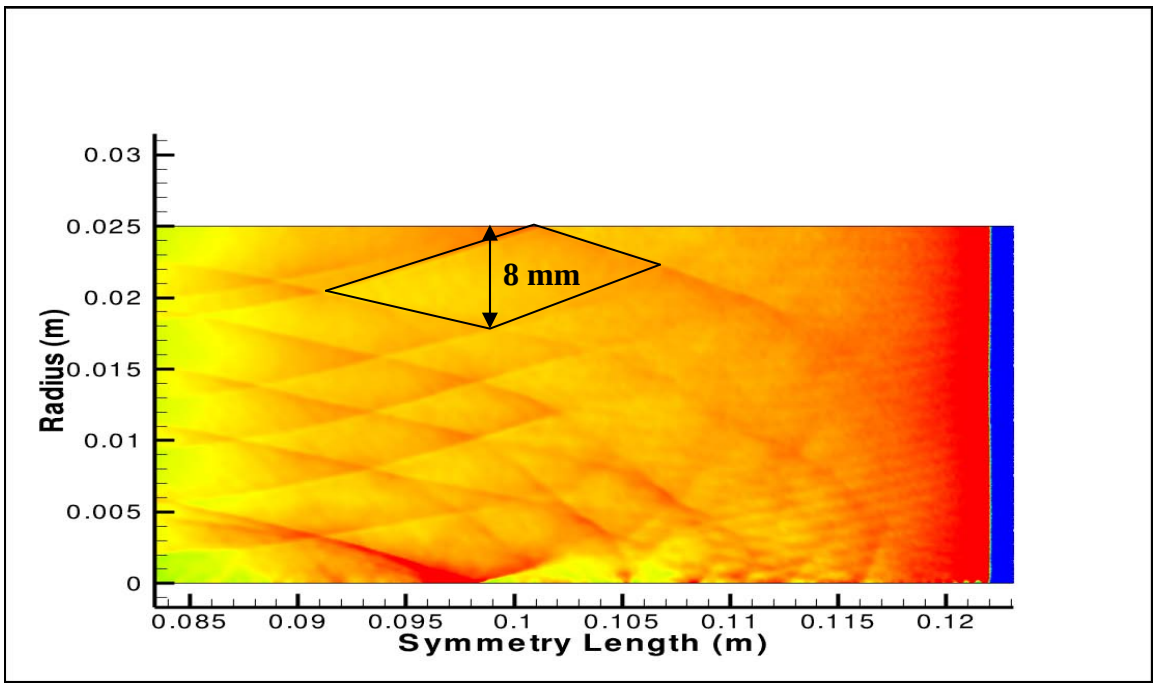

Figure 33. Close-up view of detonation wave structure

This concludes the grid sensitivity analysis and establishes that the cell size of 0.0625 mm (~ one-quarter induction length) is sufficient to capture the detonation wave physics in a PDE cylinder configuration. The same computational cell size will be used in subsequent simulations with a modified configuration for analysis of axi-symmetric toroidal implosions.

C. IMPLOSION ANALYSIS

Using the modified PDE configuration illustrated in Figure 18, a detonation wave was assumed to propagate at the inlet with stagnation pressure and temperature equal to 3.95 MPa and 2942 K with the detonation products obtained from NASA CEA. The reactant conditions were specified to be at an initial pressure of 1 atm and temperature of 298 K. This was similar to the conditions simulated for the grid sensitivity analysis. The cell size used was 0.0625 mm as determined previously, which was required to capture the complex flow field governing the shock physics. The same test case model for stoichiometric reaction of H_2-Air mixture assuming a chemical kinetic reaction setup of 18 reactions and 9 species listed in Table 2 was used for the implosion analysis.

In order to determine whether the propagating detonation wave can be sustained by the implosion process, the detonation velocity was evaluated along the mid-axis of the inlet (which would be the center of the implosion event) and along the symmetry axis of the shock tube configuration as shown in Figure 34. The resultant detonation velocity was compared against the C-J velocity to see if the wave can persist as a detonation wave. Therefore, the corresponding analysis are decoupled into two portions, the first pertaining to the mid-axis inlet (implosion) and the second pertaining to the symmetry axis.

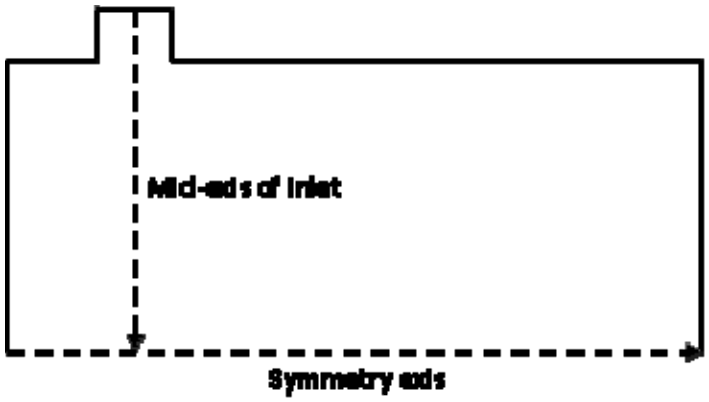

Figure 34. Evaluation of C-J wave speed for implosion study

1. Implosion Along the Mid-axis Inlet

Results of the normalized detonation wave velocity to C-J velocity versus run distance along the mid-axis of the inlet were plotted in Figure 35. From the graph, the detonation wave velocity decreases initially up to a run distance of 15 mm (~ 0.4 of the total radius) below C-J velocity as it travels along the radial direction towards the symmetry axis. This can be attributed to rarefaction effects as the detonation wave starts to expand from the inlet entrance. This can explicitly illustrated from the respective snapshot pressure and temperature contours in Figures 36 and 37 for the imploding wave at a run distance of 10 mm. From Figure 36, there is an expansion zone whereby the starting detonation wave decreases in pressure from specified inlet stagnation conditions along the inlet axis all the way to the reaction zone attached to the lead shock front that is propagating at the wave velocity. This reaction zone is a region of compression where the pressures start to build up fueled by the chemical reaction of the fuel-oxidizer mixture. Notice that this zone is localized only at the tip of the spherical wave front due to the nature of the toroidal imploding geometry and is a typical example of a shock focusing technique. There is a large high temperature region approximately equal to C-J temperature throughout the spherical shock wave except for the region immediately to the left and right of the inlet entrance whereby no communication exists between the flow field within the shock and reactant conditions. The observed high temperature region is supported by the heat release due to the reaction of the fuel-oxidizer mixture due to the

interaction of the multi-dimensional wave structure as the shock front implodes towards the symmetry axis. The pressures, temperatures as well as the kinetic chemical reaction rates are clearly driving the spherical wave front.

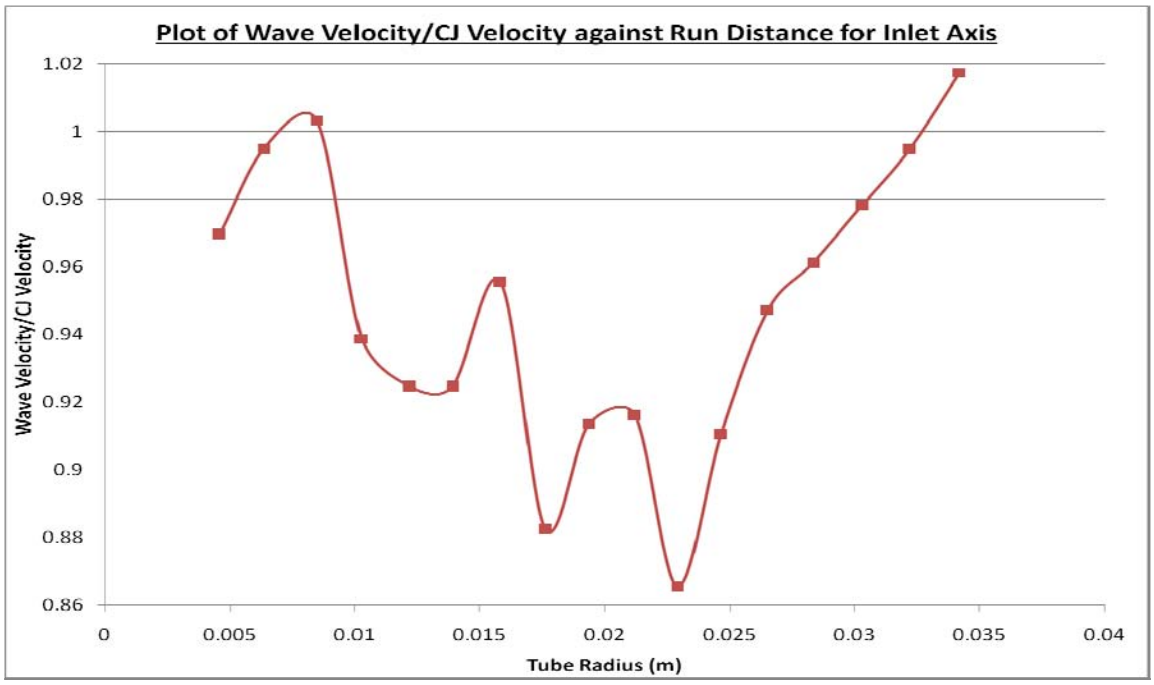

Figure 35. Plot of wave velocity/CJ velocity against tube radius along mid-axis of inlet

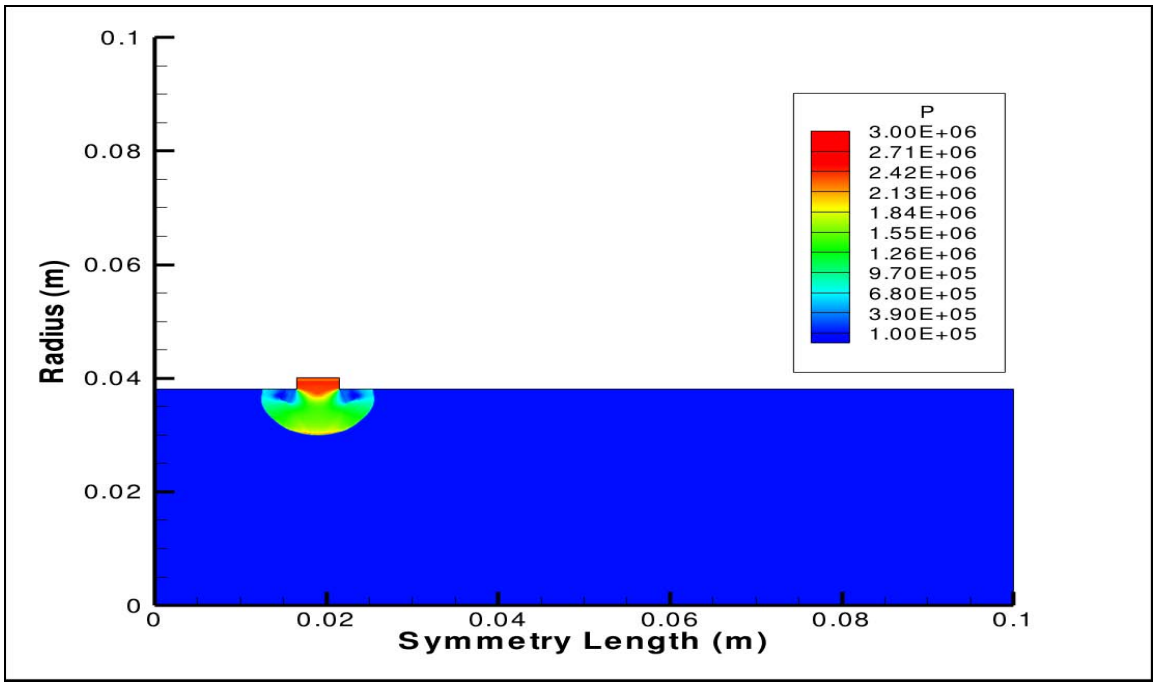

Figure 36. Pressure contour for imploding geometry at run distance of 10 mm along inlet axis

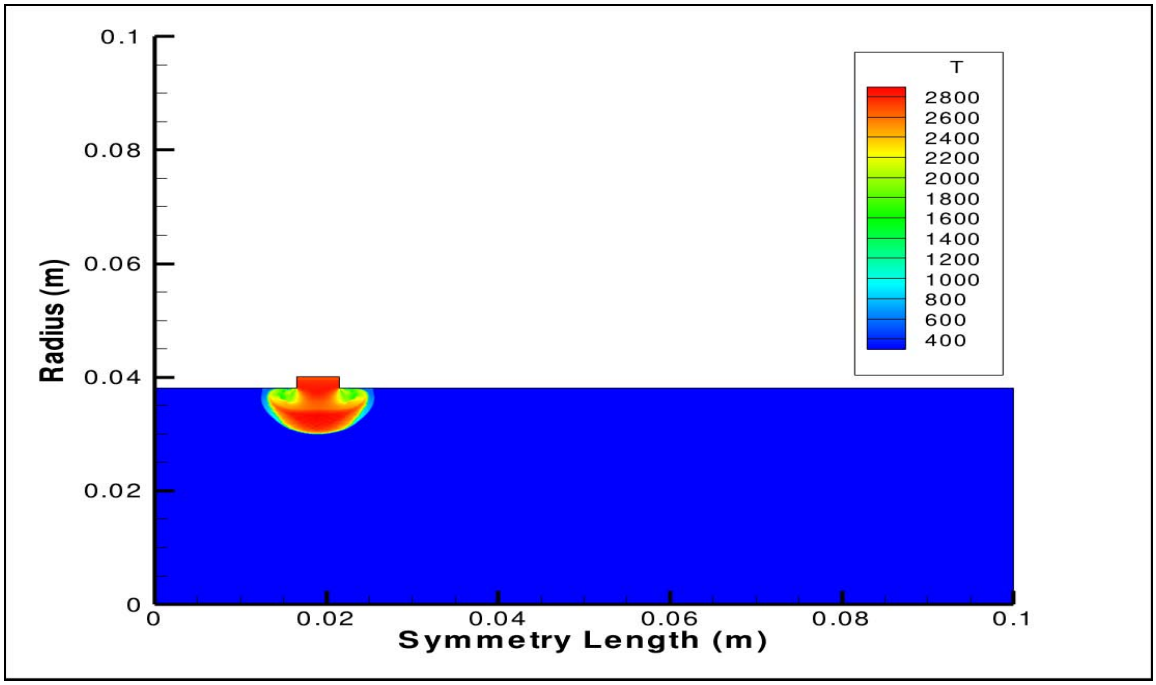

Figure 37. Temperature contour for imploding geometry at run distance of 10 mm along inlet axis

As the wave propagates beyond 15 mm towards the symmetry axis, the wave velocity starts to increase back upwards towards C-J velocity by virtue of the imploding geometry. This illustrates the fact that the detonation wave is continuously supported by the shock focusing process that can be determined from the C-J velocity. The pressure and temperature contours corresponding to a run distance of 20 mm are illustrated in Figures 38 and 39 respectively. The spherical wave front from the previous run distance of 10 mm has now transformed into little spherical wavelets coalescing into the leading edge of the detonation wave. This is due to little compression waves that are accelerated due to generation of heat release from the reaction of the fuel-oxidizer mixture. This heat release form high temperature regions that increases the sonic velocity of the gas products tries to catch up with the leading edge of the shock front. Also, extremely high localized pressure regions denoted by tiny red regions are also observed at the leading edge that is at least a factor of two greater than the C-J pressure. A look at the temperature contour reveals an interesting phenomenon, where transverse wave interactions are observed from these spherical wavelets at the protruding edge of the lead shock front extending for a distance of 10 mm along the mid-axis inlet as shown in the close-up view for the same temperature contour in Figure 40. There is also an extremely thin region separating the ambient temperature from the high temperature region – characteristic of a shock leading front. Further away from the mid-axis of the inlet on both sides, the thickness of this region increases, which indicates that the reactions are falling behind the shock front, and the detonation process is decaying due to expansion effects.

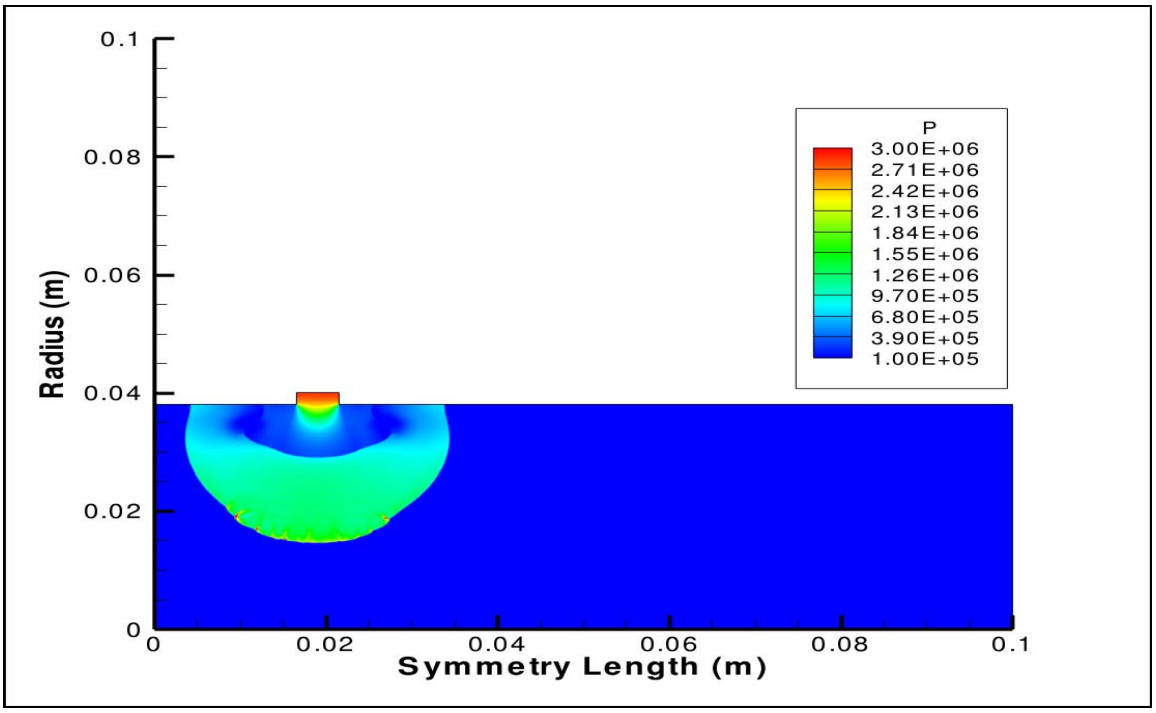

Figure 38. Pressure contour for imploding geometry at run distance of 20 mm along inlet axis

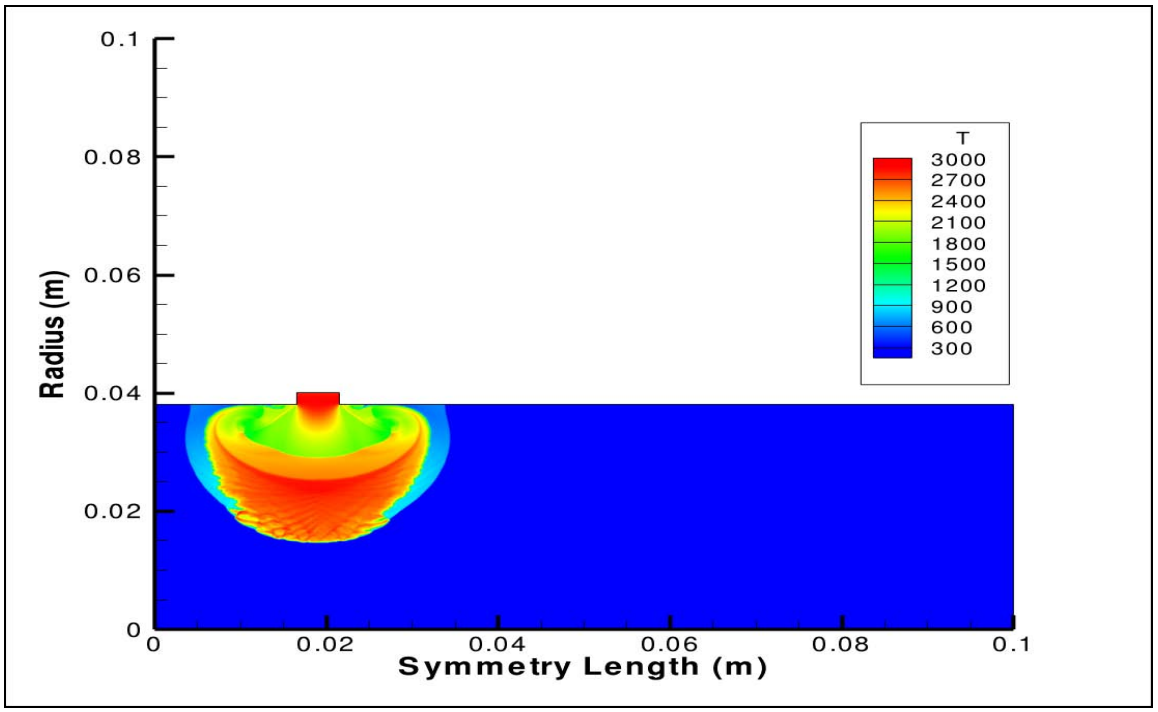

Figure 39. Temperature contour for imploding geometry at run distance of 20 mm along inlet axis

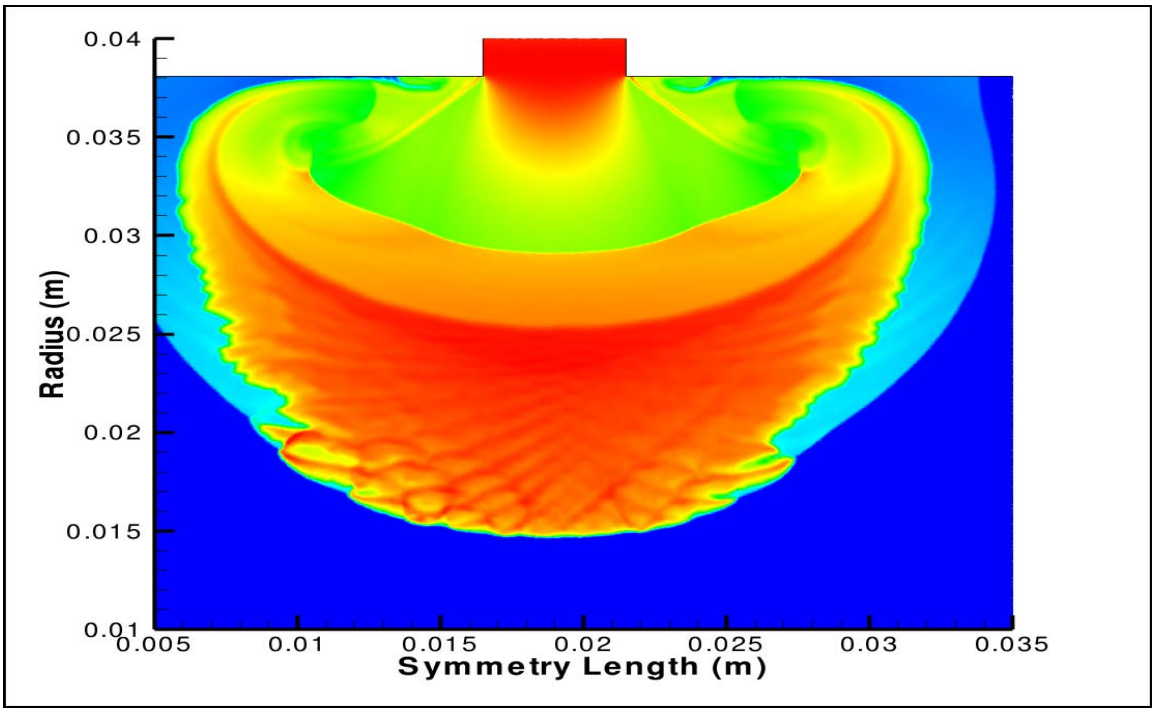

Figure 40. Close-up view of temperature contour

The pressure and temperature history plots along the mid-axis inlet are used to quantify the high pressures and temperatures driving the imploding wave as shown in Figures 41 and 42. The lead shock front is propagating at a pressure of 2.5 MPa, which essentially represents an overdriven detonation wave. Immediately behind the shock front, the pressure drops drastically to 1.2 MPa followed by a constant pressure region approximately 8 mm thick. As for the temperature at the leading edge, it increases slowly from 2500 K in an oscillating manner to almost 2900 K, which equals approximately to CJ temperature before spiraling downwards to 2000 K. This spiraling behavior is due to a huge expansion effect where the pressure decreases from the constant pressure region to ambient pressure conditions.

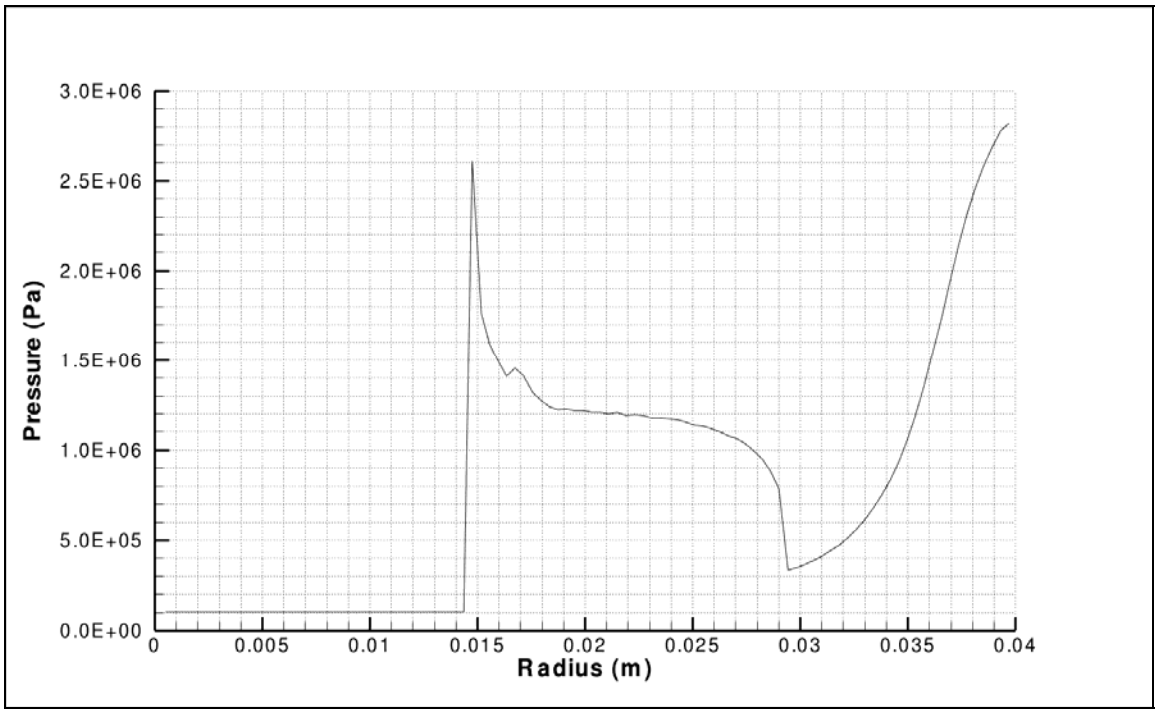

Figure 41. Pressure history of imploding wave at run distance of 20 mm along inlet axis

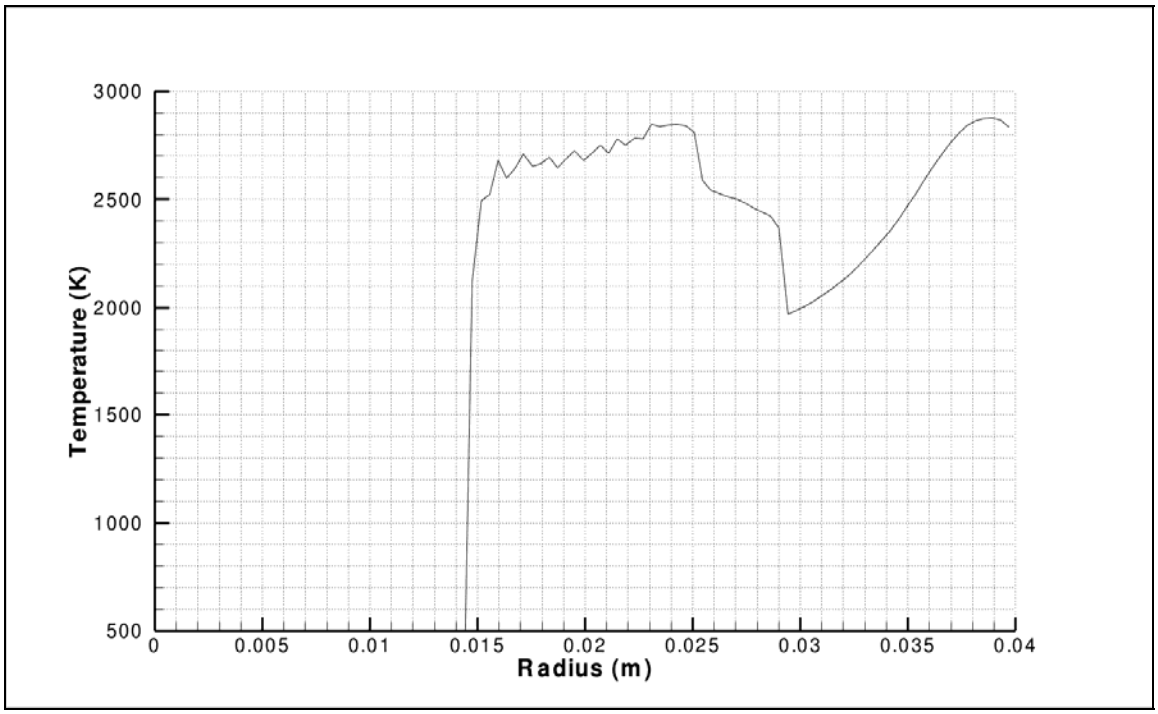

Figure 42. Temperature history of imploding wave at run distance of 20 mm along inlet axis

As the wave continues to implode towards the symmetry axis, the localized high pressure region attached to the shock front expand radially outwards with the wave at a run distance of 38 mm, which is almost the radius of the PDE tube configuration as shown in Figure 43. The pressure history in Figure 44 verifies the fact that the pressure continuously increases beyond the C-J pressure to 3.5 MPa and this further reinforces and builds up the detonation wave speed. Similarly, the expansion wave region thickness increases as the high pressure relieves itself to 0.9 MPa before a sharp decrease to ambient pressure conditions. This indicates that a second shock front is formed in front of a set of supersonic jets of products leaving the inlet region and entering the detonation tube. This phenomenon will be treated robustly in future endeavors.

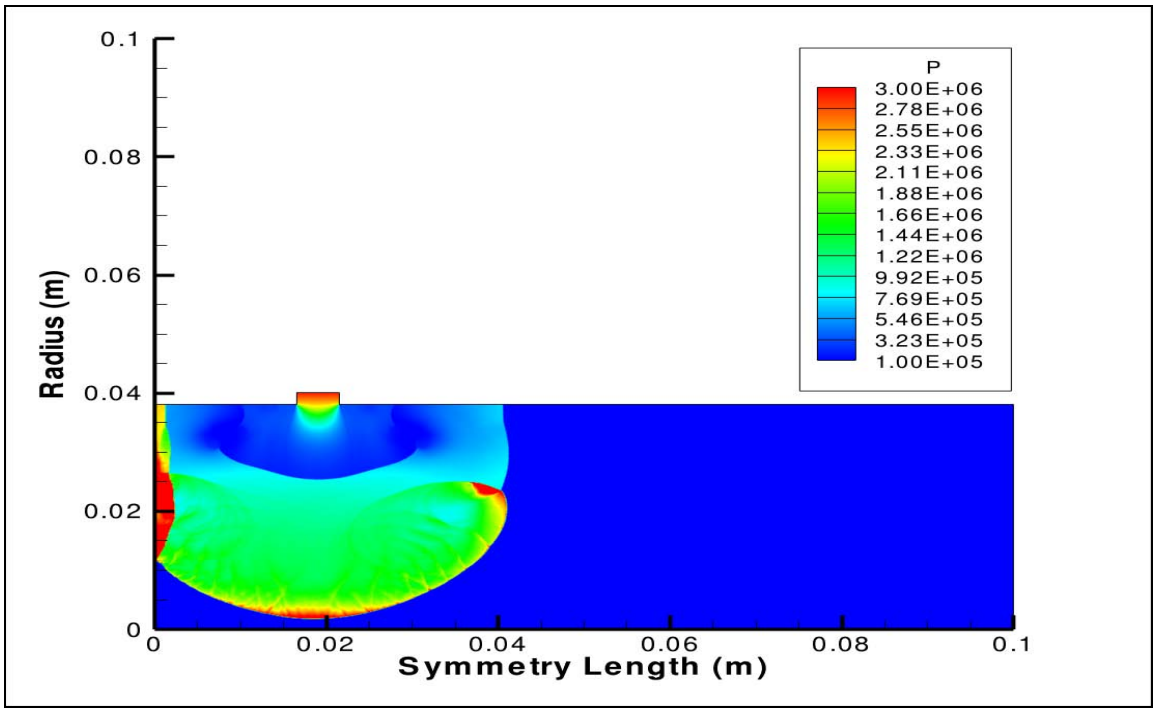

Figure 43. Pressure contour for imploding geometry at run distance of 38 mm along inlet axis

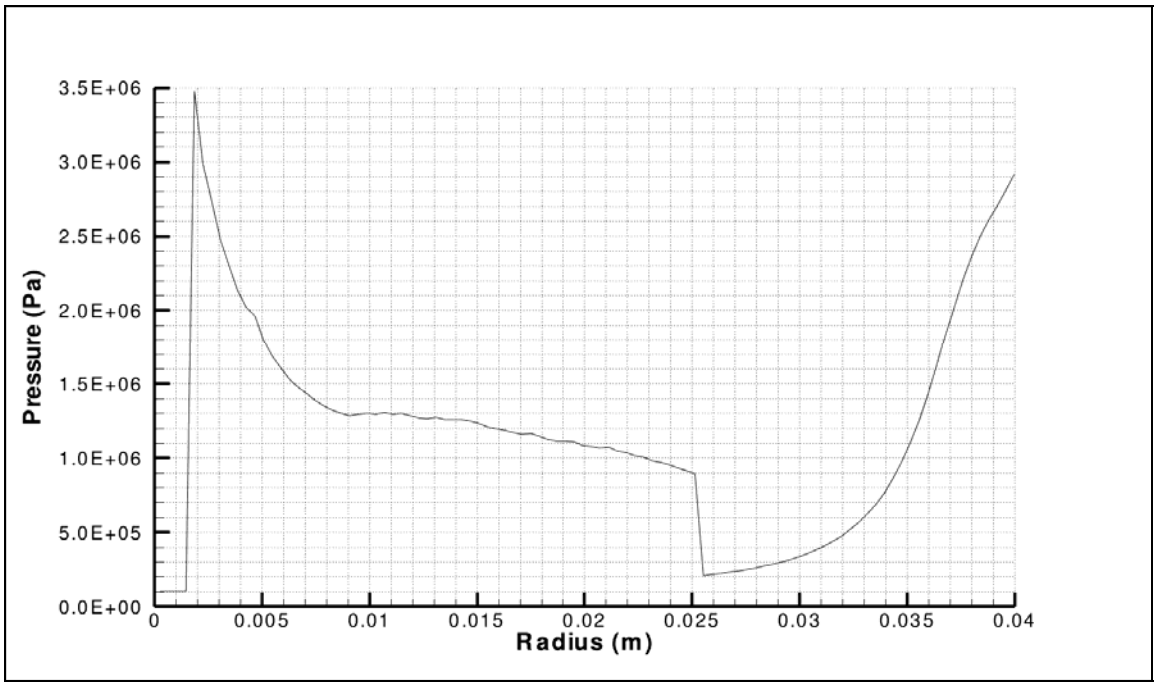

Figure 44. Pressure history of imploding wave at run distance of 38 mm along inlet axis

Similar to the observed pressures, there is a radial expansion of the high temperature region corresponding to approximately C-J temperature outwards from the inlet mid-axis as illustrated in the pressure contour of Figure 45. The temperature history plot shows an almost constant temperature region of 2900 K extending from the shock front to a thickness of 20 mm, which is almost half the radius of the PDE tube.

Analyzing the entire propagation of the toroidal wave front motion proves that even though the detonation wave initially loses its speed due to sudden expansion effects, the implosion process coupled with the reaction of the fuel-oxidizer mixture strengthens and increases the wave velocity as it propagates towards the symmetry axis. The pressure state just before the symmetry also shows that the initial wave builds up to an overdriven detonation shock wave propagating by a factor of 2.2 of the C-J pressure due to the implosion process.

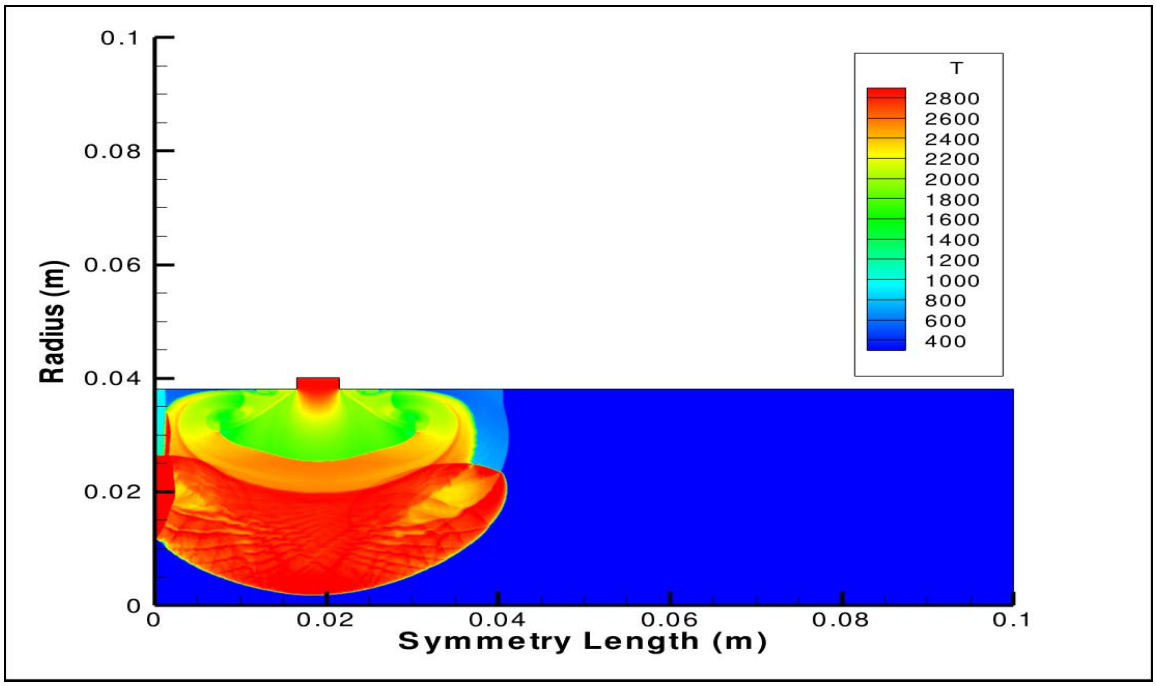

Figure 45. Temperature contour for imploding geometry at run distance of 38 mm along inlet axis

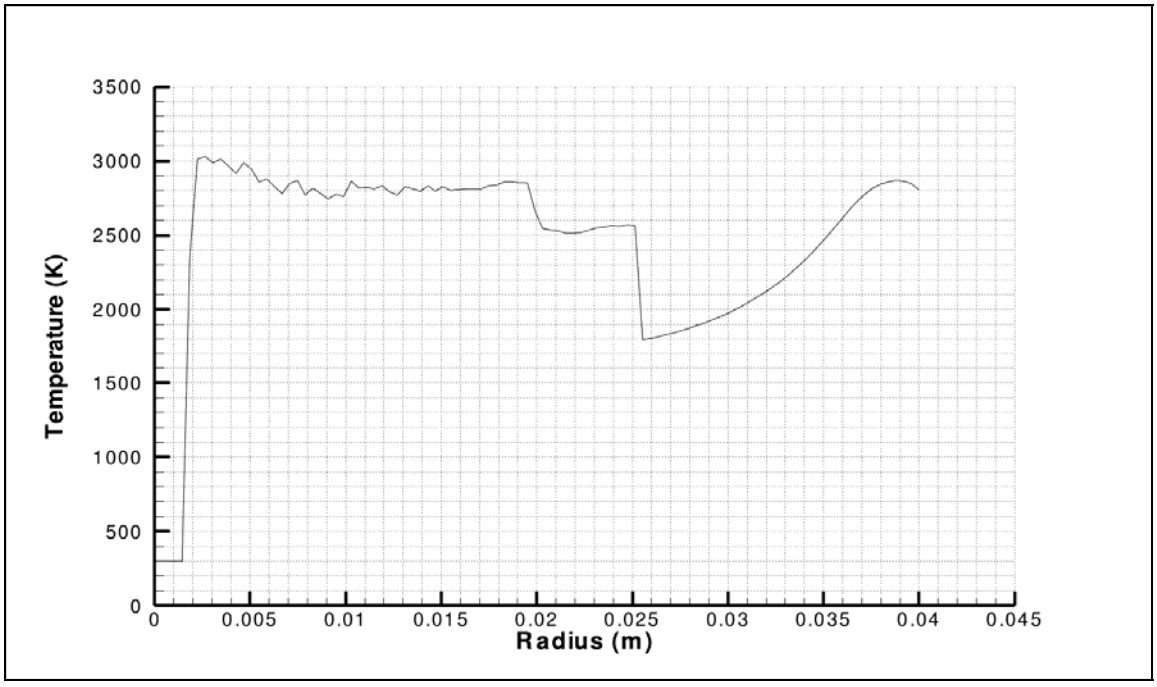

Figure 46. Temperature history for imploding geometry at run distance of 38 mm along inlet axis

2. Implosion Analysis Along Symmetry Axis

Looking at the passage of the shock front along the symmetry axis, it starts out at a highly overdriven state with a wave velocity propagating by a factor of 1.8 times the C-J velocity. This is a highly transient state that will eventually decay to the steady state C-J velocity as the wave propagates along the symmetry axis towards the end of the PDE configuration. This is shown in Figure 47. Note that the shock wave passage starts out at a run distance of 23 mm along the symmetry axis due to the implosion process at the mid-axis inlet. The first two run distance points are also discarded due to the implementation of the five point stencil finite difference method used to determine the wave velocity.

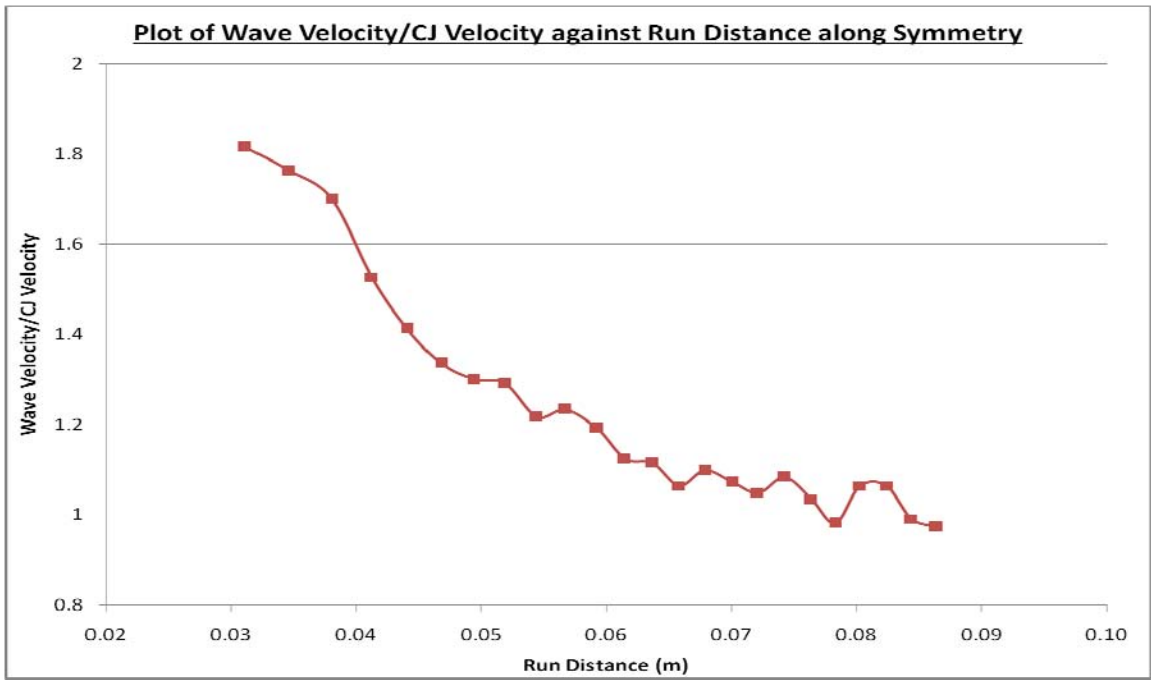

Figure 47. Plot of wave velocity/CJ velocity against run distance along symmetry axis

The snap shot pressure and temperature contours in Figures 48 and 49 denoting the point just after impact of the implosion process at a run distance of 23 mm along the

symmetry axis indicates extremely high localized pressure and temperature regions just aft of the shock front. The multi-dimensional effects of the wave interactions are explicitly observed in the temperature contour. The pressure and temperature history evaluated along the symmetry axis in Figures 50 and 51 allows for quantification of the pressure and temperature states arising from the collision of the two implosion shock waves. The localized pressure state along the symmetry axis increased to as high as 6.4 MPa with the corresponding temperature at 3700 K. In comparison to the characteristic CJ pressure, this is on the order of at least 4 times greater and the detonation wave is highly sustained by the implosion.

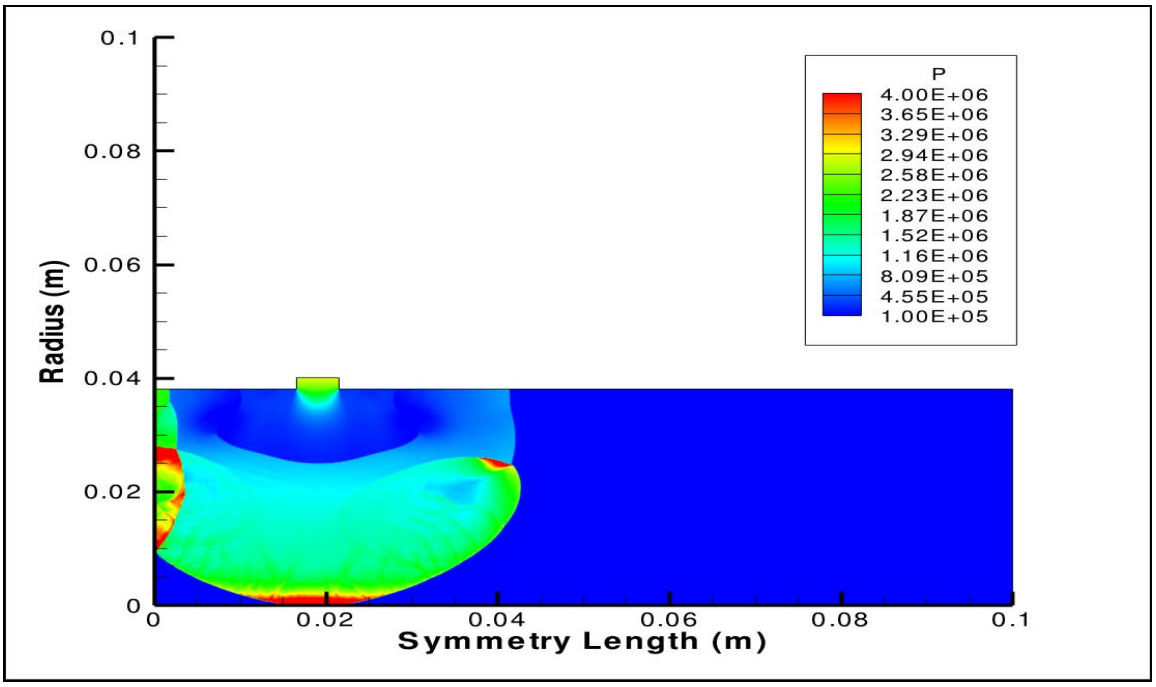

Figure 48. Pressure contour for imploding geometry at run distance of 23 mm along symmetry axis

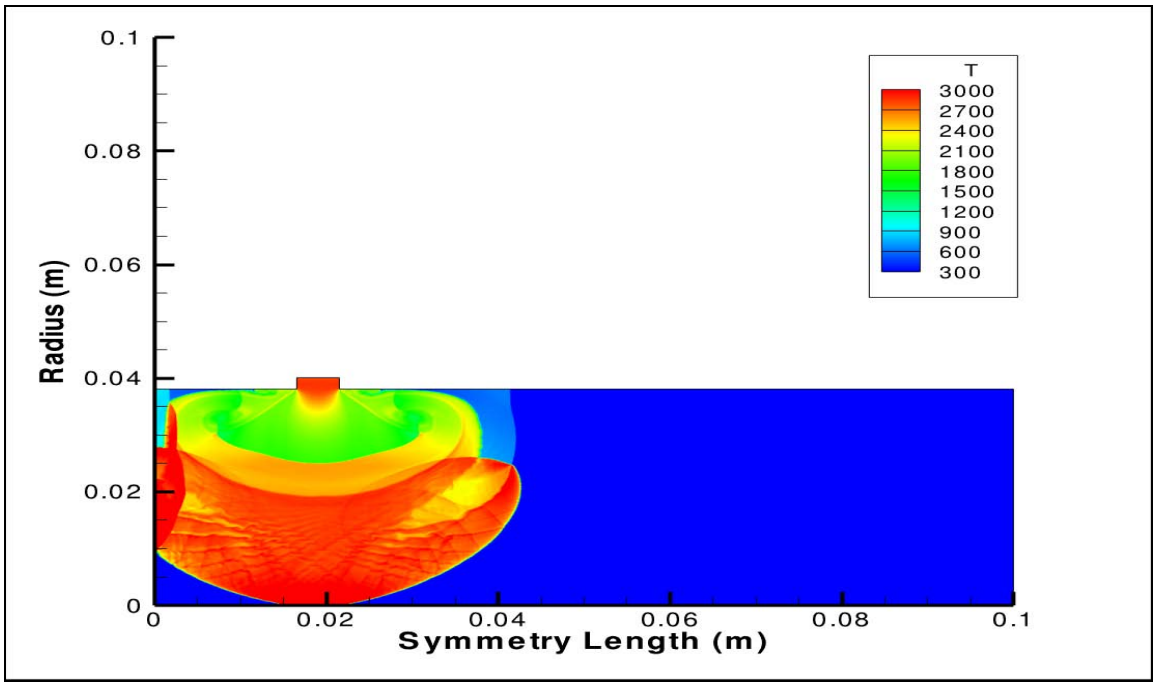

Figure 49. Temperature contour for imploding geometry at run distance of 23 mm along symmetry axis

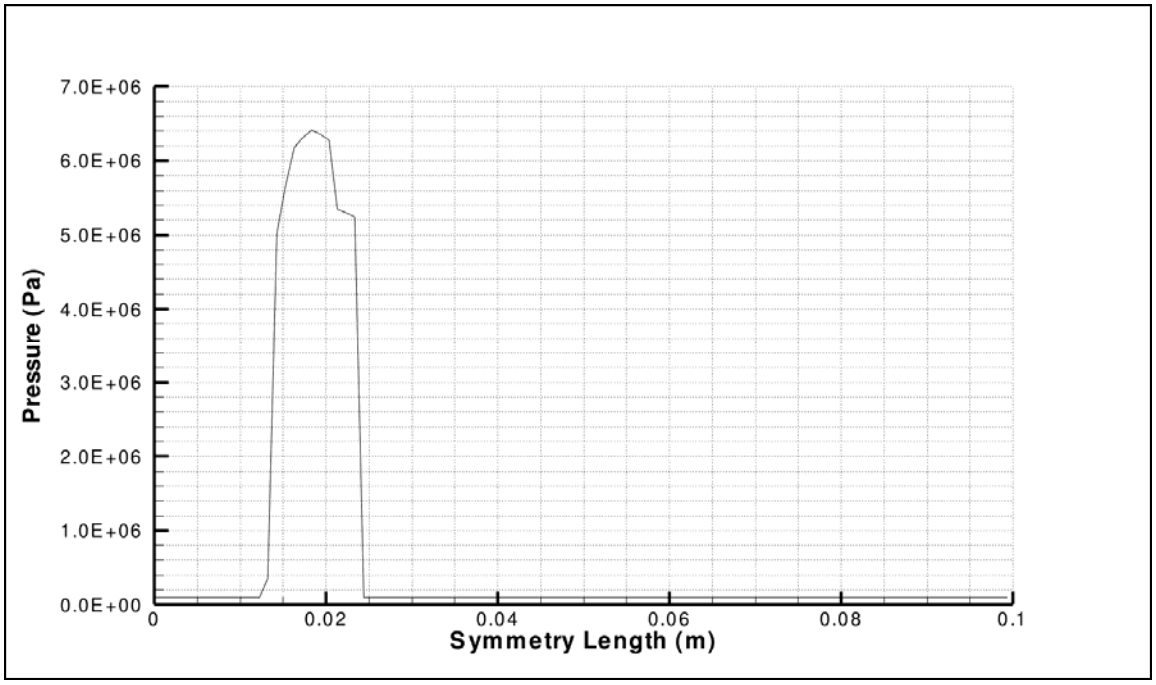

Figure 50. Pressure history of imploding wave at run distance of 23 mm along symmetry axis

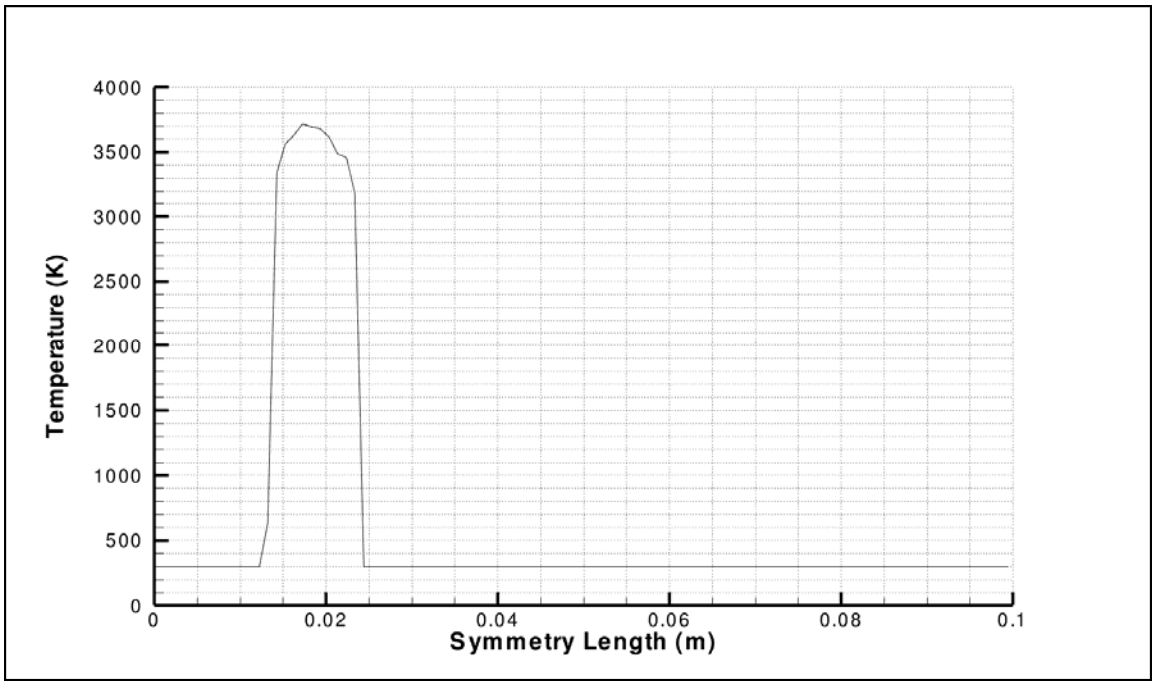

Figure 51. Temperature history of imploding wave at run distance of 23 mm along symmetry axis

As the detonation wave front propagates along the symmetry axis to a run distance of 50 mm as shown in the pressure and temperature contours of Figures 52 and 53, it catches up with the spherical wave front extending from the symmetry length to the wall of the tube configuration. The thin region behind the spherical wave is still clearly being driven by the reaction process as it stays attached to the shock front above C-J pressure and temperature while the region along the symmetry axis are propagating at extremely high overdriven pressures and temperatures fueled by the collision of the imploding shocks. The pressure and temperature history plots along the symmetry axis in Figures 54 and 55 verifies this with the lead shock front at a pressure and temperature state as high as 6.0 MPa and 4000 K respectively.

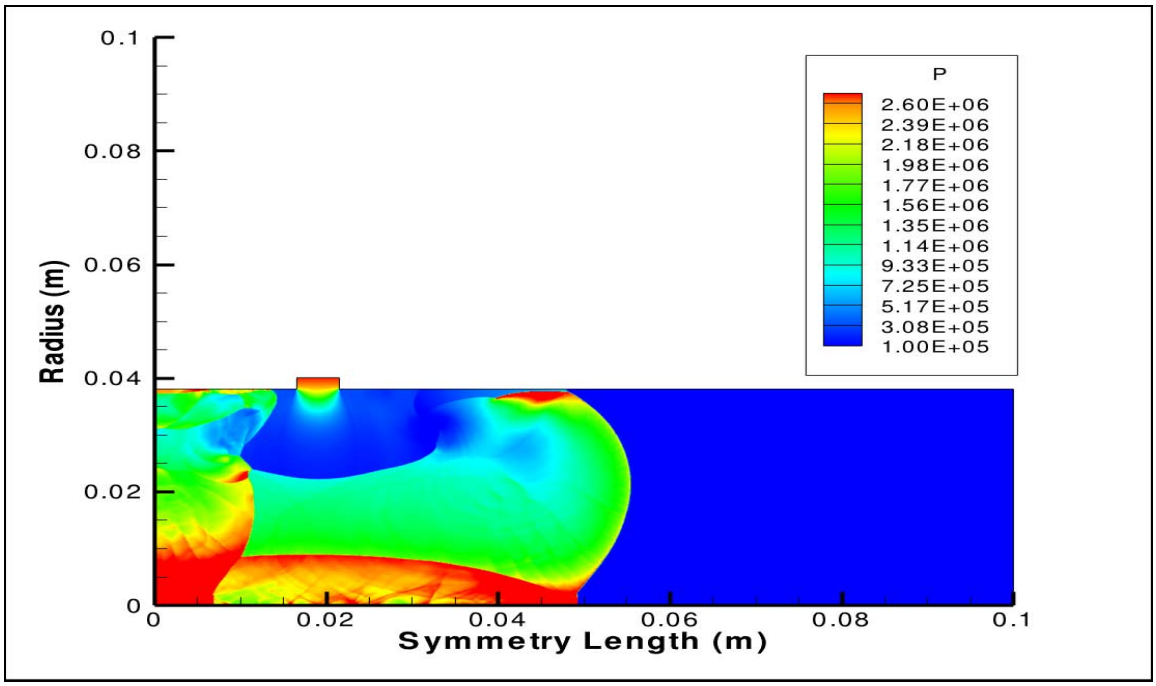

Figure 52. Pressure contour for imploding geometry at run distance of 50 mm along symmetry axis

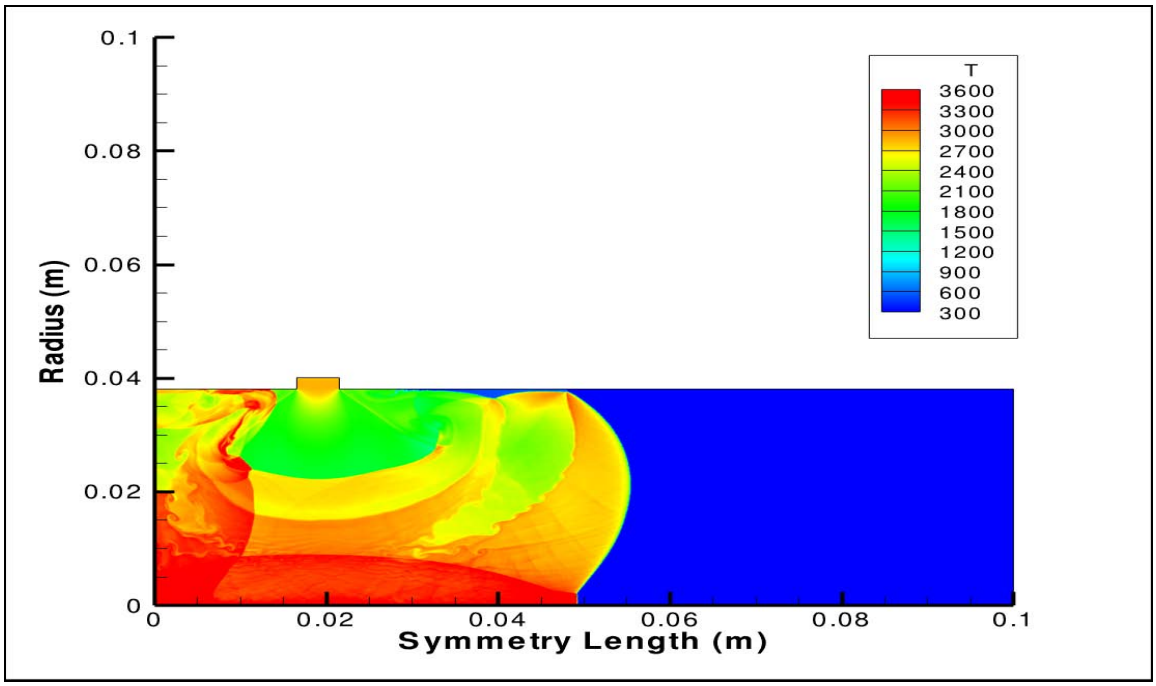

Figure 53. Temperature contour for imploding geometry at run distance of 50 mm along symmetry axis

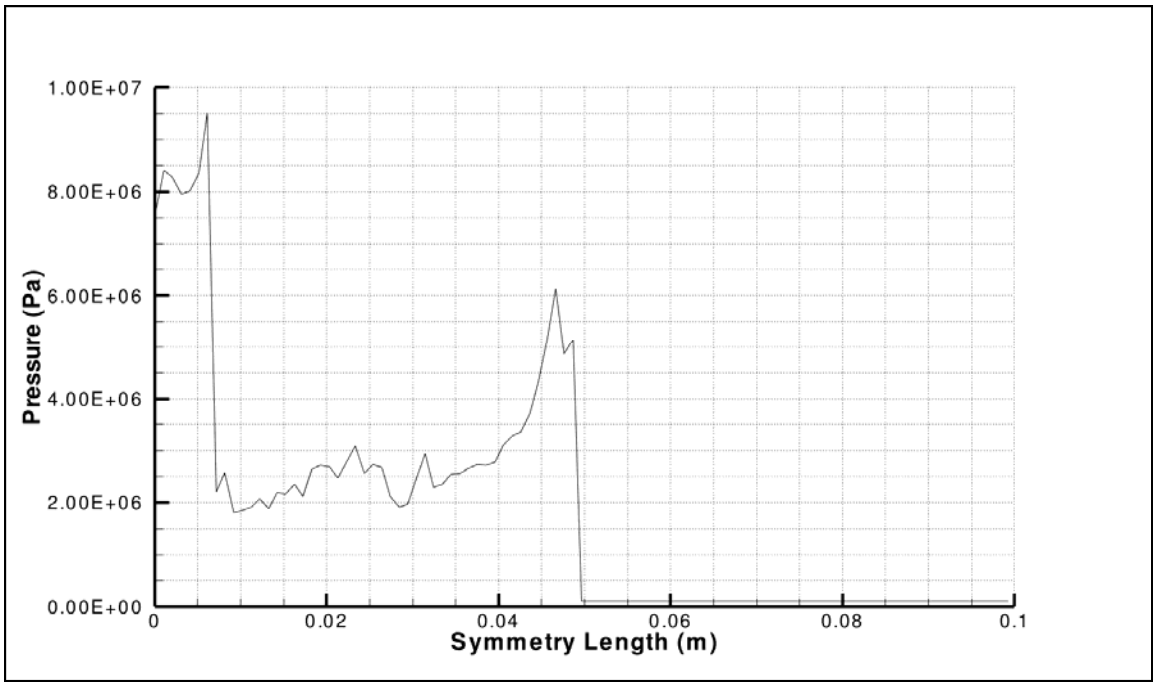

Figure 54. Pressure history of imploding wave at run distance of 50 mm along symmetry axis

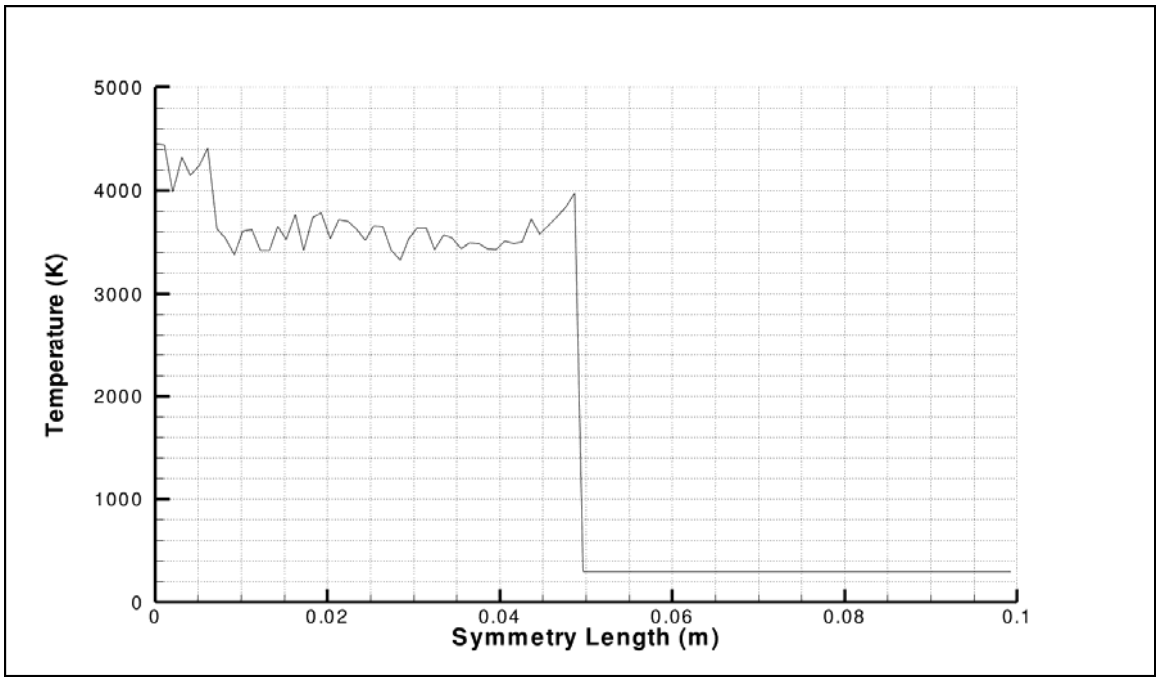

Figure 55. Temperature history of imploding wave at run distance of 50 mm along symmetry axis

At a run distance of 98 mm towards the end of the tube, the pressure and temperature contours of Figures 56 and 57 depicts the merging of the two separate waves into an almost planar wave front propagating at C-J velocity. The localized high pressure region stays highly attached to the shock front followed by an expansion region. A triple point discontinuity can be observed further upstream of the expansion region denoting the interaction of the longitudinal and transverse wave from the confined walls of the shock tube. The pressure and temperature states along the symmetry axis pertaining to the leading edge of the shock front are still at 2.0 MPa and 3000 K respectively from Figures 58 and 59 above C-J conditions, which highlight the fact that a detonation wave still persists and will continue to propagate along the length of the tube.

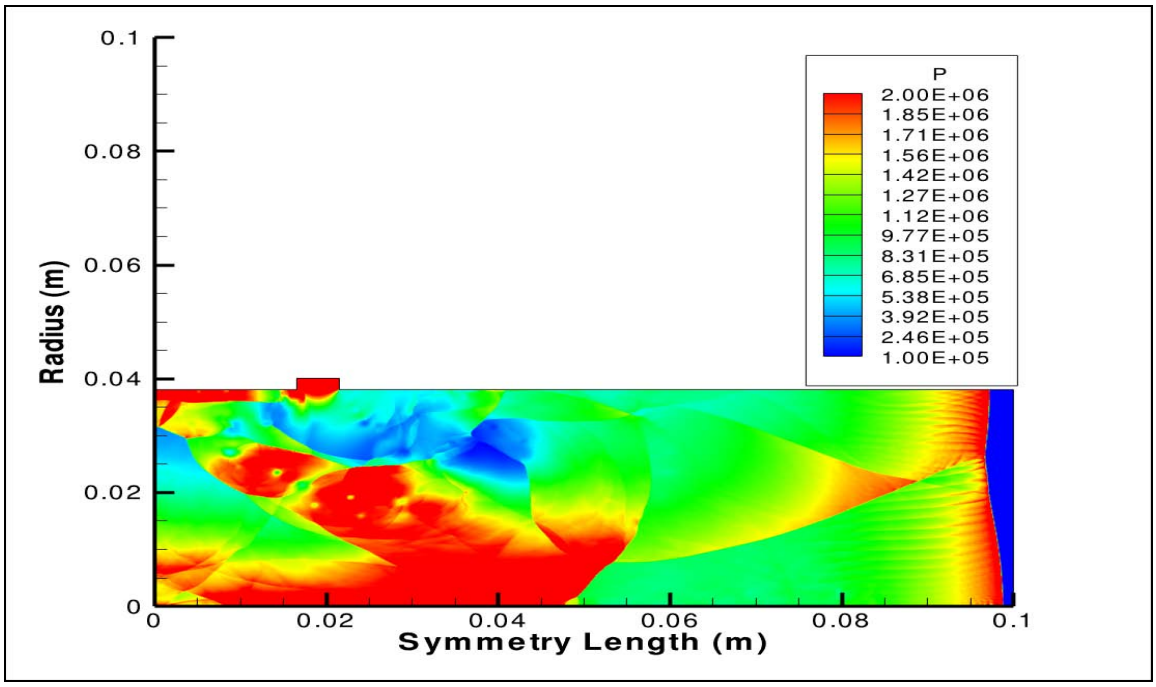

Figure 56. Pressure contour for imploding geometry at run distance of 98 mm along symmetry axis

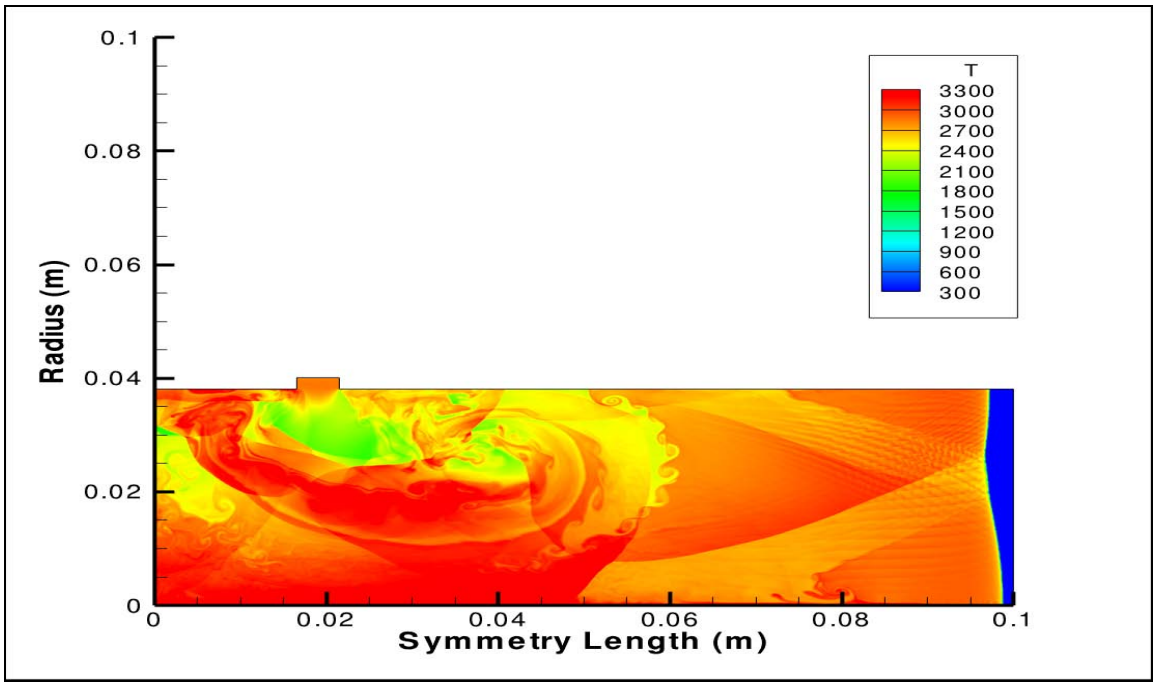

Figure 57. Temperature contour for imploding geometry at run distance of 98 mm along symmetry axis

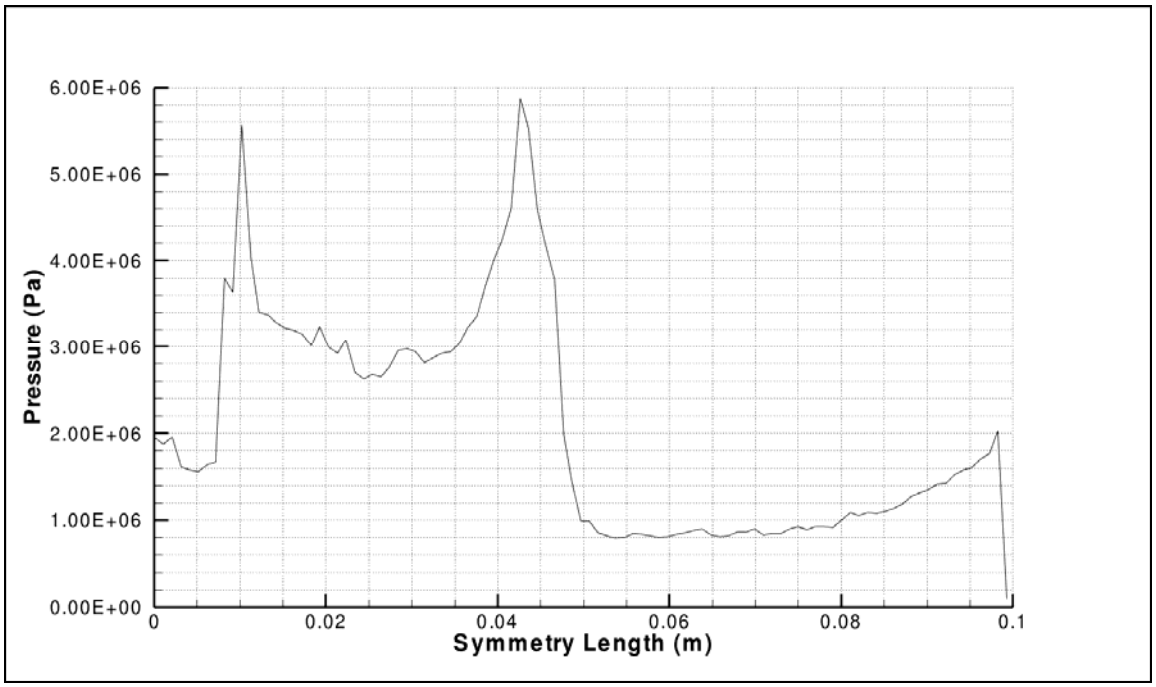

Figure 58. Pressure history of imploding wave at run distance of 98 mm along symmetry axis

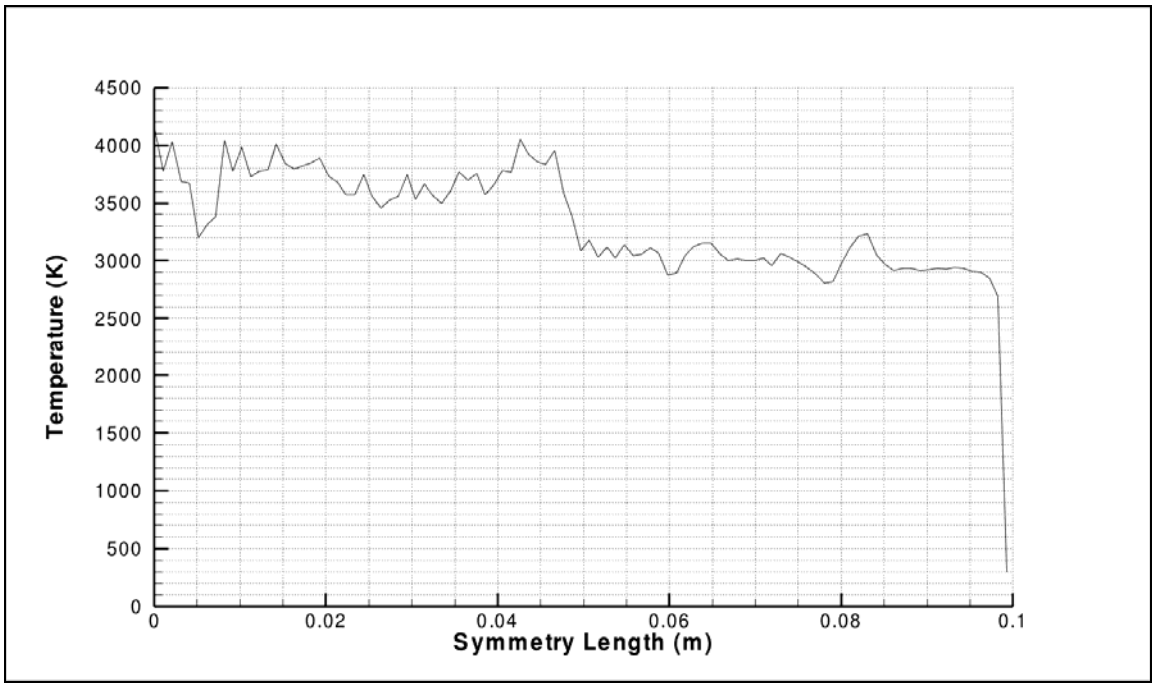

Figure 59. Temperature history of imploding wave at run distance of 98 mm along symmetry axis

Analysis of the implosion process along both the mid-axis of the inlet and symmetry axis points to the fact that a detonation shock wave persists almost throughout the entire geometry and is sustained both by the imploding wave front. This highlights the potential of introducing a toroidal implosion process for PDE type applications and allows for larger diameters to be factored into such configuration designs such that shorter tube lengths can be factored in without the need to account for DDT run distances. Subsequently, a parametric study will be conducted to evaluate exactly the extent of the diameter increase such that a detonation shock wave can be sustained for such designs.

D. PARAMETRIC STUDY

Parametric studies were performed on tube diameters of 114.3 mm and 133.35 mm respectively with the same inlet, reactant and boundary conditions specified for the toroidal implosion analysis. Note that the previous tube diameter of 76.2 mm from the implosion analysis was included as part of the parametric study. Current computational

resources could not support further exploration of tube diameters beyond 133.35 mm due to huge computational demands required and this could potentially take months to compute depending on the test case model. For the study, geometry of the shock tube as shown in Figure 18 remained the same with the exception of the diameter. The wave velocity was similarly evaluated along the mid-inlet and symmetry axis to determine if the detonation wave can be sustained.

1. Parametric Analysis Along Mid-inlet Axis

Figure 60 illustrates the detonation wave velocity as a function of the implosion shock tube radius for the different diameters specified along the mid-inlet axis.

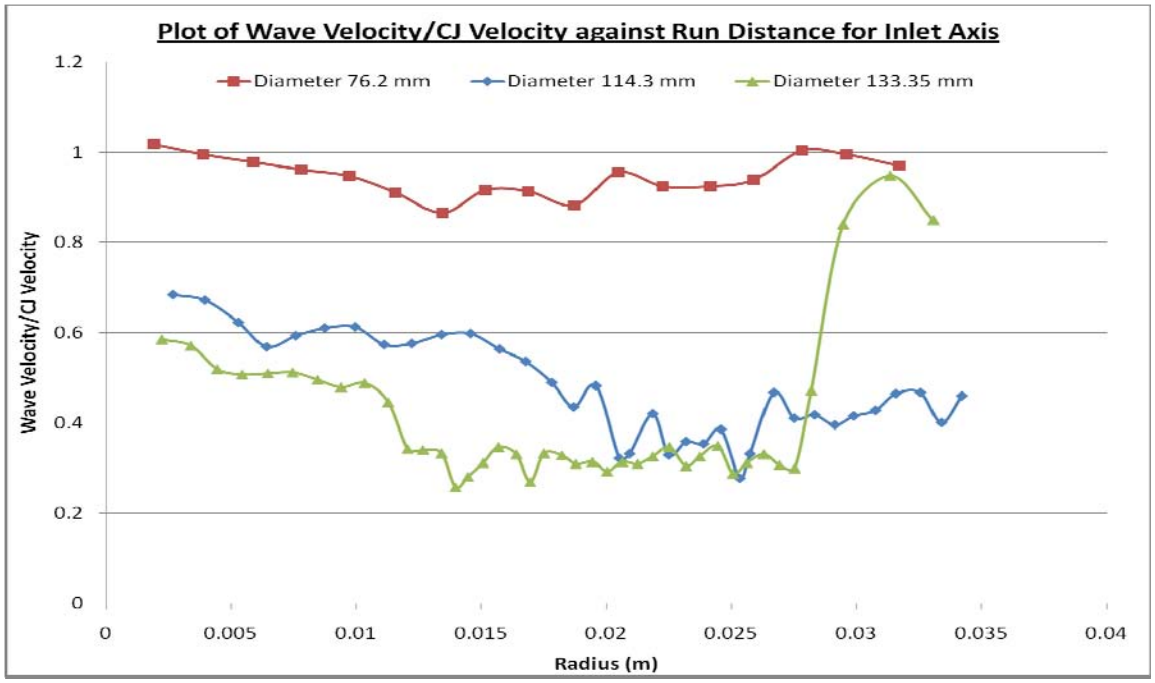

Figure 60. Plot of wave velocity/CJ Velocity against tube radius along inlet axis for different imploding shock tube diameters

As the tube diameter increases, the detonation wave velocity starts out lower as under-driven detonations due to decreased confinement effects. An analysis of the pressure and temperature contours for diameters of 114.3 mm and 133.35 mm as the

imploding wave propagates mid-way through the radius of the tube shows lower pressure and temperature states behind the lead shock front as compared to the diameter of 76.2 mm. Figures 61 and 62 illustrates the pressure and temperature contours for 114.3 mm. Figures 63 and 63 illustrates the pressure and temperature contours for 133.35 mm.

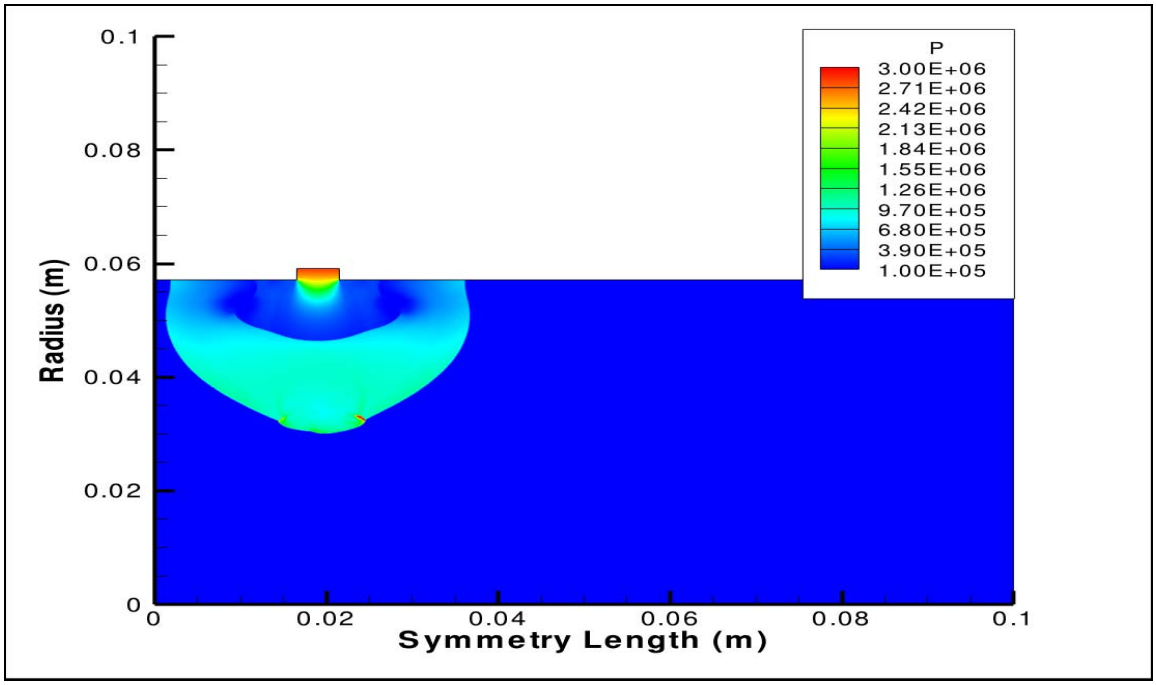

Figure 61. Pressure contour for imploding geometry at run distance of 28.75 mm for tube diameter of 114.30 mm along inlet axis

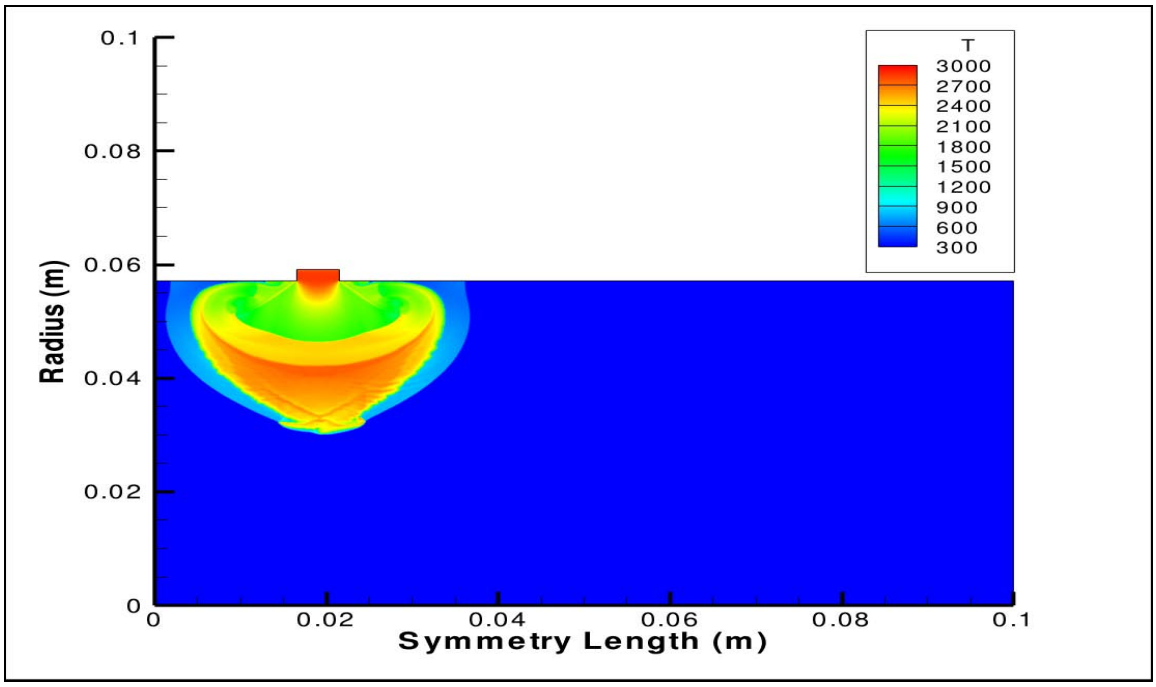

Figure 62. Temperature contour for imploding geometry at run distance of 28.75 mm for tube diameter of 114.30 mm along inlet axis

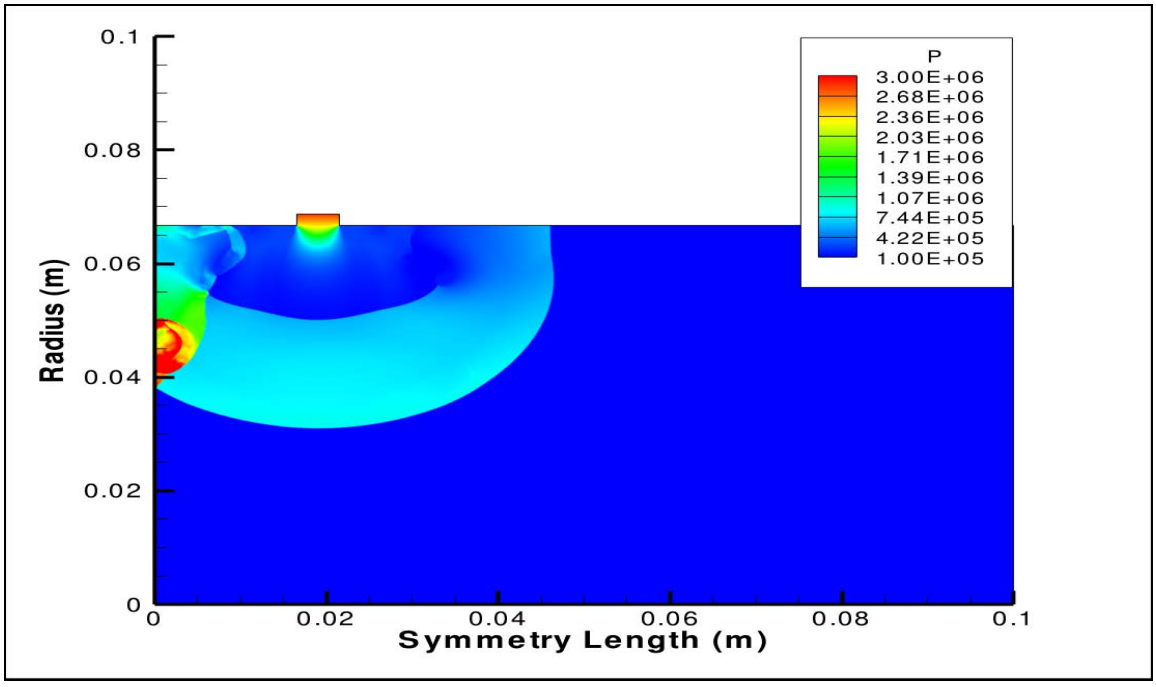

Figure 63. Pressure contour for imploding geometry at run distance of 33.34 mm for tube diameter of 133.35 mm along inlet axis

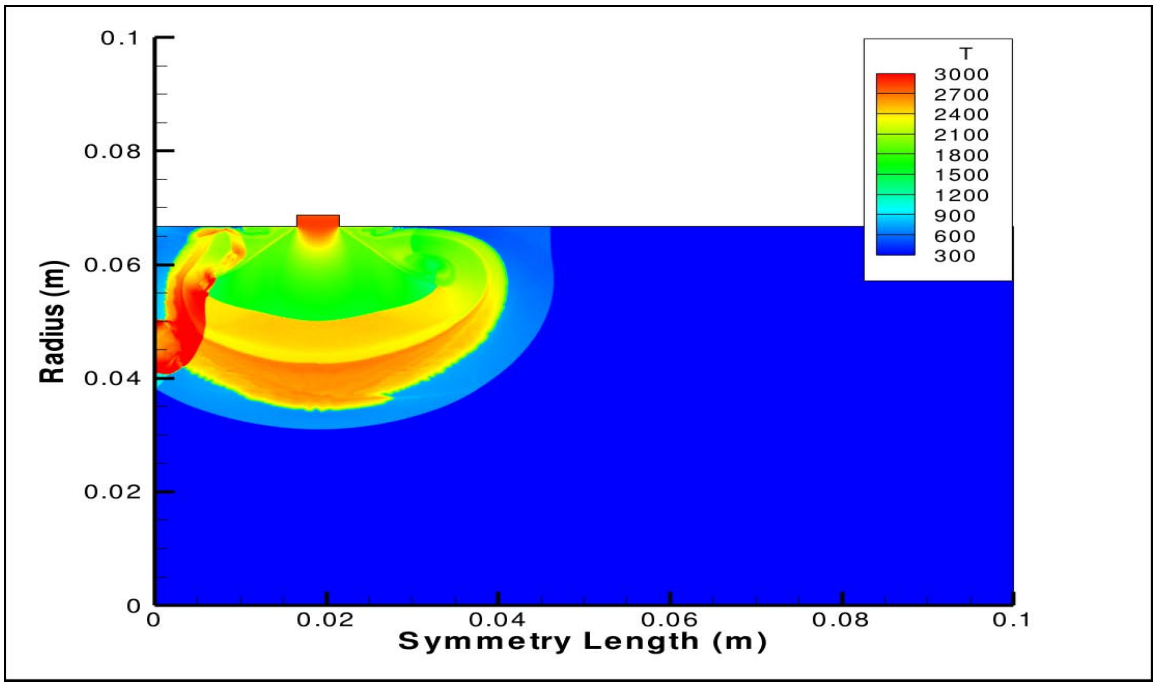

Figure 64. Temperature contour for imploding geometry at run distance of 33.34 mm for tube diameter of 133.35 mm along inlet axis

For the tube diameter pertaining to 114.30 mm, the phenomena corresponding to the coalescence of tiny spherical wavelets representing localized high pressure regions at the leading edge of the toroidal wave front could be observed similar to the implosion analysis. However the pressure states in these localized regions were lower in comparison due to geometrical differences in diameter. Similarly in comparison to the temperature contour for the implosion analysis, there is a thin separation region between the reactant conditions and the high temperature region at the toroidal front with an increasing thickness further away on both sides of the mid-axis inlet indicating a decaying detonation process due to expansion effects. These effects are however greater as compared to the test case model for 76.2 mm used for the implosion analysis and this again is a function of the diameter increase. This would account for the lower detonation velocities observed as the tube diameter is increased from 76.2 mm to 114.30 mm.

For the case study of 133.35 mm, the pressure contour indicates a weak decaying wave propagating mid-way towards the symmetry axis. The pressure region behind the decaying shock front is almost at a uniformly low pressure with a magnitude of

approximately half of CJ pressure. However due to the geometry of the imploding tube, a second reflection wave from the head end of the tube can be observed interacting in a direction perpendicular to the weak wave propagation along the mid-inlet axis. This reflection wave represents a strong detonation wave with localized pressure regions just behind the toroidal wave front starting from the head end exceeding two times of C-J pressure. Likewise, as for the temperature contour, there exists a thick uniform region of separation between the reactant temperature and high temperature region along the toroidal wave front with an interacting reflection wave from the shock tube head end. The weaker pressure and temperature states behind the decaying shock front account for even lower detonation velocities as compared to the tube diameter corresponding to 114.30 mm.

As the wave implodes towards the symmetry axis, the process fueling the lead shock front is not supported and continues to weaken and decay due to expansion effects with the exception of the test case pertaining to 133.35 mm. The second reflected wave from the head end along the symmetry axis reaches interacts with the transverse wave propagation along the mid-inlet axis, which reinforces the lead shock front and results in a sharp increase in detonation velocity towards 0.8 of C-J velocity as shown in Figure 60. The respective pressure and temperature contours in Figures 65 to 66 and 67 to 68 corresponding to the test case of 114.30 mm and 133.35 mm illustrate the observed wave propagation behavior as the shock front implodes towards the symmetry axis.

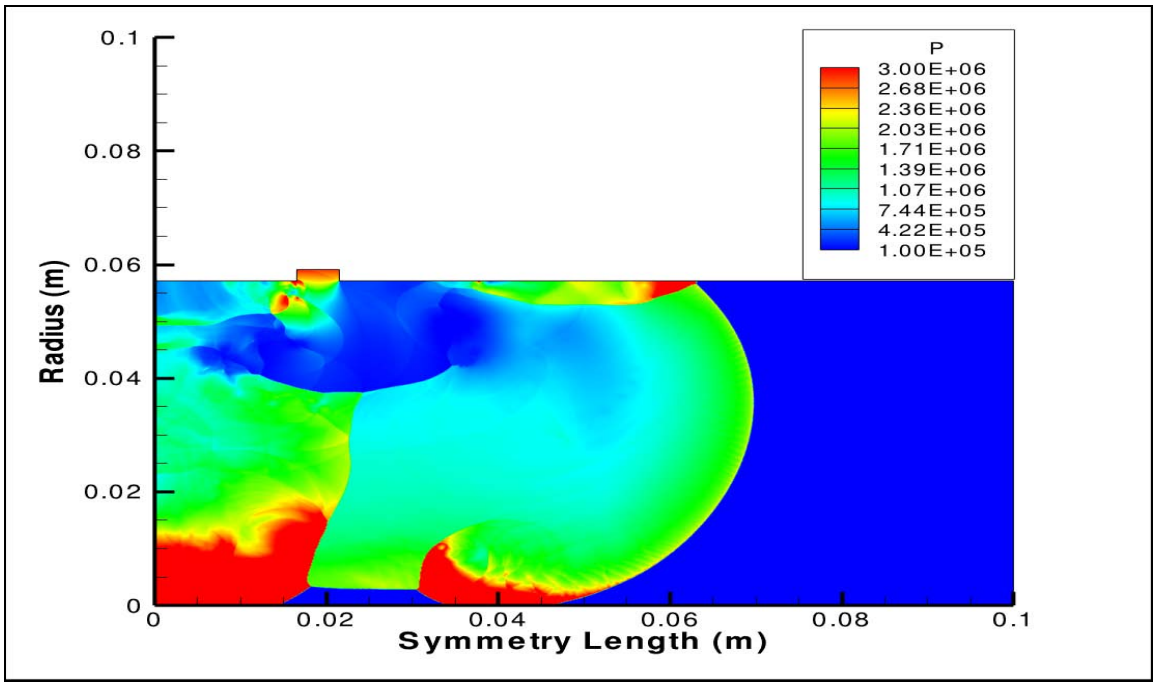

Figure 65. Pressure contour for imploding geometry at run distance of 52 mm for tube diameter of 114.30 mm along inlet axis

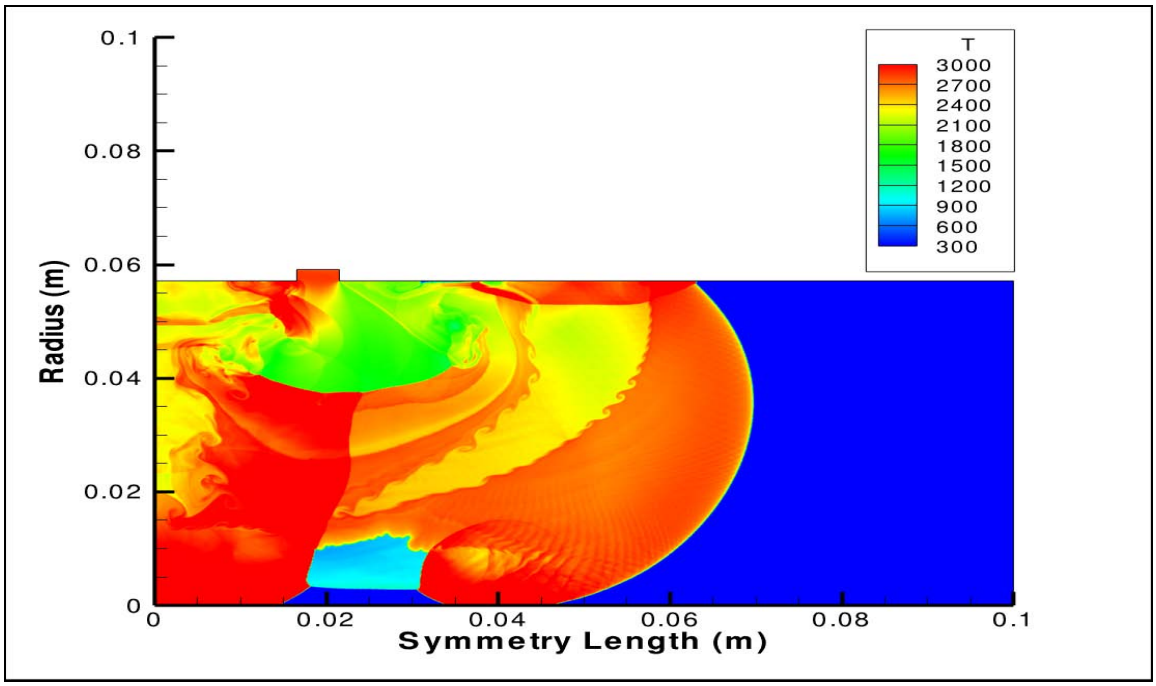

Figure 66. Temperature contour for imploding geometry at run distance of 52 mm for tube diameter of 114.30 mm along inlet axis

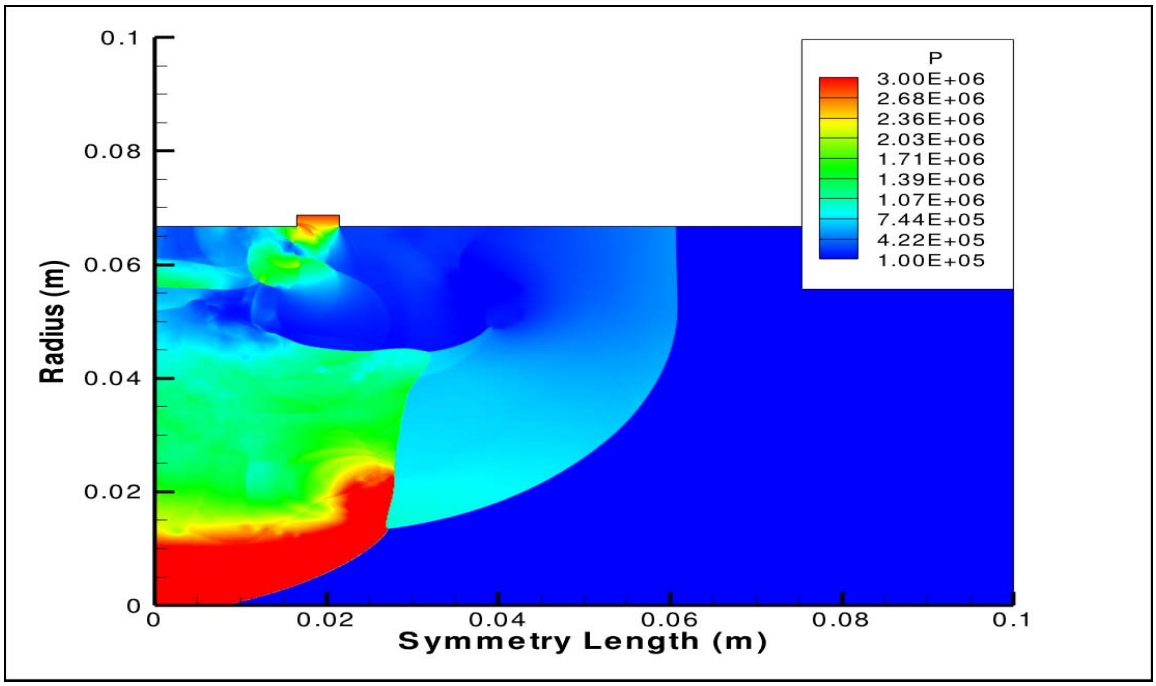

Figure 67. Pressure contour for imploding geometry at run distance of 62 mm for tube diameter of 133.35 mm along inlet axis

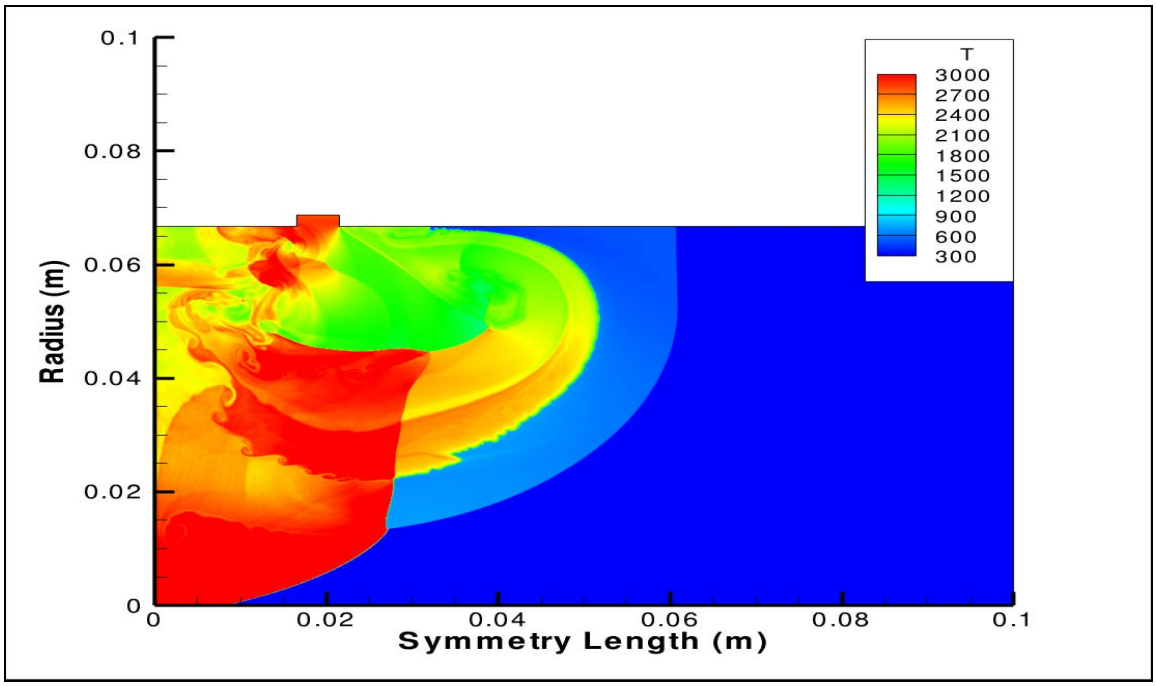

Figure 68. Temperature contour for imploding geometry at run distance of 62 mm for tube diameter of 133.35 mm along inlet axis

2. Parametric Analysis Along Symmetry Axis

Along the symmetry axis, the detonation process is supported throughout as all 3 test cases pertaining to different tube diameter geometries is observed to start from an overdriven detonation wave before decaying to a steady state wave propagating towards C-J velocity. A plot of the normalized wave velocity to C-J velocity against run distance along symmetry axis in Figure 69 depicts the observed wave propagation behavior.

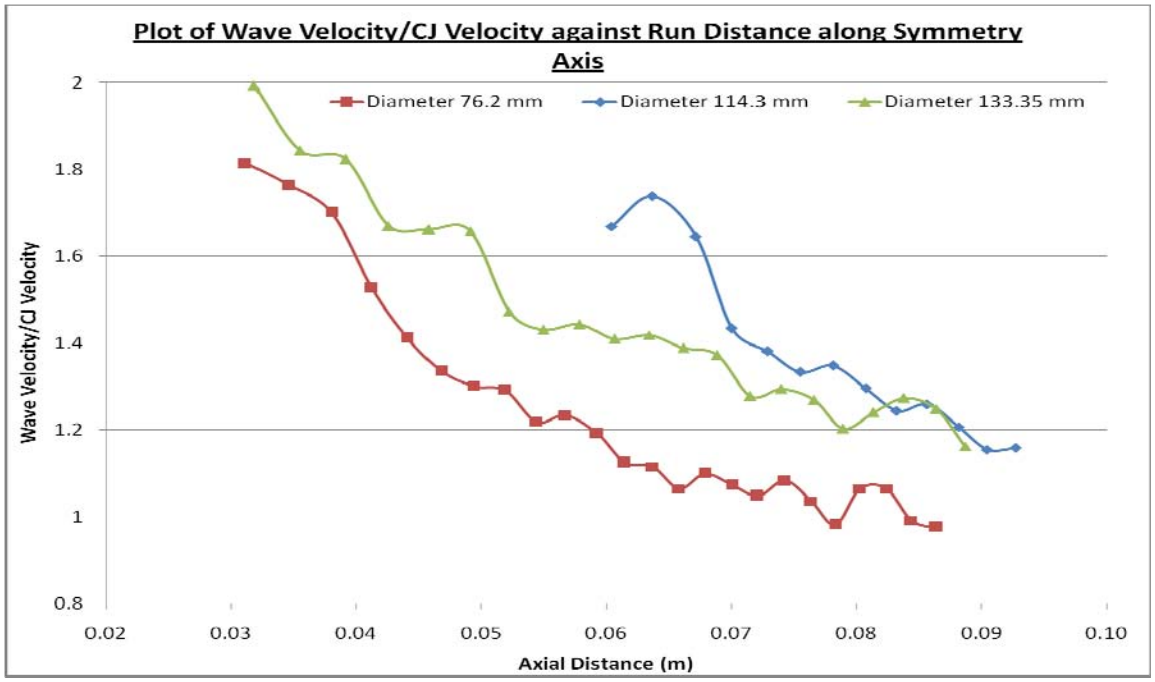

Figure 69. Plot of wave velocity/CJ Velocity against run distance along symmetry axis for different imploding shock tube diameters

The test case pertaining to tube diameter of 114.3 mm starts out immediately at 60 mm along the symmetry axis as the geometry of the wave front along the radial direction is such that at the point of implosion is almost planar throughout till the start point. The implosion process along the wave propagation drives the pressure and temperature along the symmetry plane to exceedingly high values to almost 50 times C-J pressure as shown in the pressure and temperature history of the starting wave at run distance of 60 mm as

illustrated in Figures 70 and 71. This causes a sharp increase in C-J velocity to almost 1.7 of C-J velocity, which causes the detonation wave to start out overdriven. There is also a second reflected wave from the head end of the tube, which is propagating behind the starting wave as shown in the pressure contour in Figure 72.

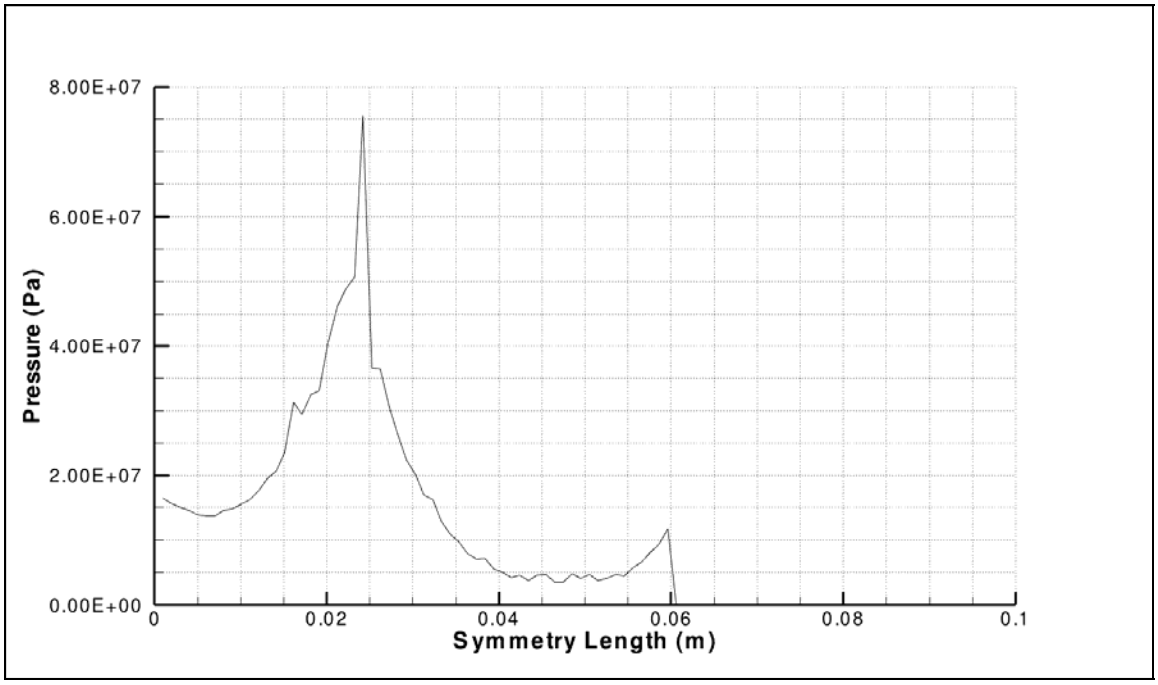

Figure 70. Pressure history of imploding wave at run distance of 60 mm along symmetry axis (diameter 114.3 mm)

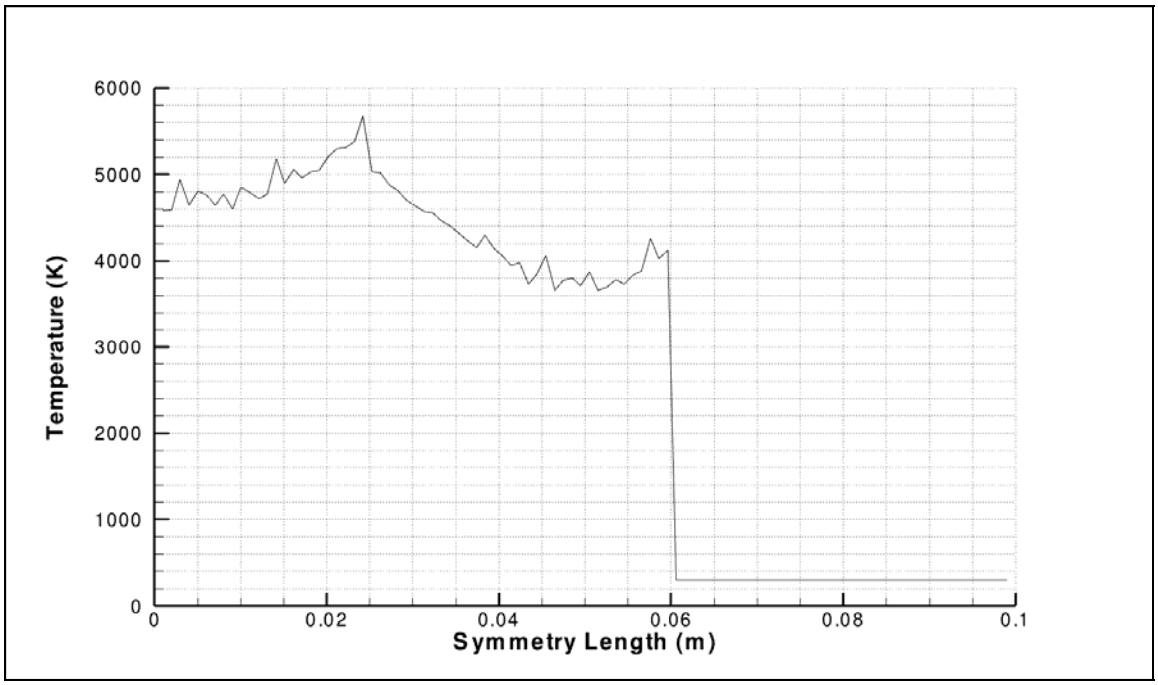

Figure 71. Temperature history of imploding wave at run distance of 60 mm along symmetry axis (diameter 114.3 mm)

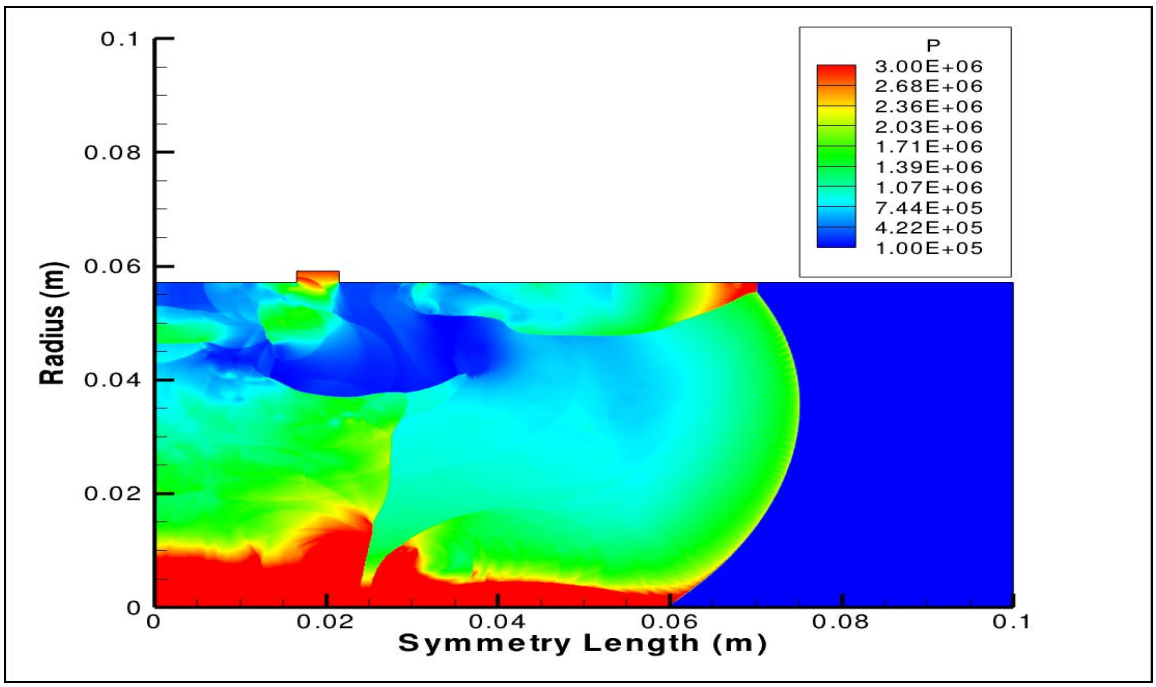

Figure 72. Pressure contour for imploding geometry at run distance of 60 mm for tube diameter of 114.3 mm along symmetry axis

The detonation process is supported throughout the symmetry axis as both pressure and temperature states decay towards C-J conditions. Even as the wave approach towards the end of the tube at a run distance of 91 mm, the pressure and temperature states at the 1-D lead shock front along the symmetry axis as denoted by the respective temperature and pressure histories in Figures 73 and 74 are still above C-J conditions. This clearly indicates that the detonation propagation process is still supported. In 2-D, the pressure contour in Figure 75 at a run distance of 91 mm illustrates a non-planar shock front followed by a closely coupled high pressure region. In this region along the transverse direction, the pressure decreases further away from the symmetry axis before increasing again towards the wall of the shock tube. Although there is a decrease of pressure in the transverse direction, the states in this closely coupled are still above C-J conditions, which highlights the potential of increasing the diameter of the tube even further and still maintain sustenance of the detonation wave.

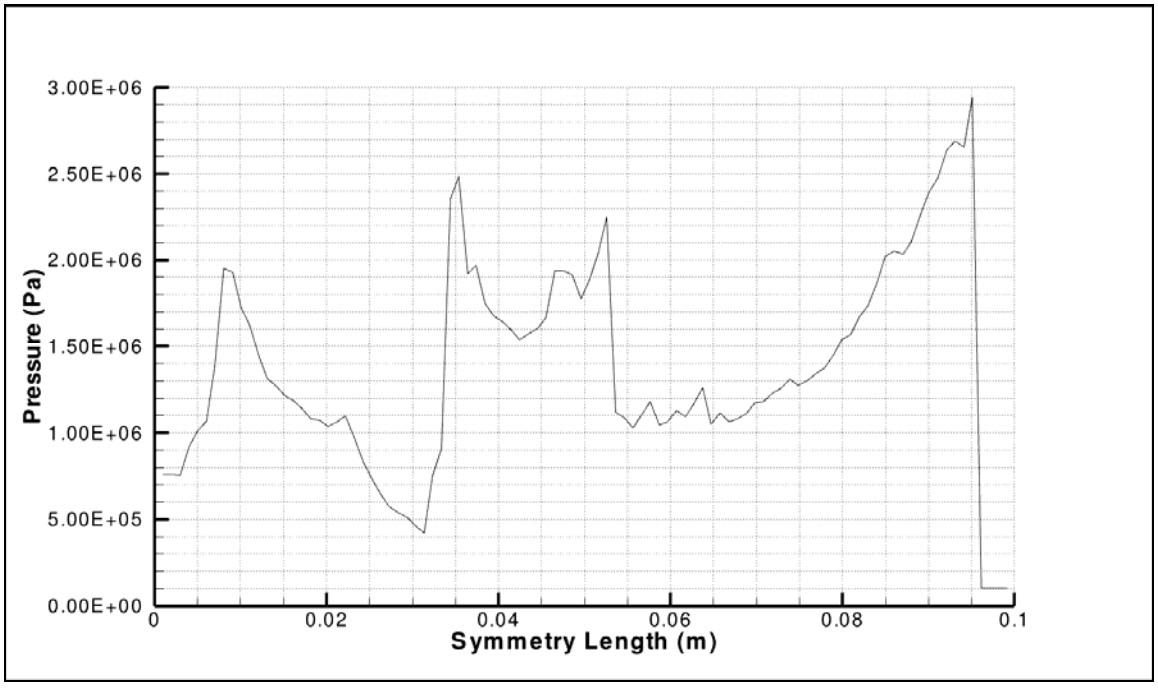

Figure 73. Pressure history of imploding wave at run distance of 91 mm along symmetry axis (diameter 114.3 mm)

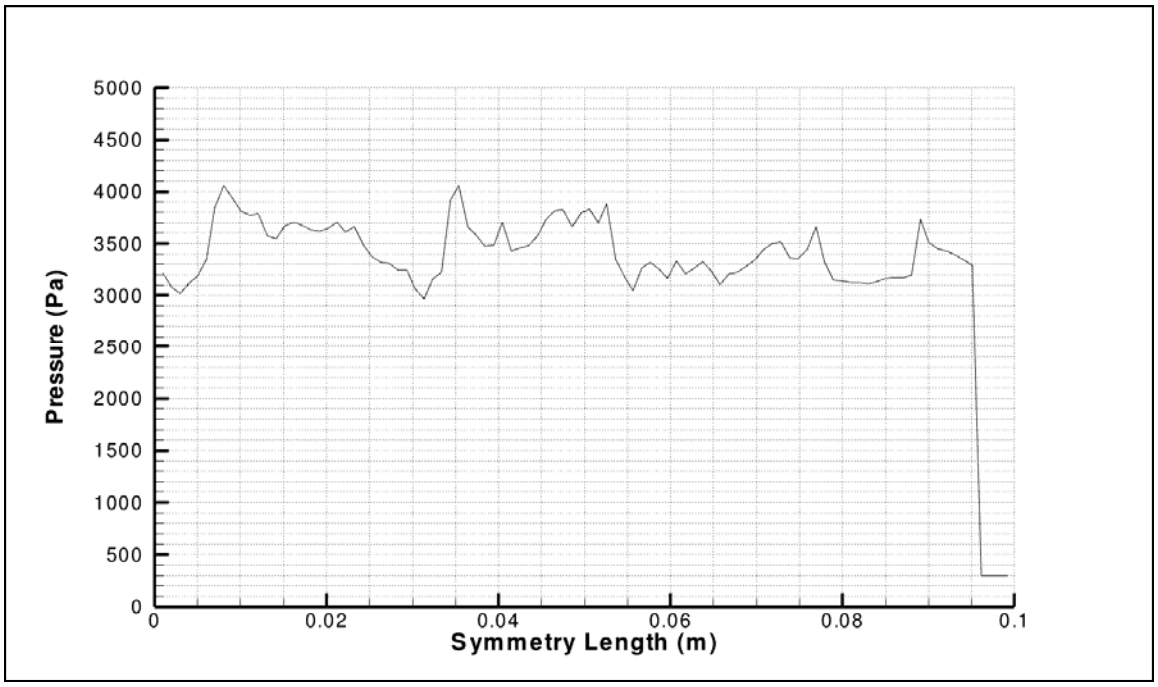

Figure 74. Temperature history of imploding wave at run distance of 91 mm along symmetry axis (diameter 114.3 mm)

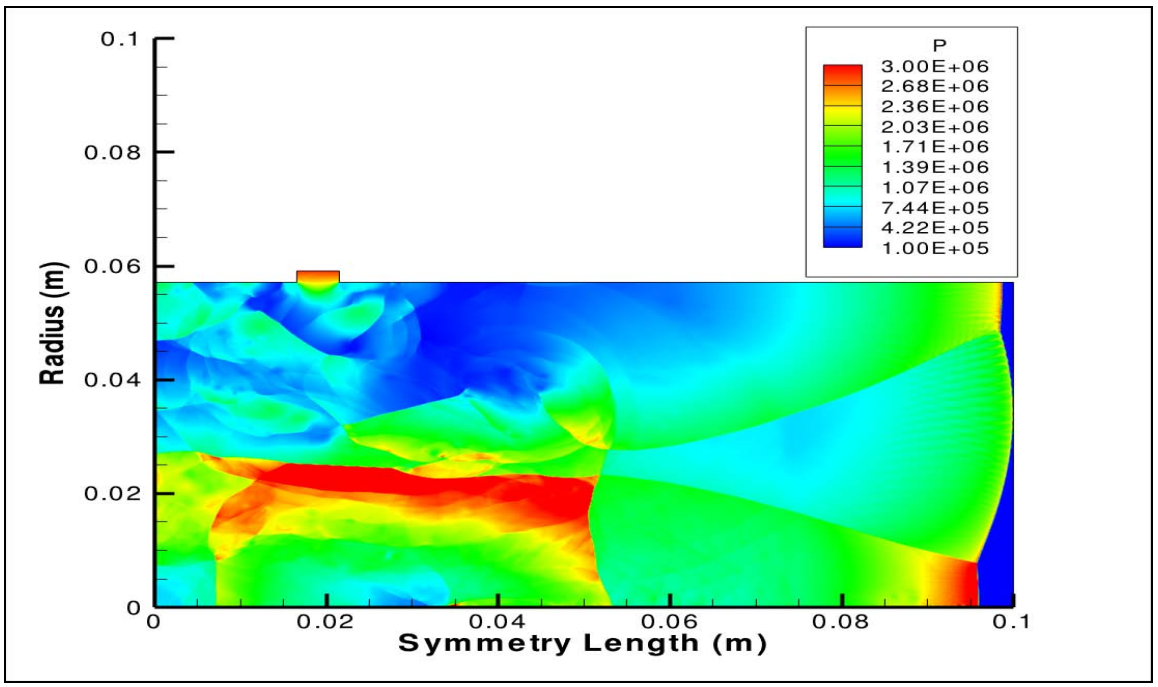

Figure 75. Pressure contour for imploding geometry at run distance of 91 mm for tube diameter of 114.3 mm along symmetry axis

For the test case pertaining to the tube diameter of 133.35 mm, there are 2 mechanisms sustaining the detonation wave propagation. The first mechanism is due to the reflection of the secondary wave from the head end of the shock tube while the second mechanism is due to the implosion process itself. At implosion, the wave starts out overdriven with pressure and temperature states behind the lead shock front way above C-J conditions. For the specified geometry, the secondary reflected wave merges with the transverse imploded wave, which magnifies the pressures and temperatures behind the lead shock front. This can be observed in the pressure and temperature histories of the wave propagation evaluated along the symmetry axis at a run distance of 30 mm in Figures 76 and 77, which reaches 32.5 MPa (~20 times C-J pressure) and 5000 K (~ 1.7 times C-J temperature). The same 2-D pressure contour in Figure 78 illustrates an observed two distinct wave structure phenomena, a detonation wave that is propagating at super C-J velocity and a weak decaying wave that is remnant of the previous toroidal wave front that is slowing down due to expansion effects.

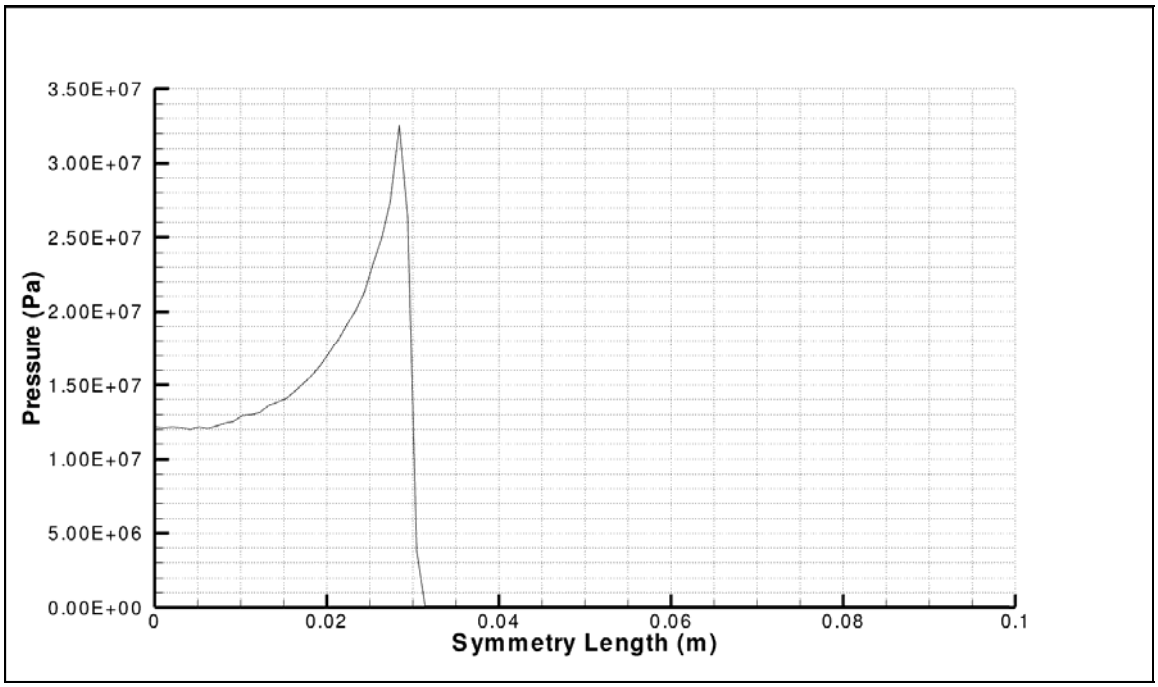

Figure 76. Pressure history of imploding wave at run distance of 30 mm along symmetry axis (diameter 133.35 mm)

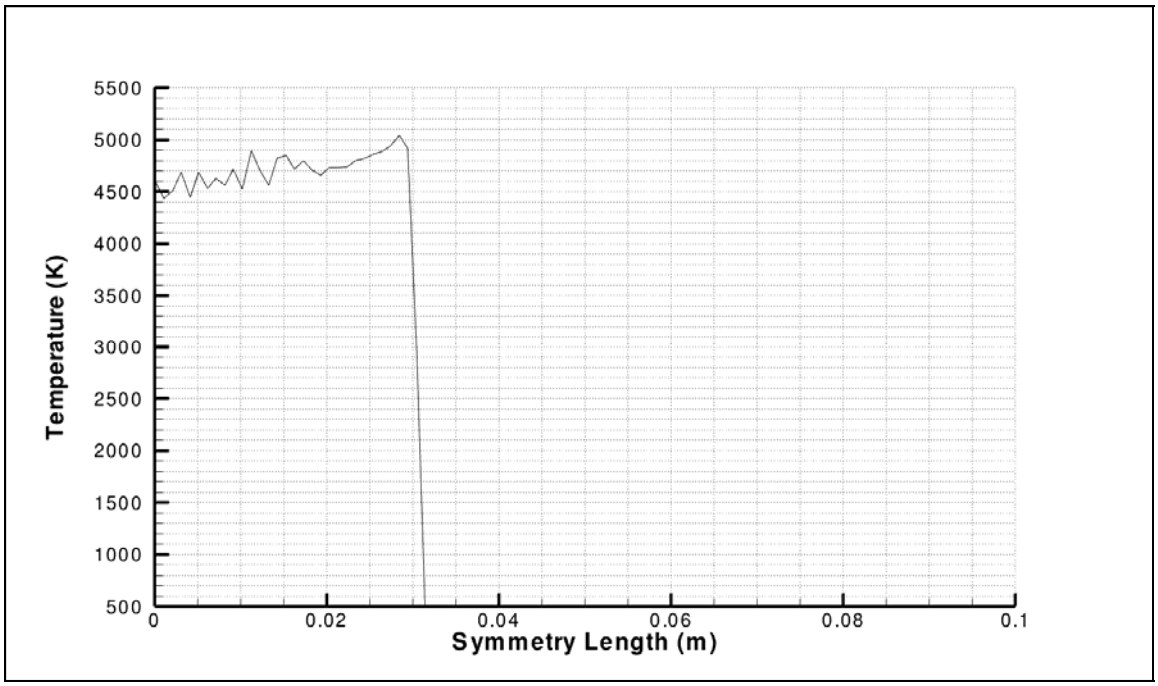

Figure 77. Temperature history of imploding wave at run distance of 30 mm along symmetry axis (diameter 133.35 mm)

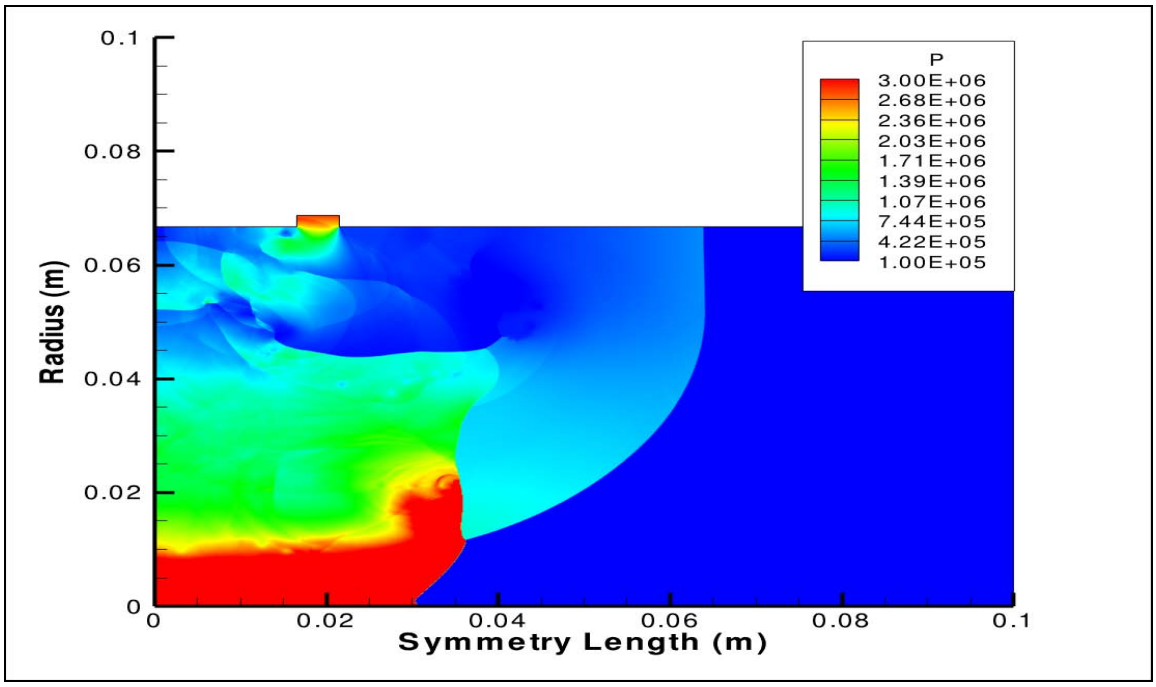

Figure 78. Pressure contour for imploding geometry at run distance of 30 mm for tube diameter of 133.35 mm along symmetry axis

The super detonation wave travelling along the symmetry axis will eventually catch up and overtake the weak expansion toroidal wave front. This is illustrated in the pressure contour in Figure 79 as the wave approaches the end of the shock tube length at a run distance of 88 mm. The super detonation wave also expands towards the walls eventually replacing the weak expansion wave front as it propagates further along the symmetry axis.

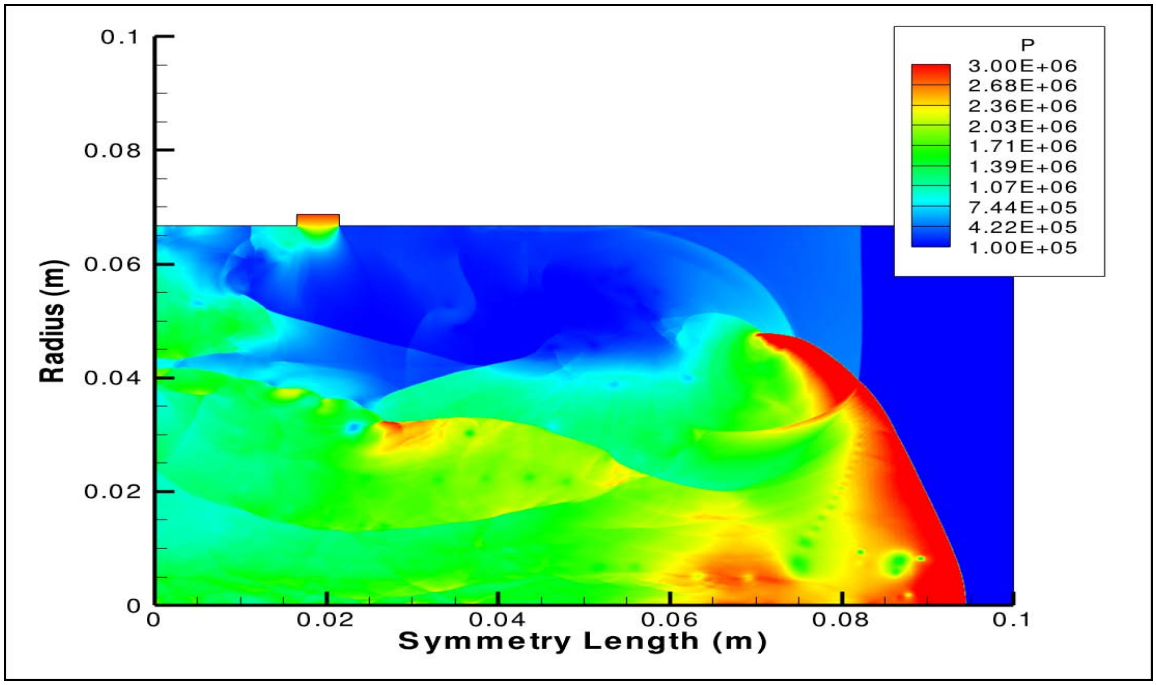

Figure 79. Pressure contour for imploding geometry at run distance of 88 mm for tube diameter of 133.35 mm along symmetry axis

The 1-D pressure and temperature histories of the same wave along the symmetry axis in Figures 80 and 81 still shows the detonation wave being supported even as it propagates towards the tube end. Here the C-J pressure and temperature states just behind the lead shock front are still at 4.0 MPa(~ 2.5 C-J pressure) and 3200 K (~ 1.1 C-J temperature), which will eventually decay to steady-state CJ velocity.

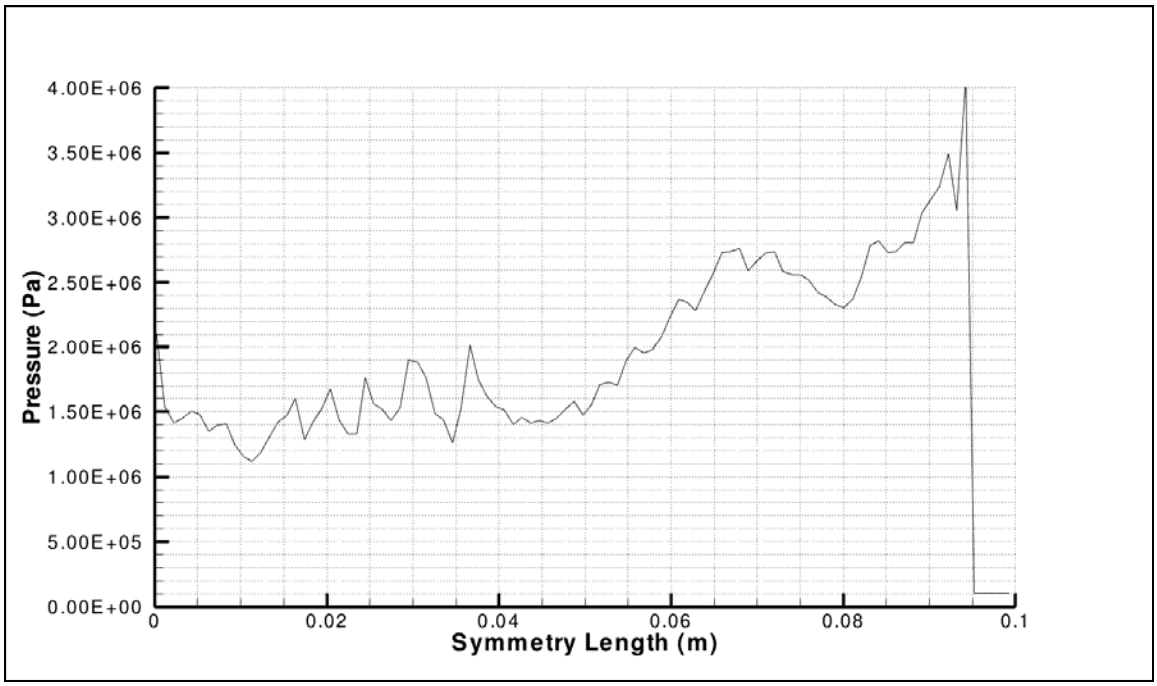

Figure 80. Pressure history of imploding wave at run distance of 88 mm along symmetry axis (diameter 133.35 mm)

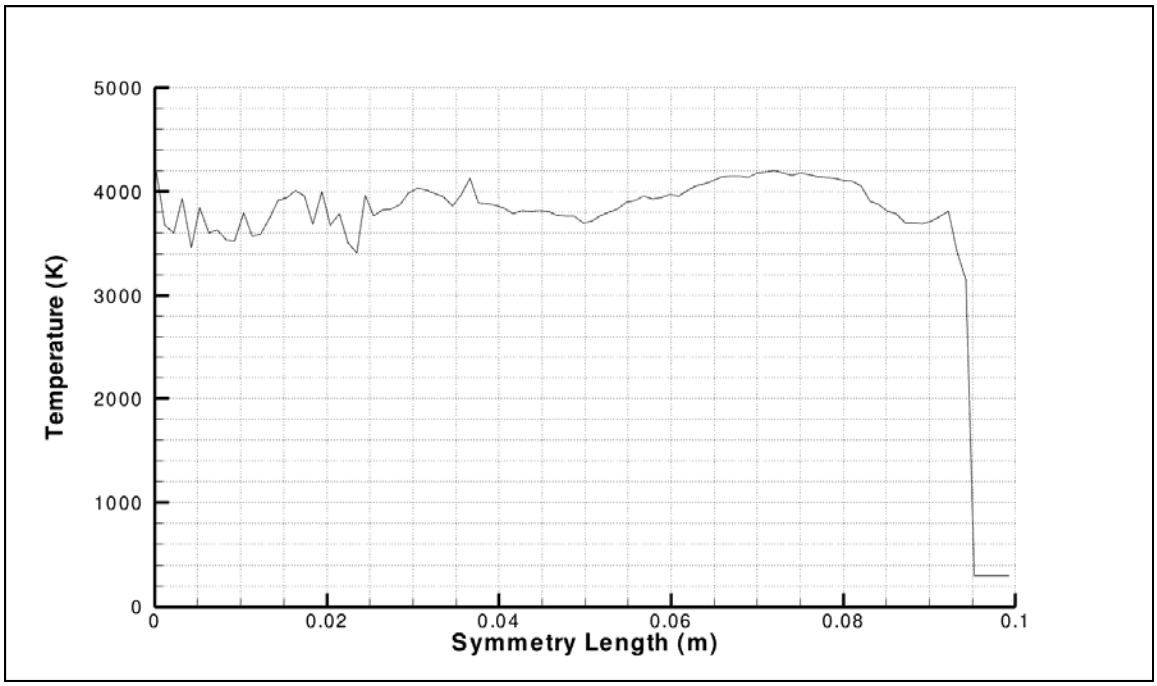

Figure 81. Temperature history of imploding wave at run distance of 88 mm along symmetry axis (diameter 133.35 mm)

The parametric study highlights the immense potential of utilizing a shock focusing technique such as toroidal implosion to increase specific thrust in pulse detonation engines with no requirements to factor in tube length for DDT transitions as the diameter of the tube is further increased. Even when the diameter was increased to beyond 1.5 times the original length, the detonation process was still supported throughout as shown by the simulation results. The mechanisms supporting the detonation process was due to the implosion process itself as well as the secondary reflection wave from the tube head end. It would have been ideal to obtain the optimal tube diameter at which the implosion process fails to support the detonation process; however it was not possible to go beyond the tube diameter of 133.35 mm due to the limitation of the available computational resources. A two-fold increase in tube diameter results in a four-fold increase in required computational resource due to the number of mesh size. It is evident from the outcome of the parametric study that diameters way beyond 133.35 mm is possible to support the detonation process due to the simultaneous interaction and reinforcement of not only the implosion process itself, but also supplemented by the secondary reflection wave from the head end of the tube.

THIS PAGE IS INTENTIONALLY LEFT BLANK

V. WAY FORWARD AND RECOMMENDATIONS

Steps to conduct further parametric studies to determine the optimal diameter such that detonation process can be supported will be addressed in future endeavors. The specialized CFD solver from Metacomp Technologies requires extensive parallel node-to-node communications based on the computational cell size required to capture the complex physics governing the shock wave propagation process. This results in latency issues that contribute to substantial computational downtime whereby current supercomputing architecture on campus using infiniband interconnects is unable to support. Subsequent studies will be ported over to a high performance computing architecture off-campus with minimal latency and as such simulation time can be drastically reduced in order to allow for reasonable time for analysis of results.

Additionally, it is desired not only to maximize the tube diameter based on the given geometry, but also the location of the inlet for the starting toroidal wave front. The location of the inlet from the head tube end will not only optimize the imploding detonation wave towards the symmetry axis but also optimizes the secondary reflected wave as it catches up with the toroidal wave front and aids as a supplementary mechanism to support the detonation wave propagation throughout the shock tube along the symmetry axis.

Once the optimal configuration geometry has been established for imploding detonations for hydrogen-air, future endeavors will also address test cases for hydrocarbon fuels such as ethylene-air and JP10-air. Moreover, optimal tube geometries can be further determined by using the practical computational cell size established for this thesis study as well as a set of viable reduced set of chemical kinetic reaction models specific to these fuel-oxidizer mixtures. Note that JP10 is a military qualified jet aviation fuel that due to its high energy density represents the best realizable fuel of choice for PDE applications.

The future should focus on building an experimental test rig based on the imploding geometry to not only validate the simulation results, but in the process allow for a paradigm shift in future PDE designs that need not factor in multiple tube configurations and as such maximizing specific thrust.

THIS PAGE INTENTIONALLY LEFT BLANK

VI. CONCLUSION

A novel method to increase specific thrust in PDEs via imploding detonations has been investigated in this study. High fidelity simulations were required in order to capture the physics governing such complex flow fields. In this study, a practical computational mesh size on the order of one-quarter induction length was determined and deemed sufficient based on a reduced set of 18 reactions and 9 species chemical reaction model for hydrogen-air mixture. It was also found that the corresponding computed detonation cell width coincided with actual experimental data for the same fuel-oxidizer mixture.

A set of simulations were carried out on an enhanced PDE design configuration utilizing implosion concepts and results indicate that the detonation wave was supported with pressure and temperature states persisting above CJ conditions behind the lead shock front throughout the entire geometry. Further parametric studies were conducted to evaluate and determine the extent of diameter increase for such design configurations and it was found that the detonation propagation process was still well supported even up to 1.75 times the original diameter. This represents a three-fold increase in thrust per PDE tube, which roughly translates into a two-fold increase in specific thrust for similar total thrust PDE systems. However, there is a need to evaluate much bigger diameters. Due to the limitations of current parallel computing architecture, future endeavors will be addressed by using the Department of Defense (DoD) High Performance Computing systems that consists of a parallel computing platform with minimal latency in order determine the maximum diameter at which the detonation structure fails to persist in the specified geometry.

THIS PAGE IS INTENTIONALLY LEFT BLANK

APPENDIX A: NASA CHEMICAL EQUILIBRIUM ANALYSIS OUTPUT

```
         NASA-GLENN CHEMICAL EQUILIBRIUM PROGRAM CEA2, FEBRUARY 5, 2004
                    BY  BONNIE MCBRIDE AND SANFORD GORDON
       REFS: NASA RP-1311, PART I, 1994 AND NASA RP-1311, PART II, 1996


*************************************************************************
********

 output massf
 prob case=00002142 det
 phi=1

 p(atm)=1
 output short
 output trace=1e-10

 reac
 oxid  Air  t,k= 298 wt%=  100.
 fuel  H2  t,k= 298 wt%=  100.
 end

                      DETONATION PROPERTIES OF AN IDEAL REACTING GAS
 CASE = 00002142

             REACTANT                              WT FRACTION        ENERGY
TEMP
                                                (SEE  NOTE)          KJ/KG-MOL
K
 OXIDANT      Air                                    1.0000000       -129.895
298.000
 FUEL         H2                                     1.0000000         -4.325
298.000

 O/F=   34.29623  %FUEL=  2.833164  R,EQ.RATIO= 1.000000  PHI,EQ.RATIO=
1.000000

 UNBURNED GAS

 P1, BAR           1.0132
 T1, K             298.00
 H1, KJ/KG          -4.36
 M1, (1/n)         21.008
 GAMMA1            1.4015
 SON VEL1,M/SEC     406.6

 BURNED GAS
```

P, BAR	15.801
T, K	2943.63
RHO, KG/CU M	1.5500 0
H, KJ/KG	1333.33
U, KJ/KG	313.90
G, KJ/KG	-29833.7
S, KJ/(KG)(K)	10.5880
M, (1/n)	24.008
(dLV/dLP)t	-1.00954
(dLV/dLT)p	1.2062
Cp, KJ/(KG)(K)	3.3542
GAMMAs	1.1637
SON VEL,M/SEC	1089.2

DETONATION PARAMETERS

P/P1	15.595
T/T1	9.878
M/M1	1.1428
RHO/RHO1	1.8042
DET MACH NUMBER	4.8335
DET VEL,M/SEC	1965.1

MASS FRACTIONS

*Ar	1.2550-2
*CO	1.3093-4
*CO2	2.6525-4
COOH	2.6149-9
*H	2.4760-4
HCO	1.0225-9
HNCO	2.395-10
HNO	3.1235-6
HNO2	8.9839-7
HNO3	1.028-10
HO2	1.5250-5
*H2	2.6254-3
HCOOH	3.735-10
H2O	2.2035-1
H2O2	2.3080-6
*N	1.1146-6
*NH	4.5040-7
NH2	2.7000-7
NH3	3.4969-7
NH2OH	4.217-10
*NO	9.4235-3
NO2	6.6339-6
*N2	7.2938-1
N2O	2.7711-6
*O	1.3571-3
*OH	1.3522-2
*O2	1.0117-2
O3	6.2078-9

* THERMODYNAMIC PROPERTIES FITTED TO 20000.K

NOTE. WEIGHT FRACTION OF FUEL IN TOTAL FUELS AND OF OXIDANT IN TOTAL OXIDANTS

THIS PAGE IS INTENTIONALLY LEFT BLANK

APPENDIX B: CONVERGENCE PLOTS FOR RESIDUAL ERRORS

A. GLOBAL RESIDUAL ERROR PLOT FOR MESH SIZE OF 0.25 MM

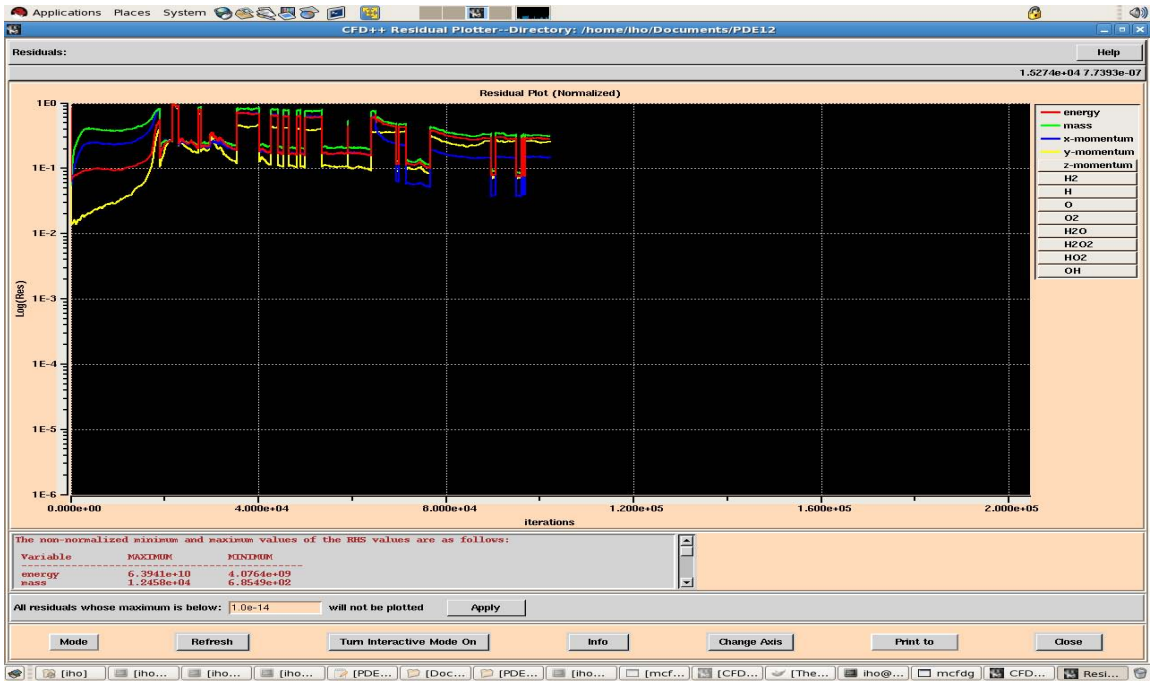

B. INNER RESIDUAL ERROR PLOT FOR MESH SIZE OF 0.25 MM

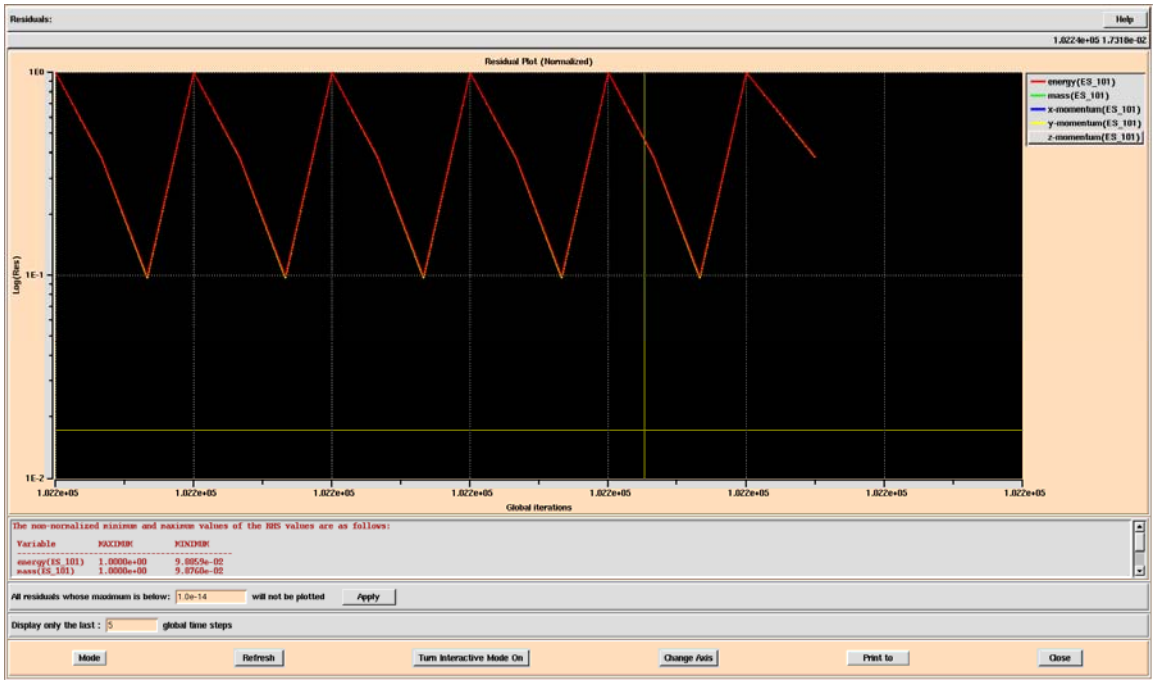

C. GLOBAL RESIDUAL ERROR PLOT FOR MESH SIZE OF 0.50 MM

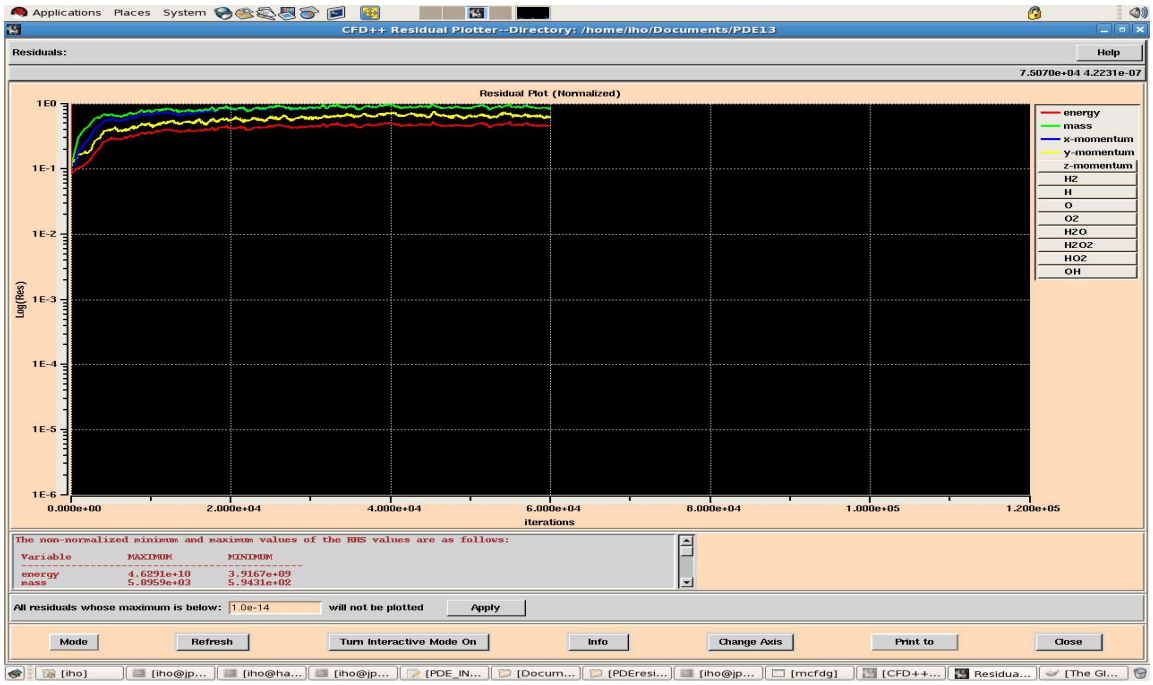

D. INNER RESIDUAL ERROR PLOT FOR MESH SIZE OF 0.50 MM

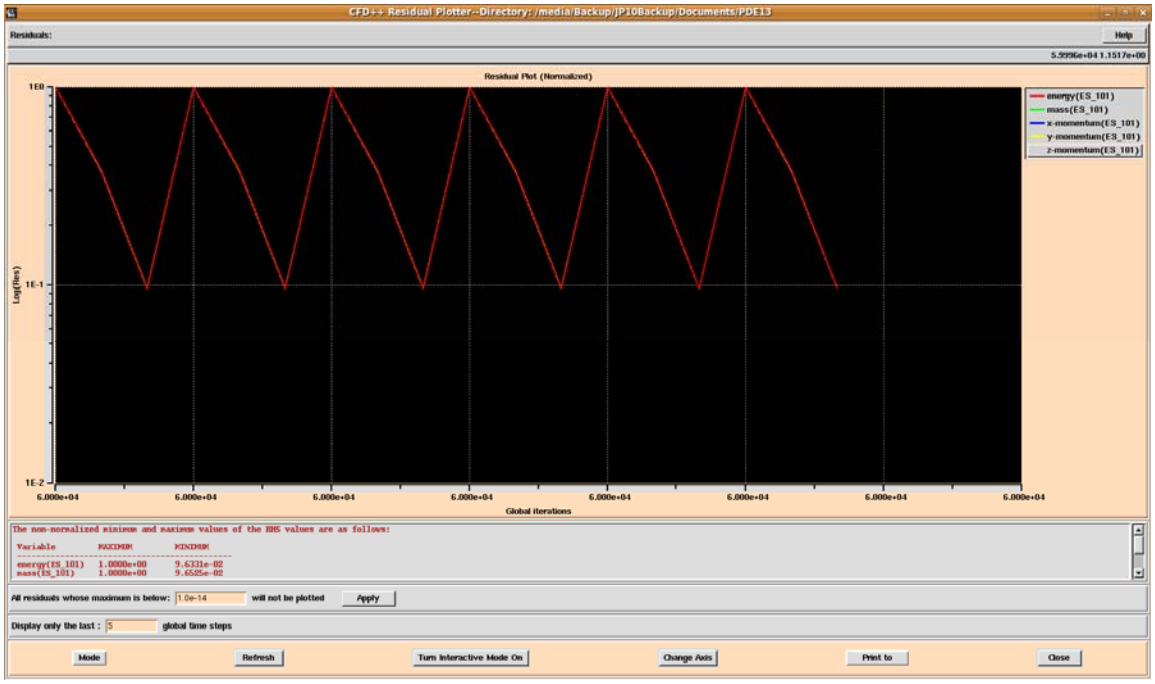

E. GLOBAL RESIDUAL ERROR PLOT FOR MESH SIZE OF 1.00 MM

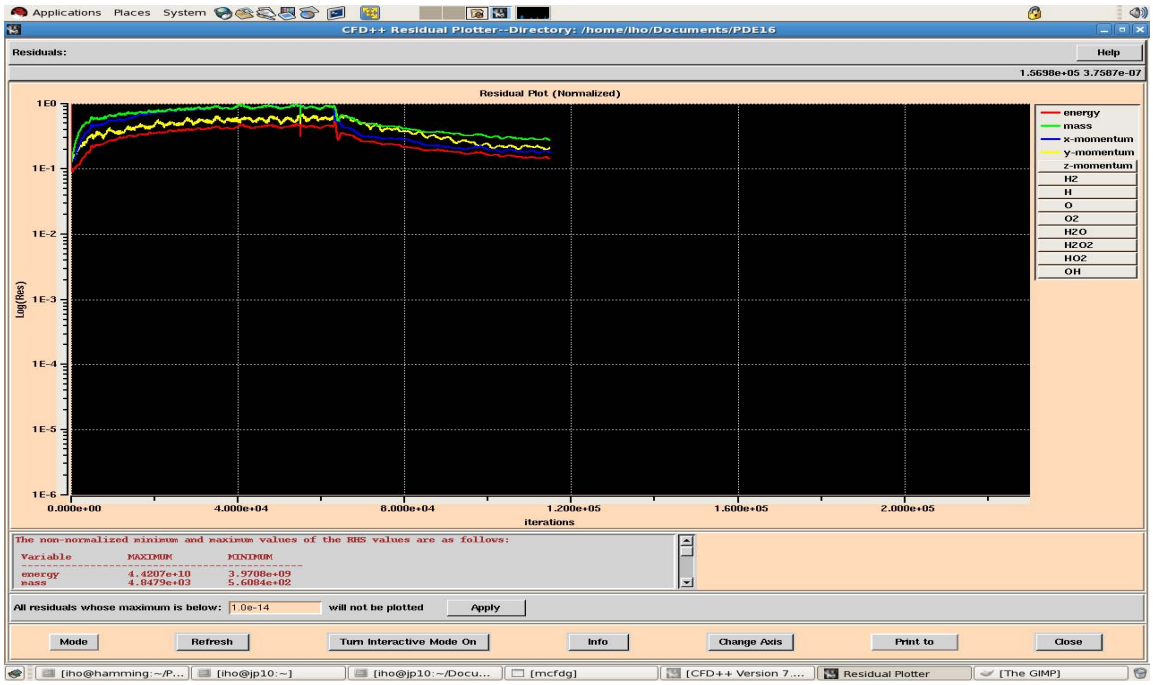

F. INNER RESIDUAL ERROR PLOT FOR MESH SIZE OF 1.00 MM

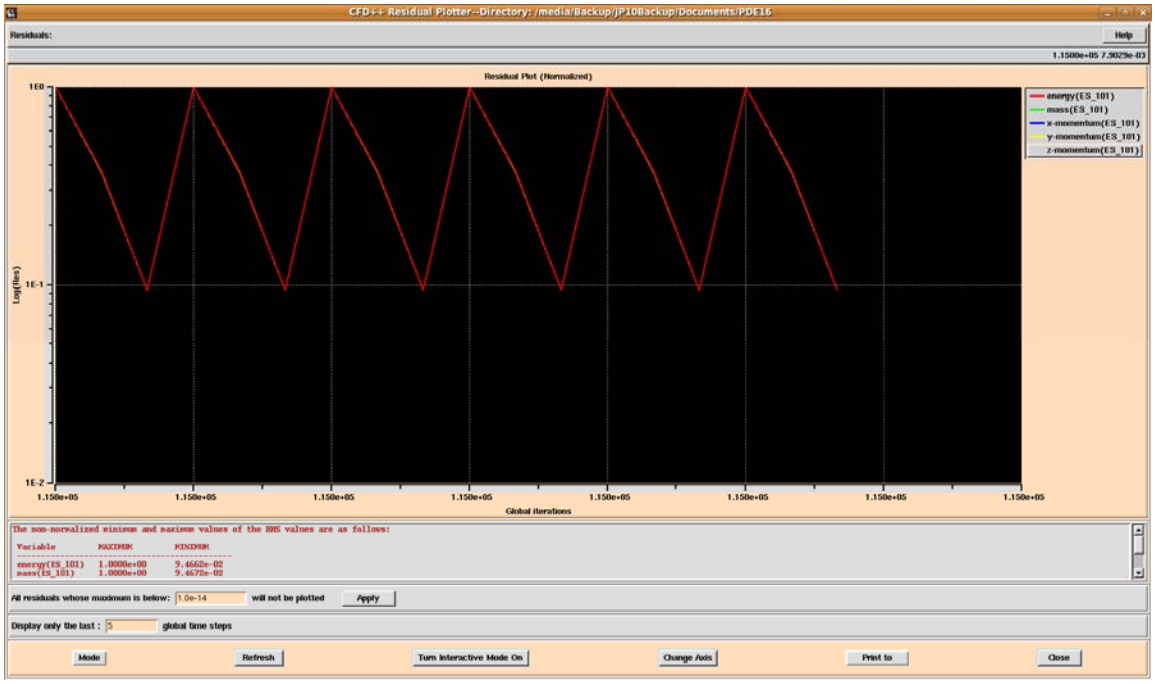

G. GLOBAL RESIDUAL ERROR PLOT FOR MESH SIZE OF 0.0625 MM

H. INNER RESIDUAL ERROR PLOT FOR MESH SIZE OF 0.0625 MM

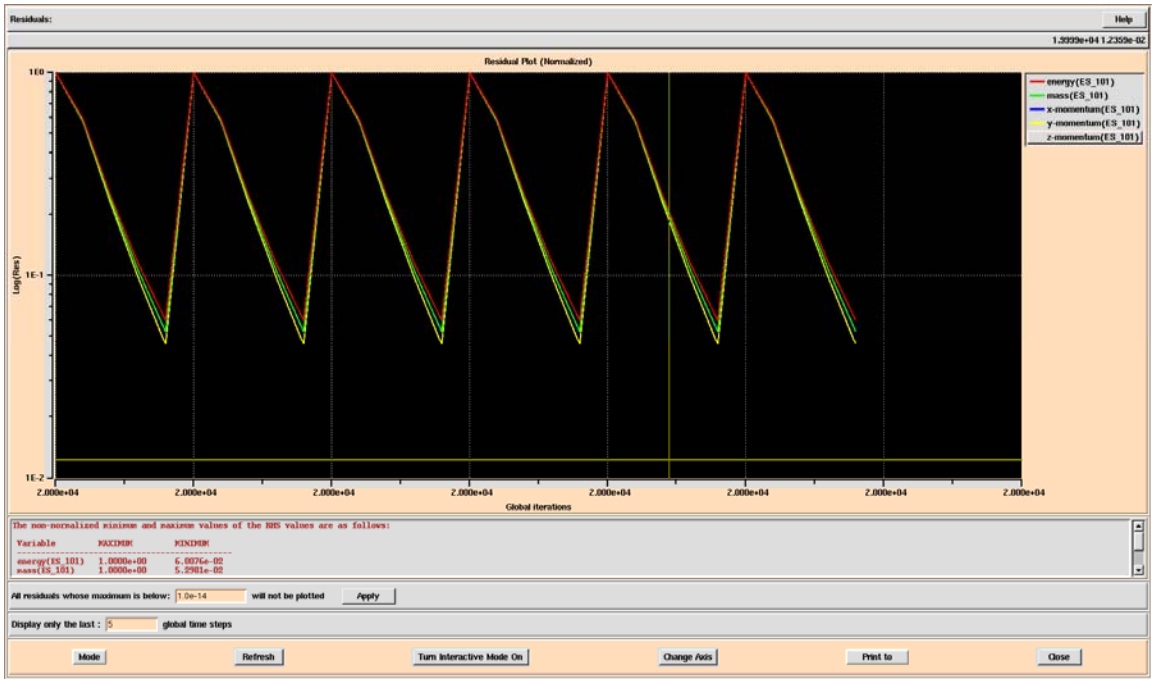

I. GLOBAL RESIDUAL ERROR PLOT FOR MESH SIZE OF 0.05 MM

J. INNER RESIDUAL ERROR PLOT FOR MESH SIZE OF 0.05 MM

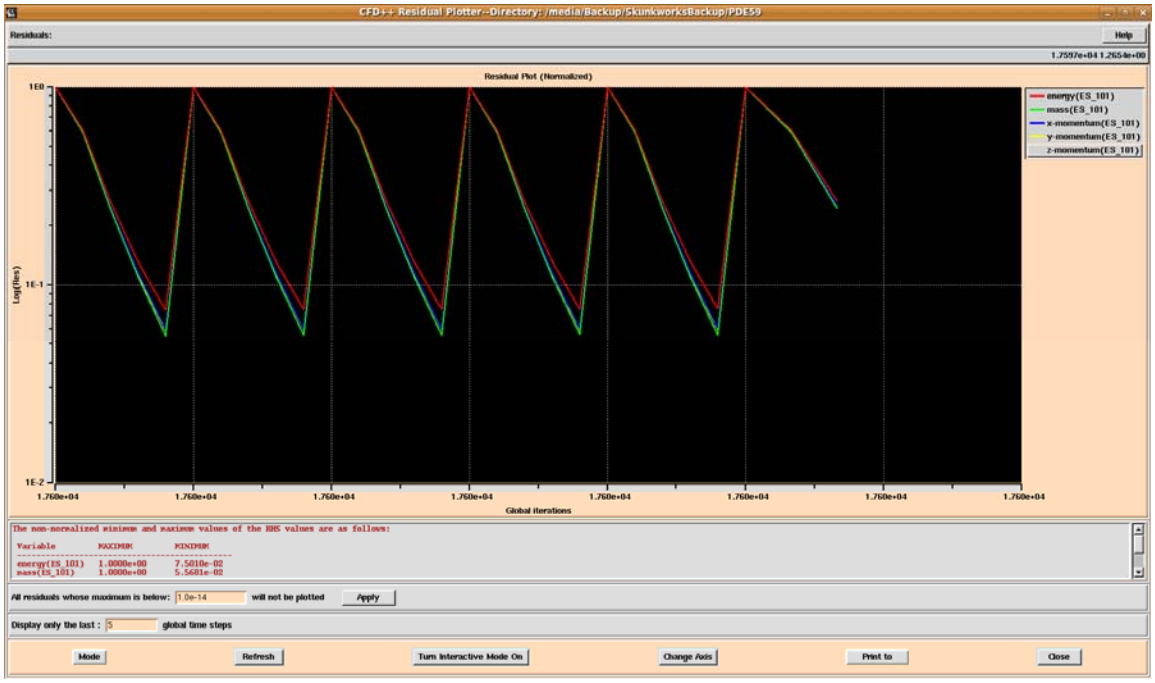

K. GLOBAL RESIDUAL ERROR PLOT FOR IMPLOSION (76.2 MM)

L. INNER RESIDUAL ERROR PLOT FOR IMPLOSION (76.2 MM)

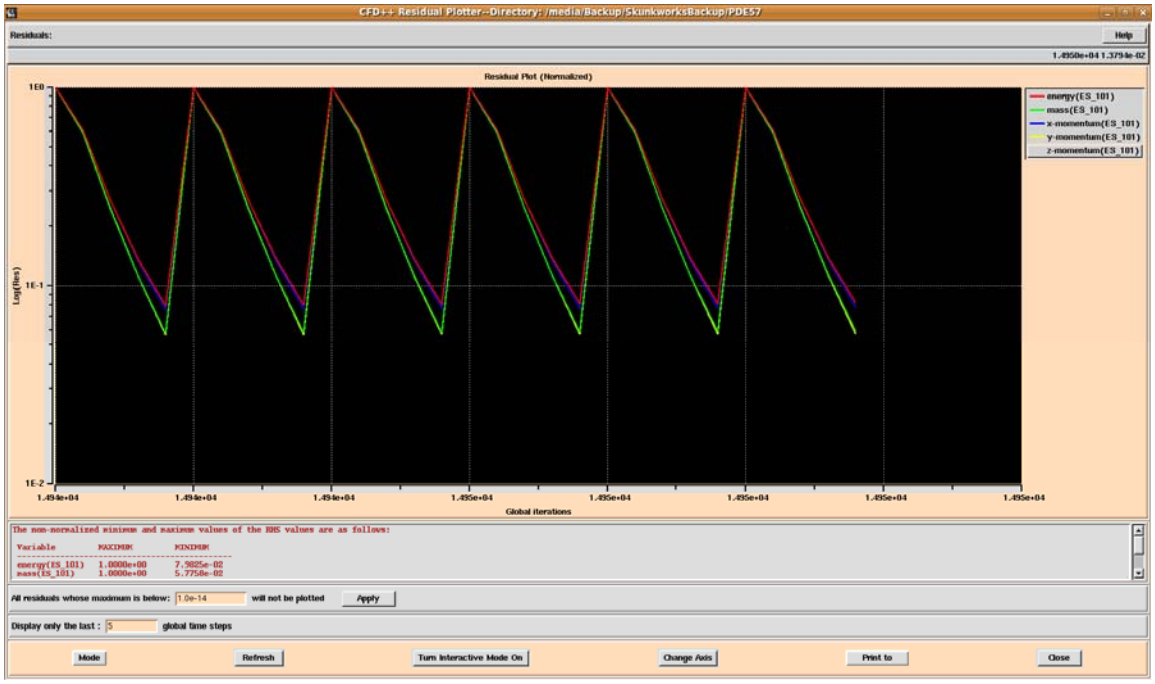

M. GLOBAL RESIDUAL ERROR PLOT FOR IMPLOSION (114.30 MM)

N. INNER RESIDUAL ERROR PLOT FOR IMPLOSION (114.30 MM)

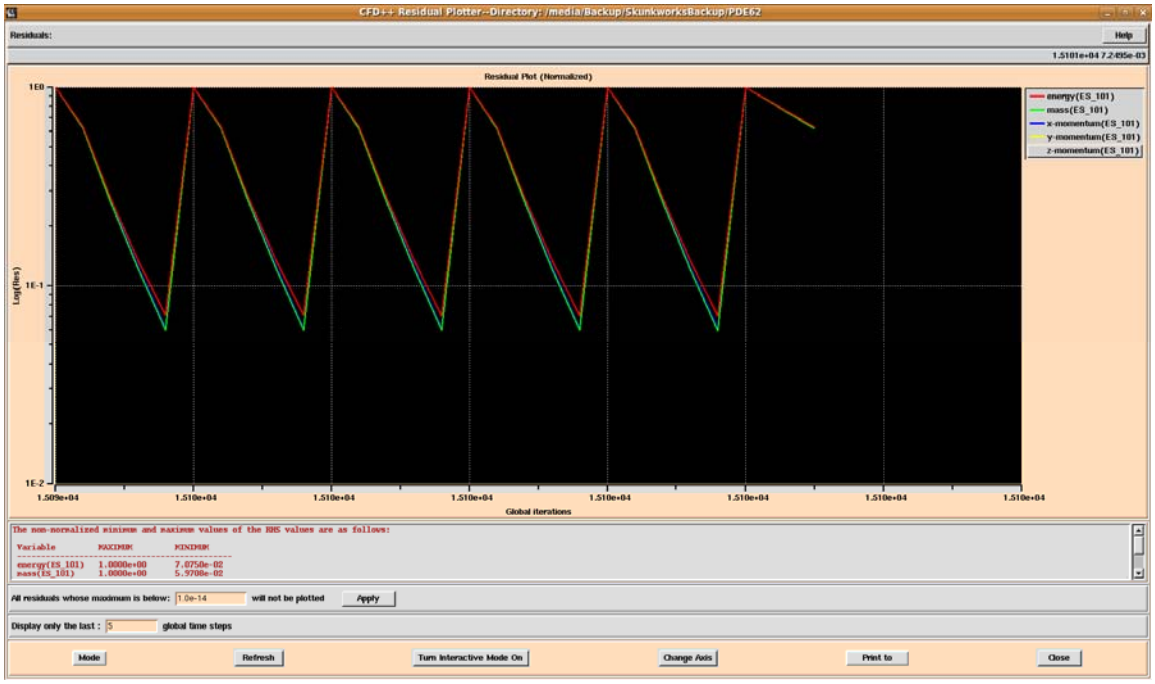

O. GLOBAL RESIDUAL ERROR PLOT FOR IMPLOSION (133.35 MM)

P. INNER RESIDUAL ERROR PLOT FOR IMPLOSION (133.35 MM)

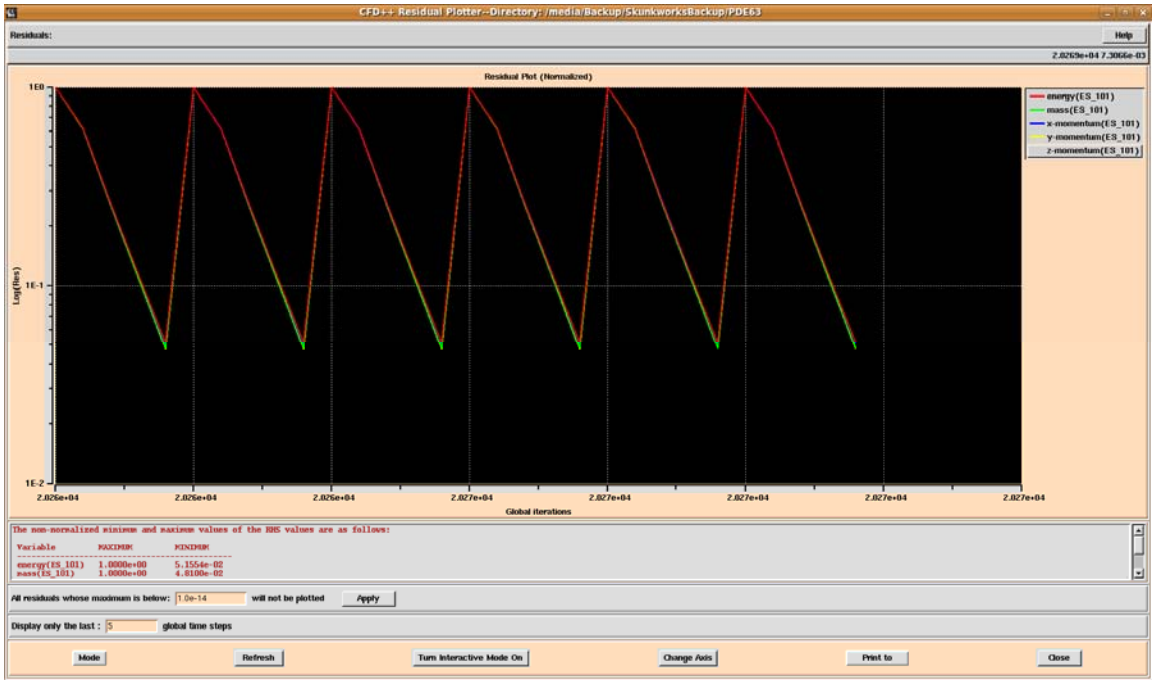

LIST OF REFERENCES

[1] S.I. Jackson, M.P. Grunthaner and J.E. Shepherd, “Wave Implosion as an Initiation Mechanism for Pulse Detonation Engines”, 39th AIAA Joint Propulsion Conference & Exhibit, 2003.

[2] P. Panicker, T.H. New, K. Lu and H.M. Tsai, “Experimental Investigations on DDT Enhancements by Schelkin Spiral in a PDE,” Aerodynamic Research Center, University of Texas at Arlington.

[3] Kenneth K. Kuo, “Principles of Combustion (2nd Edition,)” John Wiley and Sons, Hoboken New Jersey, 2005.

[4] G. Ciccarelli and J. Card, “Detonation in Mixtures of JP-10 Vapor and Air”, AIAA Journal, Vol. 44, No.2, February 2006, pp.362–367.

[5] T. Lu, Chung K. Law and Y. Ju, “Some Aspects of Chemical Kinetics in Chapman-Jouguet Detonation: Induction Length Analysis,” Journal of Power and Propulsion Vol.19, No.5, September-October 2003, pp. 901–907.

[6] R. Courant, K. Friedrichs and H. Lewy, "On the Partial Difference Equations of Mathematical Physics", IBM Journal, March 1967, pp. 215–234, English translation of the 1928 German original.

[7] M.C. Burrows and A.P Kurkov, “Analytical & Experimental Study of Supersonic Combustion of Hydrogen in a Vitiated Air Stream”, NASA TM X-2828, 1973.

[8] J.P. Drummond, R.C. Rogers and M.Y. Hussaini, “A Numerical Model for Supersonic Reacting Mixing Layers,” Computational Methods in Applied Mechanics & Engineering, Vol.64, pp. 39–60, 1987

[9] I.A. Zaev, M.I. Strelkova, I.A. Kirillov, M.V. Okun, B.V. Potapkin, V.E. Tangirala, A.J. Dean and A.M. Tentner, “Validation of a Short Kinetic Mechanism for Jet A-Air Detonations”, 43rd AIAA Joint Propulsion Conference & Exhibit, 2007.

[10] C.M. Guirao, R. Knystautas, J. Lee, W. Benedick, and M. Berman. Hydrogen-air detonations. In *19th Symp. Int. Combust. Proc.*, pages 583–590, 1982.

[11] P.A. Urtiew and C.M. Tarver. Effects of cellular structure on the behaviour of gaseous detonation waves under transient conditions. In *Prog. Astronaut. Aeronaut.*, volume 75, pages 370–384, 1981.

[12] G. Ciccarelli, T. Ginsberg, J. Boccio, C. Finfrock, L. Gerlach, H. Tagawa, and A. Malliakos. Detonation cell size measurements in high-temperature hydrogen-air-steam mixtures at the bnl high-temperature combustion facility. Technical Report NUREG/CR-6391, BNL-NUREG-52482, Brookhaven National Laboratory, 1997.

[13] W.B. Benedick, R. Knystautas, and J.H.S. Lee. Large-scale experiments on the transmission of fuel-air detonations from two-dimensional channels. In *Prog. Astronaut. Aeronaut.*, volume 94, Pp. 546–555, 1984.

[14] J. Shepherd, Detonation Database, May 27 2002, http://www.galcit.caltech.edu/detn_db/html/C2H2-Air2.html, accessed June 1 2009.

[15] NASA CEA, NASA computer program for calculating of the Chemical Equilibrium with Applications, NASA Glenn Research Center, Cleveland, OH.

[16] J. E Shepherd, "Chemical Kinetics of Hydrogen-Air Diluent Detonations", Sandia National Laboratories, Albuquerque, New Mexico.

[17] W. Fickett and W.C. Davis, "Detonation Theory and Experiment."

[18] M. Abramowitz and I.A. Stegun, "Handbook of Mathematical Functions with Formulas, Graphs and Mathematical Tables", Ninth Printing, Dover, 1970.

INITIAL DISTRIBUTION LIST

1. Defense Technical Information Center
   Ft. Belvoir, Virginia

2. Dudley Knox Library
   Naval Postgraduate School
   Monterey, California

3. Graduate School of Engineering and Applied Sciences
   Naval Postgraduate School
   Monterey, California

4. Prof. Jose O. Sinibaldi
   Department of Physics
   Naval Postgraduate School
   Monterey, California

5. Prof. Christopher M. Brophy
   Department of Mechanical and Aeronautical Engineering
   Naval Postgraduate School
   Monterey, California

6. Prof. Knox T. Millsaps
   Department of Mechanical and Aeronautical Engineering
   Naval Postgraduate School
   Monterey, California

7. Prof. Andres Larraza
   Department of Physics
   Naval Postgraduate School
   Monterey, California

8. Mr. Ivan Chin Kian Ho
   Naval Postgraduate School
   Monterey, California

9. Dr. Gabriel Roy
   Office of Naval Research
   Arlington, Virginia